NOTE TO USERS

Control and Simulation Investigation of Wing Rock Phenomenon

Zeng Lian Liu

A Thesis

in

The Department

of

Mechanical and Industrial Engineering

Presented in Partial Fulfilment of the Requirements
for the Degree of Doctor of Philosophy at
Concordia University
Montreal, Quebec, Canada

December 2004

Your file Votre référence
ISBN: 0-494-04061-0
Our file Notre référence
ISBN: 0-494-04061-0

ABSTRACT

Control and Simulation Investigation of Wing Rock Phenomenon

Zeng Lian Liu, Ph. D.
Concordia University, 2004

Wing rock phenomenon is manifested by a limit cycle oscillation predominantly in roll about the body axis. This self-induced rolling oscillation is highly annoying to the pilot and poses serious limitation to the combat effectiveness. The maneuvering envelope of an aircraft exhibiting this behavior is also seriously restricted because the maximum angle of attack (AOA) is often limited by the onset of wing rock before the occurrence of stall. This thesis deals with the control and simulation investigation of wing rock phenomenon by the five new control schemes for the different assumptions of wing rock model.

First, a variable phase control scheme, based on the results of energy analysis of wing rock hysteresis, is developed for wing rock suppression. Its main advantage is small control power need. For the tracking control of wing rock at a fixed AOA, fuzzy PD control is then designed; however, if wing rock suffers from external disturbance, fuzzy PD control exhibits a big tracking error. To overcome this disadvantage, variable universe fuzzy PD control is proposed to achieve the precise tracking control. For the tracking control of wing rock with a time-varying AOA and uncertainties, the NDOFEL scheme, a nonlinear disturbance observer (NDO) combined with a feedback-error-learning (FEL) strategy, is proposed for a class of time-varying nonlinear systems with

unknown disturbances, where the nominal model of wing rock control is assumed available. The proposed NDOFEL not only extends the NDO into time-varying nonlinear systems but also improves the precision of tracking control. Finally, because aircraft at a high AOA operate in nonlinear flight regimes in which the dynamics are very complex, aircraft's wing rock model is usually unavailable. A reinforcement adaptive fuzzy control scheme is presented to guarantee the stability of the closed-loop system and the convergence of the tracking error.

The proposed control schemes emphasize stability, robustness, and simplicity such that they can be applied for on-line learning and real-time control. Numerical cases in each scheme are used to confirm the effectiveness and robustness of the proposed schemes.

I dedicate this thesis to *Junping, Yijun, and Eunice*

ACKNOWLEDGEMENTS

I would like to express my profound and sincere appreciation to my supervisors Dr. Chun-Yi Su and Dr. Jaroslav Svoboda for their constant encouragement and invaluable guidance and significant support throughout the course of this study.

I also would like to thank the members of my Ph. D qualifying examination committee, who have given me the encouragement and support through their constructive suggestions and advices.

I am indebted to my father, parents-in-law, brothers, and sisters for their constant encouragement and solid support.

Last, but not the least, I wish to express my thanks particularly to my wife Junping Liu, whose love, invaluable support, patience and understanding made the course of this work possible and successful, and also to my daughters Yijun and Eunice without whom my study and completion of this work would not have been possible.

TABLE OF CONTENTS

LIST OF FIGURES

Chapter 1

Introduction

1.1 Limit Cycle Oscillation

Limit cycle oscillation (LCO), as described in Reference [1], is a term that has come into widespread use since the mid-1970s to describe the aeroelastic response of certain aircraft and external store configurations that encounter sustained, periodic, but not catastrophically divergent motion in portions of the flight envelope. In practice, the term LCO ignores the origin issue and simply describes the nature of the motion associated with the phenomenon. Specifically, the amplitude of the motion is cyclic (repetitive in a given period of time) and oscillatory (the amplitude varies above and below a mean value). What this means is that LCO in its purest form is characterized by sinusoidal motion.

Dimitriadis and Cooper in Reference [2] explained the mechanism by which limit cycles are created. Around a stable limit cycle, only a certain amount of energy is drawn from the free stream; as a result, when a system undergoing such an LCO is displaced to a higher energy state, it cannot maintain its energy level and winds back on the limit cycle. If the system is at a lower energy state, it receives more energy than it is dissipated by the

damping and moves up to the limit cycle. On the limit cycle, the rate of energy input from the free steam is equal to the rate of energy dissipation, resulting in a stable periodic motion.

The stability of LCO is based on stability principles of nonlinear systems. If a system has a nonlinear stiffening term, in most occasions the amplitude of oscillation will grow until an LCO is reached. LCOs, though stable in the sense of Lyapunov, are not asymptotically stable. This means that although the final state is bounded, the system will not asymptotically approach its original equilibrium point as time grows. In addition, Patil *et al.* in Reference [3] pointed out that LCOs can be induced by certain disturbances, if it is sufficiently large, even when the given equilibrium state is stable. Basically, if the disturbances are not small, the response of LCO cannot be predicted by linear system theories.

Because of the nonlinearities involved, classical linear flutter analysis techniques fail to predict the onset of LCO. Although no instance of a structural failure has ever been reported, when an LCO has suddenly and rapidly grown in amplitude, it is unclear at what level the divergent behavior will have stopped, or if it will have stopped at all short of a structural failure. Especially for fighter aircraft, LCOs can be highly annoying to the pilot and may pose serious limitation to the combat effectiveness. Besides, Katz in Reference [4] explained the case of jet-engine airplanes with high swept wings. The angle of attack (AOA) of the airplanes must increase to obtain reasonable landing speeds. Under such high AOA landing conditions, both flight tests and experimental data have

indicated that lateral instabilities in the form of LCO may be presented. Therefore, the efficient control of LCO is a very important issue.

Most LCO investigations of aircraft are concerned with two aspects: aeroelastic systems and lateral flight dynamics. References [5-11] are some examples of LCO research in other engineering fields.

1.2 Aircraft's Limit Cycle Oscillations

1.2.1 LCO in Aeroelastic Systems

In aeroelastic systems, which study the interaction of structural, inertial, and aerodynamic forces, limit cycle behavior occurs in level flight and during elevated aircraft load factor maneuvers. Ko *et al.* in Reference [12] described this type of LCO. For a typical LCO, the amplitude is constant only in stabilized flight conditions. Once above the onset speed and accelerating to a new higher speed, the amplitude of the LCO grows. The motion appears to be diverging until the new target speed is reached. When the speed is again stabilized, the motion will become sinusoidal, but with bigger amplitude than it had at the earlier speed. Some engineers consider this phenomenon to be closely linked to classical *flutter* characterized by the loss of system damping due to the presence of unsteady aerodynamic loads.

Denegri in Reference [13] provided flight test results and a detailed description of the aircraft/store LCO phenomena. LCO flight test of a fighter aircraft with external stores

shows three distinct categories of response behavior as follows:

(a) Classical flutter behavior is characterized by the sudden onset of high-amplitude wing oscillations.

(b) Typical LCO is characterized by the gradual onset of sustained limited amplitude wing oscillations where the amplitude progressively increases with increasing Mach number and dynamic pressure.

(c) Nontypical LCO is characterized by the gradual onset of sustained limited amplitude wing oscillations where the amplitude does not progressively increase with increasing Mach number.

1.2.2 LCO in Lateral Flight Dynamics

Flight at a high AOA allows for enhanced maneuverability and increased lift during takeoff and landing. In this flight condition, the aerodynamics of aircraft is dominated by separated flow, vortex shedding, and possibly vortex breakdown. These unsteady aerodynamic effects at a high AOA generate LCO in roll, which in some case is coupled with yaw oscillation. This phenomenon is called as Dutch-roll LCO. However, this motion, as claimed in Reference [14], becomes more of a pure rolling motion as the AOA is increased. In flight tests, Ross in References [15-16] observed that the Dutch roll oscillation is stable at a low AOA and does not diverge completely at a large AOA, but exhibits a limit-cycle type motion with a constant amplitude in angle of bank of 30^0 or so. The researchers in References [17-18] analyzed the characteristics of this motion.

On the other hand, wing rock phenomenon, as defined in Reference [19], is manifested by

an LCO predominantly in roll about the body axis. The control of many aircraft at a high AOA is limited by wing rock phenomenon. High-speed civil transport and combat aircraft can fly in conditions where this self-induced oscillatory rolling motion is observed. Shue and Agarwal in Reference [20] asserted that such oscillations lead to a significant loss in lift and can cause a serious safety problem during maneuvers such as landing or takeoff. The maneuvering envelope of an aircraft exhibiting this behavior is also seriously restricted because the maximum incidence angle is often limited by the onset of wing rock before the occurrence of stall.

The researchers in References [21-26] investigated large-amplitude wing rock phenomena. With AOA increasing, normal wing-rock limit cycles build up gradually in amplitude, whereas large-amplitude wing rock results from a jump at a saddle-node bifurcation point of the periodic solutions. Ananthkrishnan and Sudhakar in Reference [21] explained that inertial and kinematical coupling terms are primarily responsible for the jump in limit cycle amplitude while the aerodynamic nonlinearities cause the onset of wing rock and restrict the unstable Dutch roll model to a limit cycle.

However, the mechanism that leads to these LCOs is not clear. Kurdila in Reference [27] claimed that, in part, this might be attributed to the difficulty in understanding the nature of the contributing nonlinear structural and nonlinear aerodynamic interactions that account for the LCO motion. From this point of view, Figure 1.1 is drawn to interpret the interaction of aircraft structure and aerodynamics to produce some LCOs in the following forms:

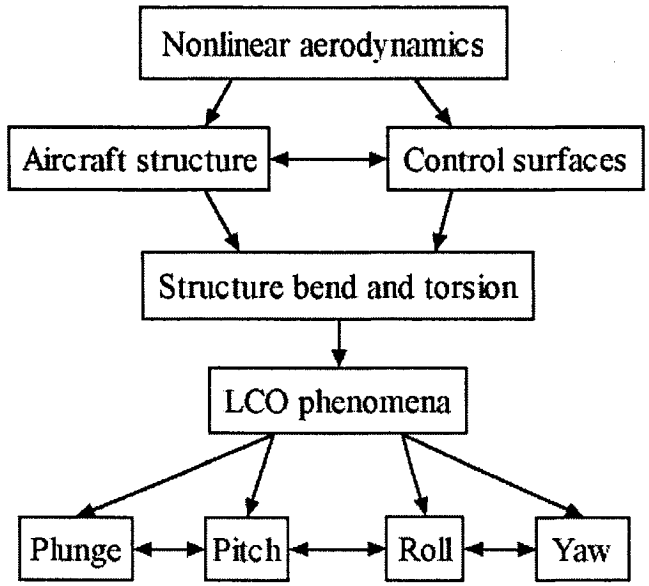

Figure 1.1 Interaction of aircraft structures and aerodynamics

(a) Pitch and plunge LCOs (in aeroelastic systems),

(b) Dutch-roll LCO (combining with roll and yaw motions), and

(c) Roll LCO (wing rock phenomenon).

In this thesis, we will focus on the control and simulation investigations of wing rock phenomenon. Of course, these investigations could also be applied in the other LCO controls of aircraft.

1.3 Wing Rock Phenomenon

Wing rock phenomena in the literature can be traced back to Ross's research paper in 1972. Ross in Reference [15] described this "nonlinear motion" experienced by the Handley Page 115 research airplane. Nelson and Andrew in Reference [28] reported that

wing rock phenomenon is not limited to a few aircraft; in fact, over 13 modern aircraft have been documented to exhibit this phenomenon. Levin and Katz in Reference [29] explained that the principal source of wing rock is the wing itself. To understand wing rock phenomenon, most researchers focus on the wing rock of free-to-roll delta wing models. It is interesting to note that only those delta wings whose leading-edge sweep is 75^0 or more to exhibit wing rock. Moreover, it is generally accepted that only thin, highly swept slender delta wings exhibit wing rock.

The wing rock phenomenon of a thin, sharp-edged 80^0 delta wing model has received considerable attention in the literature. At a high AOA, the 80^0 delta wing model loses roll damping. On receiving a disturbance, the model starts oscillating and its amplitude builds up rapidly, as shown in Figure 1.2. Even a small disturbance in the form of wind-tunnel turbulence or flow unsteadiness is usually sufficient to initial the rocking motion. Such wing rock in References [30-31] is often called a *self-induced wing rock.*

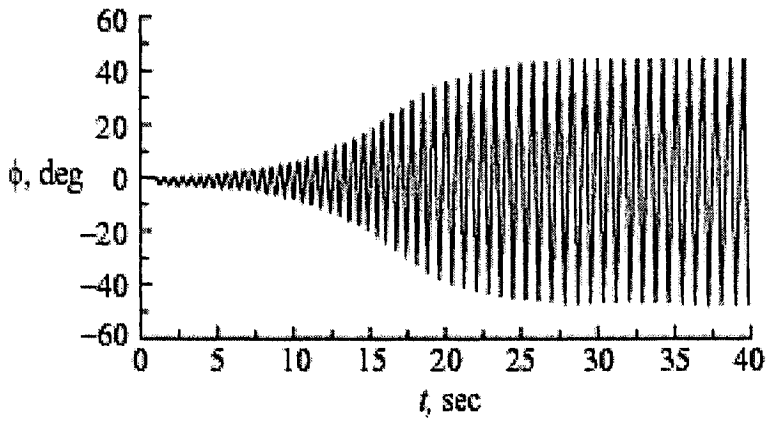

Figure 1.2 Free-to-roll test wing rock at AOA =30° [28]

However, aircraft configurations not having highly swept delta wings but featuring fuselages with long, slender forebodies, even when the wing is removed, are also known to exhibit wing rock. This type of wing rock in References [30-31] is called *forebody-induced wing rock.* It may also be noted that thin, sharp-edged rectangular wings of very low aspect ratio, usually less than 0.5, also exhibit wing rock, which is generated by the dynamic motion of the side edge vortices.

Figure 1.3 shows some wing tunnel test results on the 80^0 delta wing models in the literature. When $20^0 < AOA < 60^0$, the models exhibit wing rock, but the oscillation amplitude at the same AOA is different due to the different free-to-roll apparatus.

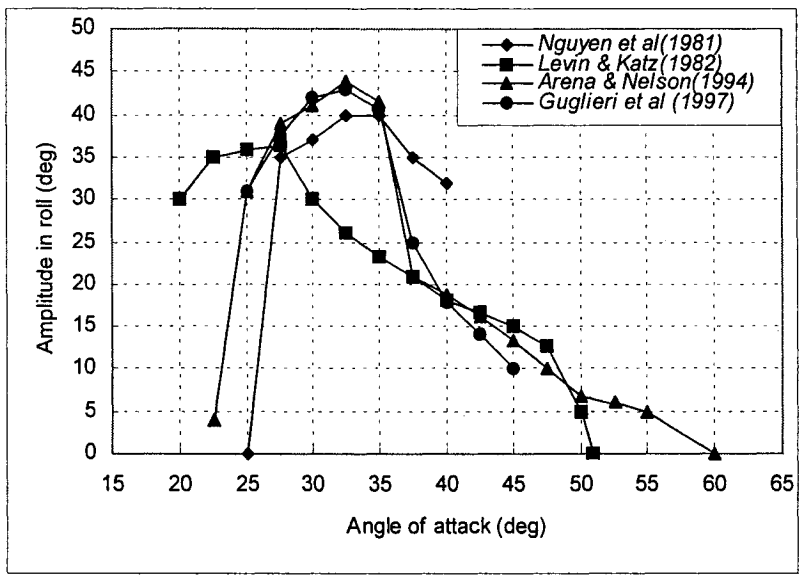

Figure1.3 Some wing-rock experimental results

In Figure 1.3, we have also observed some difference in the AOA of the onset of wing rock. Various researchers measure the AOA at which the onset of wing rock. The main

reason for these variations is believed to be the bearing friction in the free-to-roll apparatus. If the bearing friction is high, the wing rock starts at a higher AOA because a larger destabilizing aerodynamic moment is necessary to set the model rolling. *In fact, in free flight, it will exhibit wing rock at a much lower AOA than measured in the free-to-roll tests.* It is interesting to observe that the limit cycle amplitude is reached within a few oscillations. The maximum amplitude and the frequency of wing rock vary with the AOA.

Pamadi and Bandu in Reference [30] indicated that a loss of damping in roll at a high AOA makes a configuration susceptible to wing rock but does not necessarily generate a sustained wing rock. Some additional aerodynamic causes are necessary to generate a sustained wing rock motion. The various causes that have been identified so far are:

(a) Nonlinearities in lateral-directional aerodynamic characteristics,

(b) Aerodynamic hysteresis in the variation of rolling moment with sideslip/roll angle, and

(c) Nonlinear variation of roll damping such that negative damping (destabilizing) exists at low values of sideslip/roll angle and positive damping (stabilizing) at higher values of sideslip/roll angle.

1.4 Problem Definition

One of the most common dynamic phenomena experienced by slender wing aircrafts flying at a high AOA is the phenomenon known as wing rock. Wing rock phenomenon is a complicated motion that typically affects several degrees of freedom simultaneously.

However, as the name implies, the primary motion is an oscillation in roll. This rolling motion is a self-induced motion characterized by a limit cycle behavior

In general, wing rock phenomenon investigation is based on numerous experimental observations. The experiments demonstrate the role of the leading edge vortices in driving the motion. Katz in Reference [4] explained the experimental results that the rolling moment versus roll angle indicates a reversal of the hysteresis near the edges of the loop compared to its center, providing clues about where the motion is being driven and where the motion is being damped.

Wing rock mathematical modeling is based on the parameter identification of experimental data. The simplified geometries in free-to-roll tests exhibit stable limit cycles and correctly reproduce the dominant effect of primary wing vortices. Most researchers use the mathematical models of some LCOs with one-degree-of-freedom (one-DOF) to describe wing rock phenomenon.

As for wing rock control approaches, we may choose forebody blowing methods or nonlinear control algorithms. By comparison, nonlinear control algorithms obviously show high potential in inexact dynamic model and uncertain operating environments.

In this thesis, we will study the nonlinear control schemes of wing rock phenomenon that has the different model assumptions. These assumptions are:

(a) The mathematical model of wing rock phenomenon is known at different AOAs,

as many researchers have done numerical studies about wing rock suppression.

(b) The mathematical model is a known time-varying nonlinear system with AOA.

(c) The mathematical model is a known time-varying nonlinear system with unknown disturbances.

(d) The mathematical model is an uncertain nonlinear system with unknown disturbances; but we know its nominal model.

(e) Not only the mathematical model is an uncertain nonlinear system with unknown disturbances, but also its nominal model is unavailable because the analytical modeling of wing rock is very difficult to be obtained for real aircraft.

We are interested in the following two problems about wing-rock control without and with disturbances.

(a) *Suppressing control*: achieve the system output to be zero roll angle, $\phi(t) = 0$, and zero roll rate, $\dot{\phi}(t) = 0$, to suppress wing rock.

(b) *Tracking control*: achieve the system output to follow a desired trajectory.

1.5 Literature Review

Wing-rock control methods reported in the literature can be classified into two groups: forebody blowing methods and nonlinear control schemes.

1.5.1 Forebody Blowing Methods

Wing rock phenomenon is caused by the wing vortices, the forebody vortices, or an

interaction between these two vortices. The loss of damping in roll at a high AOA initiates the wing rock, and some form of vortex-asymmetry-switching mechanism sustains it as an LCO. Therefore, the key to suppressing wing rock by passive aerodynamic methods is to manipulate the vortices so that the vortex-asymmetry-switching mechanism is suppressed and the vortices are forced to assume a symmetric disposition. The researches in References [32-37] employed this technique to achieve wing rock suppression.

1.5.2 Nonlinear Control Schemes

Generally, if physical systems are inherently nonlinear, these nonliearities lead to the systems not described by linear representations. Moreover, nonlinear control laws, as claimed in Reference [38], can improve control precision and widen stability boundaries when flight must be conducted at high angles or high angular rates and when the control actuator limits must be challenged. Various nonlinear control schemes in the literature have been tried to control wing rock. Some of the prominent approaches are: 1) adaptive control, 2) neural networks, 3) optimal control, 4) fuzzy logic control, 5) robust control, 6) bifurcation analysis, and 7) sliding mode control. Each of these approaches is briefly described below.

1) Adaptive Control

An adaptive control system, as defined in Reference [39], is a feedback control system intelligent enough to adjust its characteristics in a changing environment so as to operate in an optimal manner according to some specified criteria. To date, most adaptive flight

control designs have addressed the issue of the uncertain aerodynamic effects within the context of linear control. Calise and Rysdyk in Reference [40] assured them that aircraft of the future will benefit from an adaptive control system based on the full nonlinear dynamics of the vehicle while avoiding prohibitively complex gain scheduling. Therefore, there is presently a strong interest in the development of adaptive control methods that are applicable to flight control problems where the aircraft characteristics are poorly understood or are rapidly changing.

Monahemi and Krstic in Reference [41] used the tuning function method of adaptive backstepping to develop a wing-rock regulator. They have claimed precise tracking and maximum performance can be achieved if there is sufficient rolling moment derivative. Araujo and Singh in Reference [19] presented the variable structure model reference adaptive control of wing-rock motion, using only input and output signals. Gazi and Passino in Reference [42] proposed direct adaptive control scheme and dynamic structure fuzzy systems for wing-rock control problem. Ordonez and Passino in Reference [43] also developed a direct adaptive control method with a time-varying structure using a Lyapunov approach to construct the stability proof.

2) Neural Networks

Neural network (NN) control has great potential since artificial NNs are built on a firm mathematical foundation that includes versatile and well-understood mathematical tools. It is suitable for nonlinear dynamic systems and offers powerful control mechanisms in conjunction with NN-based system identification techniques. Furthermore, the authors in

References [44-45] showed that NN function as highly nonlinear adaptive control elements offers distinct advantages over more conventional linear parameter adaptive controllers in achieving desired performance.

Singh *et al.* in Reference [46] presented conventional adaptive and neural adaptive control methods for wing rock control. A radial basis function network is used for synthesizing the controller and an adaptation law is derived for adjusting the parameters of the network. Joshi *et al.* in Reference [47] also proposed a single neuron control scheme for wing rock suppression. They have demonstrated the robustness by suppressing wing rock not only in the software simulation but also in the real-time experiments conducted in a wind tunnel on an 80^0 swept back wing.

3) Optimal Control

Optimal control, as defined in Reference [48], tries to find a feasible control such that the system starting from the given initial condition transfers its state to the objective set to minimize a performance index.

Luo and Lan in Reference [49] used Beecham-Titchener's averaging technique to derive an optimal control input for wing-rock suppression. Since the control input is a function of time, an approximate state-variable feedback control input is obtained using the least-squares method. Rogers in Reference [50] presented an algorithm for determining the optimal constant coefficients directly and applied to parameter optimal control of wing rock. Besides, Shue *et al.* in Reference [51] proposed nonlinear optimal feedback control

using the Hamilton-Jacobi-Bellman (HJB) equation. The control of wing rock is asymptotically stable in the large, as both the closed-loop Lyapunov function and performance index are positive definite. Recently, Tewari in Reference [52] presented an optimal control scheme and considered self-induced rolling motion, yawing motion, and an aileron actuator model.

4) Fuzzy Logic Control

Fuzzy logic control (FLC) uses fuzzy set theory. Control decisions can be generated based on the fuzzy sets and functions with rules. The authors in References [53-54] indicated that fuzzy control has attracted increasing attention, essentially because it can provide an effective solution to the control of plants that are complex, uncertain, ill-defined, and have available qualitative knowledge from domain experts for their controllers design. This ability of FLC's makes them suitable for control applications to plants like aircraft that have nonlinear dynamics and operate in uncertain environments

Tarn and Hsu in Reference [55] developed a rule-based fuzzy controller for wing-rock suppression. They have employed the fuzzy sets of three terms for the fuzzification of the control variables and presented numerical results at two AOAs to demonstrate the robustness of the fuzzy controller in small initial conditions. Sreenatha *et al.* in Reference [56] presented the design and implementation of FLC for wing-rock suppression. The forty-nine fuzzy rules are tried out with the delta wing model in the wind tunnel. The numerical and experimental results indicate the effectiveness and robustness of the FLC. Lim and Sreenatha in Reference [57] analyzed the stability and robustness of FLC using

Liapunov's theorem. In addition, Nho and Agarwal in Reference [58] presented a fuzzy model-based predictive control strategy. The control action can be obtained by an error-minimized optimization procedure. The adaptive network-based fuzzy inference is employed as an adaptive predictor for the future state values.

5) Robust Control

Controlled system robustness, as described in References [59-60], is the ability to maintain satisfactory performance in the presence of parametric or structural uncertainties in either the aircraft or its control system. All controlled systems must possess some degree of robustness against operational parameter variations. The design of a robust control system is typically based on the worst case so that the system usually does not work at optimal status in the sense of control performance under normal circumstances. Once the controller is designed, the parameters do not change and control performance is guaranteed.

Crassidis in Reference [61] presented the robust control approach of nonlinear systems, which employs an optimal real-time nonlinear estimator to determine model-error corrections to the control input. This synthesis method is used in conjunction with a variable structure controller to suppress wing-rock motion. Stalford in Reference [62] investigated the control of wing rock using the robust control theory for linear uncertain systems. Shue and Agarwal in Reference [20] also proposed a nonlinear H_∞ robust method to control wing rock.

6) Bifurcation Analysis

The dynamic characteristics of complex systems can be investigated through the solution of their governing nonlinear differential equations. This analysis is performed by calculating all steady states of the differential equations. The stability of the dynamic system at each steady-state condition is determined by the local stability of the linearized system around the steady state. A system is defined to be locally stable if the real parts of all the linearized eigenvalues are negative. Stability changes are characterized by a crossing of the imaginary axis of one or more eigenvalues between successive steady states. These stability changes result in qualitative changes in the system dynamics, which is called *bifurcation* [63]. A particularly important example is the Hopf bifurcation that occurs when a complex-conjugate pair of eigenvalues crosses the imaginary axis. Thus a Hopf bifurcation indicates a point at which LCO behavior starts.

Liebst in Reference [64] used bifurcation theory and root-locus techniques to analyze a F-15 model and found that an effective control scheme to delay the onset of wing rock is to combine roll rate and sideslip fixed gain feedback. Goman and Khramtsovsky in Reference [65] performed the design of a global stability augmentation system for severe wing-rock motion by using bifurcation diagrams. The nonlinear control law is derived, considering both local stability characteristics and domains of attraction.

7) Sliding Model Control

The technique of sliding mode control (SMC) is a natural extension of the concept of variable structure systems (VSS). The VSS philosophy, as discussed in References [66-

68], can be considered as one in which the system trajectories in the state-space are forced to slide along a switching manifold by the application of discontinuous control. The system trajectory is maintained on the manifold and is rendered insensitive to uncertainties in the process. This is clearly of use for systems in which the model is poorly defined or time varying.

Based on variable structure control (VSC) theory and the direct method of Lyapunov, Jafarov and Tasaltin in Reference [69] designed robust flight laws for a simplified aircraft model F-18. They have applied the derived control laws for the tracking and positioning of longitudinal dynamics of the F-18 aircraft model. In addition, Singh *et al.* in Reference [70] designed a flight control law based on VSC for a simplified F-14 aircraft model. They have derived the control law for the control roll angle, lateral velocity, and yaw rate in spite of aerodynamic parameter uncertainty.

Fernand in Reference [71] presented discrete sliding mode control (DSMC) for nonlinear, autonomous, single input, one-DOF plants modeled by continuous or discrete equations. The DSMC system of wing rock can remain asymptotically stable at a sampling frequency of five times the open-loop fundamental frequency.

1.6 Motivation

The research of limit cycle problems dates back to the early investigations of *Poincare'* in the 1880's. Unfortunately, a very few results have been found even though it was restricted within the analysis to small-amplitude limit cycle behavior. On the other hand,

in many engineering fields, see References [5-11], the limit-cycle phenomenon is usually observed. These phenomena like friction usually cause the loss or degradation of the system function. Therefore, the limit-cycle phenomenon research is an important and challenging issue.

In aerospace industry, most modern fighters are required to have high performance capabilities for enhanced air superiority. Such requirements necessitate aircraft at a high AOA to operate in nonlinear flight regimes in which the dynamics are very complex. For example, Ericsson in Reference [72] summarized these challenges into three critical issues.

(a) Cause and effect of asymmetric forebody flow separation with associated vortices: the coupling between vehicle motion and flow separation is the cause of experimentally observed forebody-induced nose-slice and coning motions, as well as of the associated vortex-induced *wing rock phenomenon.*

(b) Effect of asymmetry and breakdown of leading edge vortices: for slender delta wings ($\Lambda > 75^0$) vortex asymmetry is the flow mechanism causing the observed large amplitudes of slender wing rock, and vortex breakdown is the flow mechanism setting the upper limit of the wing rock amplitude.

(c) Effect of vehicle motion on dynamic airfoil stall: the observed large difference in dynamic stall characteristics between pitching and plunging airfoil oscillations is caused by the opposite moving wall effects.

The challenge extends the present knowledge to include the coupling between novel

aerodynamic controls and the vehicle dynamics of agile aircraft operating at a high AOA. Ericsson in Reference [73] also stressed the increased interest in improving the safety and handling qualities of highly maneuverable fighter airplanes and of very slender space-plane configurations results in a focused effort to study *wing rock* phenomena.

Ko *et al.* in Reference [12] pointed out that many researchers have examined the nonlinearities inherent in structural models. However, efforts to examine nonlinear aeroelasticity and active control strategies are limited. Surprisingly, less progress has been made in active control methodologies for these inherently nonlinear dynamic phenomena. Even in the case where it is known that LCOs may be observed in real flight envelope, and active control methodologies are employed to attenuate response, there are very few analytical results that characterize the stability of the closed-loop system. Owing to the highly nonlinear nature of the flight dynamics at a high AOA, wing rock phenomenon is not well understood. No satisfactory method has been developed by the aircraft industry to solve this problem.

Additionally, note that many wing rock control schemes in the literature used a simple 80^0 plate plane delta wing model with small disturbance or without disturbance. My efforts try to expand this model into a real aircraft model by using different assumptions. Meanwhile, I will propose some new suppressing control and tracking control schemes. In this thesis, the following five issues have been focused on:

(a) To understand wing-rock phenomenon, most researchers investigate the characteristics of wing-rock aerodynamics such as vortex flow, vortex breakdown, and locations of vortex breakdown. But, in this thesis we study the

phase plane and energy mechanism of wing rock phenomenon, and then find a relationship between the rate of wing rock energy change and wing rock hysteresis loops.

(b) Based on above results of energy analysis, we try to use a phase control algorithm to suppress wing rock phenomenon in such a way as to force the rate of energy change less than zero, that is, $dE/dt<0$. Since the phase control algorithm of open-loop linear systems is limited, we seek the variable phase control method of closed-loop nonlinear systems to remove the effect of wing rock hysteresis such that wing rock phenomenon can be suppressed.

(c) To control wing rock phenomenon, we first choose fuzzy PD control method to achieve a satisfactory performance if external disturbance is ignored. If the disturbance is considered, then its performance is limited.

(d) If aircraft fly in a moderate or high AOA environment, the real wing rock model should include a time-varying part, non-modeled dynamics, and external disturbance. These factors offer a challenge to nonlinear control theory. Variable universe fuzzy PD control is proposed to achieve the tracking control of wing rock with unknown disturbance. Furthermore, a new learning control scheme, NDOFEL, is proposed to control a class of time-varying nonlinear systems with unknown disturbances, but the nominal model is available.

(e) Note that the wing rock model is based on the parameter identifications of the free-to-roll test data of a simple 80^0 flat-plate delta wing. In fact, the test results of Reference [74] for four military aircraft show that aircraft's wing rock at a high AOA is a very complex, uncertain, and time-varying nonlinear system. This

implies that the wing rock model of real aircraft and its nominal model are unavailable. For this case, a reinforcement adaptive fuzzy control scheme is proposed to guarantee the robustness and stability of the control system.

The control schemes to be proposed should have the following features:

(a) Have stable online learning ability;

(b) Quickly track the desired trajectory;

(c) Maintain high control performance in the presence of disturbances and uncertainties such as parameter variations and non-modeled dynamics;

(d) Guarantee stability of the control system by Lyapunov theorem;

(e) Use simple tuning algorithms for real-time control; and,

(f) Alleviate the chattering problem of sliding-mode control.

Besides, all control algorithms should be simulated by Matlab/Simulink software of Math Works Inc. to verify the effectiveness of the proposed control schemes.

1.7 Contributions of the Thesis

Over the past thirty years, there has been a continuously increasing interest in the investigation of wing rock phenomenon. Even though a number of extensive investigations in the source, behavior, fluid mechanism, modeling, prediction, suppression, and control strategy have been carried out, there is not a valid control solution in aircraft industry.

In this thesis, further research is made on both the mechanism and the control schemes of wing rock phenomenon. The following contributions have been achieved:

(a) Presented a phase plane analysis of wing rock phenomenon and gave numerical simulation results.

(b) Proposed an energy analysis method of wing rock hysteresis and established a relationship between the rate of energy change of wing rock phenomenon and the wing rock hysteresis.

(c) Proposed a variable phase control scheme of wing rock phenomenon and extended the phase control of open-loop linear systems into a variable phase control of closed-loop nonlinear systems.

(d) Proposed a fuzzy PD control scheme with four fuzzy rules for wing rock suppression.

(e) Proposed a new variable universe fuzzy PD control scheme for wing rock tracking control with unknown disturbance.

(f) Proposed a new learning control scheme, NDOFEL, for a class of time-varying nonlinear systems tracking control with unknown disturbances. The proposed NDOFEL not only extends nonlinear disturbance observer into time-varying nonlinear systems but also improves the precision of tracking control.

(g) Proposed a new reinforcement adaptive fuzzy control scheme if aircraft's wing rock nominal model is unavailable. The proposed algorithm is derived by Lyapunov theorem to ensure the stability of the closed-loop system and the convergence of the tracking error.

Part I

Wing Rock Phenomenon Analysis and Variable Phase Control

The objectives of Part I are to present wing rock models, to analyze the phase plane of wing rock phenomenon, and then to develop a variable phase control scheme to suppress wing rock with hysteresis.

1. Wing Rock Models

In order to suppress wing rock phenomenon, the mathematical model of wing rock should express the main behavior and nature of wing rock phenomenon. Various researchers in References [75-89], based on the test investigations of an 80^0 slender delta wing in References [77, 79-80, 82, 84-87], have proposed the one-degree-of freedom (one-DOF) models. These models are obtained by using a parameter identification approach of experimental data. Among these models, the analytical model of wing rock phenomenon proposed by Guglieri and Quagliotti in References [88-89] provides more information at different AOAs and with different Reynolds numbers than other models do.

2. Phase Plane Analysis of Wing Rock Phenomenon

As mentioned above, the analytical model of wing rock phenomenon is a one-DOF nonlinear differential equation. To understand and analyze this phenomenon, we need to determine the properties of the solution of the nonlinear differential equation. Phase plane analysis is an effective tool because the phase-portrait is the aggregate of all trajectories and therefore represents all possible solutions. Through a study of singularities in the phase plane, we have considerable insight into the qualitative aspect of the solution. A graphical representation of the location of the singularities and the types of solution curves near them present a picture in compact form of all the solutions that may exist. It shows what kind of changes may occur as the variables in the system take on all possible values, both large and small.

The phase plane analysis results of wing rock phenomenon have shown that wing rock is a typical nonlinear system with a soft self-excitation. This means that small-amplitude initial conditions lead to motions that grow to the stable limit cycle and large-amplitude initial conditions lead to motions that decay to the limit cycle. The further analysis shows that wing rock phenomenon on the entire phase plane exhibits three equilibrium points: an unstable focus at the origin and two saddle points at nonzero equilibrium points. Based on the Lyapunov stability theory, we conclude that the wing-rock limit cycle is stable but not asymptotically stable,

3. Hysteresis Mechanism of Wing Rock Phenomenon

The most useful and general approach for studying the stability of nonlinear systems is

Lyapunov's theory. Using Lyapunov's direct method, we analyze the relationship of the energy variation and hysteresis of wing rock phenomenon. The results show that within the center loop of hysteresis, the mechanical energy is increasing; outside the center loop, the energy is decreasing; on the boundary between the center loop and the two outer loops, the energy is constant. Thus, the exchange of energy during one cycle is equal to zero. This is the primary explanation of wing rock phenomenon.

4. Variable Phase Control

The hysteresis analysis of wing rock phenomenon provides clues about where the phenomenon is being driven and where the phenomenon is being damped. Based on the hysteresis mechanism of driving wing rock phenomenon, a variable phase control scheme has been proposed to compensate wing rock hysteresis so as to suppress wing rock phenomenon.

It should be noted that the phase control method focuses on the phase shift or compensation of the output signal while ignoring the magnitude compensation of the signal. To suppress wing rock phenomenon with nonlinear nature, we have proposed the variable phase control scheme of wing rock phenomenon not only to keep the benefits of the phase control but also to compensate the magnitude distortion.

Chapter 2

Wing Rock Models

In this chapter, we introduce one-degree-of-freedom (one-DOF) wing rock models in the literature, and then numerically simulate the wing rock behavior, which is studied and controlled in this thesis. This chapter is organized as follows: In Section 2.1, we recall one-DOF analytical models of wing rock phenomenon. To exhibit the wing rock behavior, we provide some numerical simulation results of wing rock models in Section 2.2. Section 2.3 summarizes this chapter.

2.1. Wing Rock Models

To describe the motion of an airplane, it is necessary to define a suitable coordinate system for formulation of the equations of motion. Figure 2.1 shows a body axes coordinate system for the aircraft with delta wing.

It is necessary to understand that at a high AOA the roll motion about the body axis reduces the effective AOA and builds up the sideslip as given by the following equations

$$\alpha = \tan^{-1}(\tan\sigma\cos\phi)$$

$$\beta = \sin^{-1}(\sin\sigma \sin\phi)$$

where $\alpha = AOA$, σ is the angle between the x-body (roll) axis and the vector V, and ϕ is the roll angle about the x-body axis, as shown in Figure 2.1.

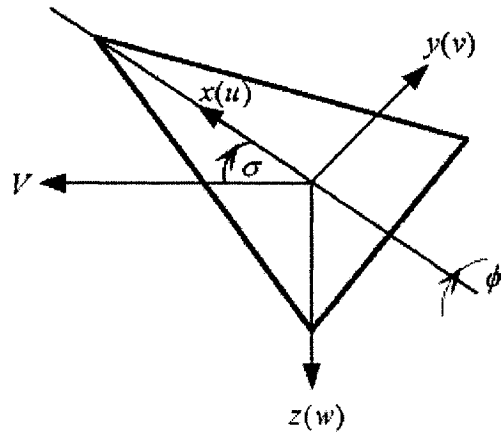

Figure 2.1 Body axes coordinate system for delta wing

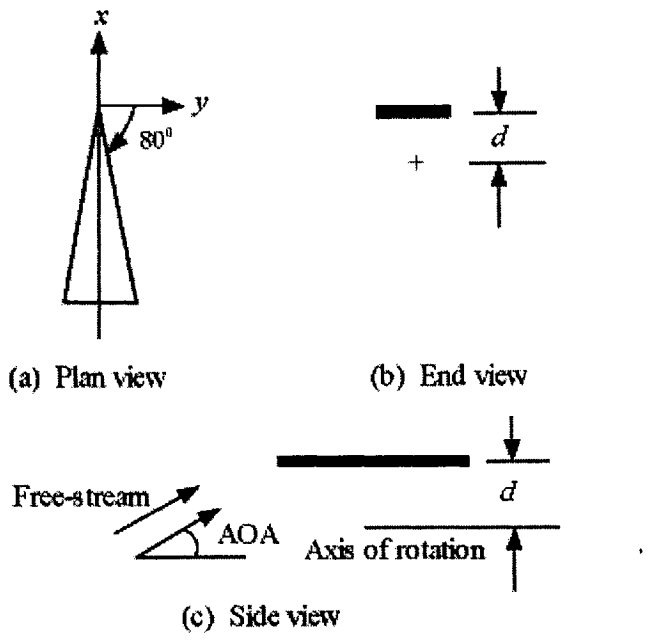

Figure 2.2 Schematic representation of a delta wing on a free-to-roll sting [80]

If $\phi = 0$ and $\alpha = \sigma$, then $\beta = 0$; if $\phi = 90^0$ and $\alpha = 0$, then $\beta = \sigma$. Thus, at extreme roll angles, all AOAs get converted to sideslip. This is a relation between angle of attack (AOA), sideslip, and roll angle in reference [90].

In the literature, the modeling of wing rock phenomenon is normally conducted based on 80^0 swept delta wing models in the free-to-roll tests. For example, Figure 2.2 shows a wing model, a uniform, plat, and thin wing, supported on a free-to-roll sting, which is used in the free-to-roll test of Reference [80].

The modeling of wing rock in Reference [80] is based on the following basic equation:

$$\ddot{\phi} = \frac{\rho U_\infty^2 Sb}{2I_{xx}} C_l + D\dot{\phi} \tag{2.1}$$

where $\phi(t)$ is the roll angle, ρ is the density of the air, U_∞ is the speed of the freestream, S is the plan form area, b is the chord, C_l is the roll-moment coefficient, I_{xx} is the mass moment of inertia of the wing around the midspan axis, D is the constant.

Mathematically, the phase plane representation of wing rock motion shows that wing rock phenomenon is dominated by nonlinear damping and a relationship established with one-DOF analytical models. Moreover, the analytical models are verified by using a parameter identification approach of experimental data. The main models in the literature are summarized in Figure 2.3. The major difference among the models is in the assumed form of C_l.

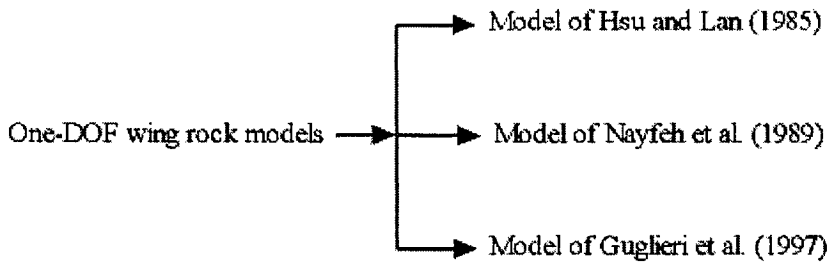

Figure 2.3 Analytical models of wing rock

1) Model of Hsu and Lan

Hsu and Lan in Reference [78] proposed the following model

$$\ddot{\phi} = L_0 + \sin\alpha\, L_\beta \phi + L_{p0}\dot{\phi} + \sin\alpha\, L_{p\beta}|\phi|\dot{\phi} + L_{pp}|\dot{\phi}|\dot{\phi} \tag{2.2}$$

where $\phi(t)$ is a roll angle, $\alpha = AOA$, L_0, L_β, L_{p0}, $L_{p\beta}$, and L_{pp} are constants. They have taken L_0 equal to zero and have not provided the values of other constants.

Following the model of Hsu and Lan, we write the rolling moment around the midspan chord as

$$C_l = a_1\phi + a_2\dot{\phi} + a_3|\phi|\dot{\phi} + a_4|\dot{\phi}|\dot{\phi} \tag{2.3}$$

Substituting Equation (2.3) into Equation (2.1), and rearranging the result, we obtain

$$\ddot{\phi} + \omega^2\phi = \mu\dot{\phi} + b_1|\phi|\dot{\phi} + b_2|\dot{\phi}|\dot{\phi} \tag{2.4}$$

where $\omega^2 = -Ca_1 = \sin\alpha\, L_\beta$, $\mu = Ca_2 - D = L_{p0} - D$, $D = 0.001$, $b_1 = Ca_3 = \sin\alpha L_{p\beta}$, $b_2 = Ca_4 = L_{pp}$, and $C = \rho U_\infty^2 Sb/I_{xx} = 0.354$.

However, the model of Hsu and Lan cannot predict more than one equilibrium point and

roll divergence. The addition of a cubic term to the moment expression in Equation 2.3 leads to additional equilibrium points and to the prediction of roll divergence. We call this as the modified model of Hsu and Lan.

$$C_l = a_1\phi + a_2\dot{\phi} + a_3|\phi|\dot{\phi} + a_4|\dot{\phi}|\dot{\phi} + a_5\phi^3 \tag{2.5}$$

Substituting Equation (2.5) into Equation (2.1) leads to

$$\ddot{\phi} + \omega^2\phi = \mu\dot{\phi} + b_1|\phi|\dot{\phi} + b_2|\dot{\phi}|\dot{\phi} + b_3\phi^3 \tag{2.6}$$

where $b_3 = Ca_5$ and other parameters remain the same in Equation (2.4).

2) Model of Nayfeh, Elzebda, And Mook

Nayfeh *et al.* in Reference [80], instead of expressing the rolling moment coefficient in Equation (2.3), used the following form

$$C_l = a_1\phi + a_2\dot{\phi} + a_3\phi^3 + a_4\phi^2\dot{\phi} + a_5\dot{\phi}^2\phi \tag{2.7}$$

which leads to a governing equation of the form

$$\ddot{\phi} + \omega^2\phi = \mu\dot{\phi} + b_1\phi^2\dot{\phi} + b_2\phi\dot{\phi}^2 + b_3\phi^3 \tag{2.8}$$

The values of the coefficients a_i in Equations (2.4) and (2.6) for different AOAs are shown in Table 2.1.

Table 2.1 Coefficients for wing rock models

AOA	a_1	a_2	a_3	a_4	a_5
21.5^0	-0.04207	0.01456	-0.18583	0.24234	0.04714
22.5^0	-0.04681	0.01966	-0.22691	0.59065	0.05671
25^0	-0.05686	0.03254	-0.3597	1.4681	0.07334

3) Model of Guglieri And Ouagliotti

Guglieri and Quagliotti in References [88-89] also developed an analytical nonlinear model of wing rock, based on parameter identification of experimental data. Figure 2.4 shows the experimental setup.

The free-to-roll experiments were performed on a delta wing for AOA from 21^0 to 45^0, V from 15 m/s to 40 m/s, Reynolds number from 486000 to 1290000. The model was an 80^0 delta wing with sharp leading and trailing edges, made in aluminum alloy. The dimensions are root chord c = 479mm, span b = 169mm, and thickness 12mm. The wing longitudinal body axis and the bearings axis coincide.

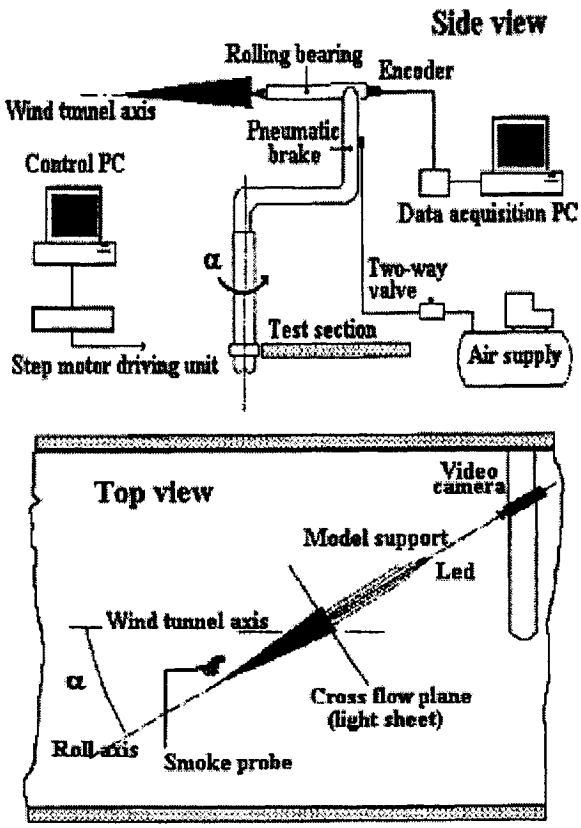

Figure 2.4 The experimental setup [89]

The model was connected to a horizontal shaft supported by rolling bearings. To minimize the friction of the angular transducer, an optical encoder, linked with the rotating shaft using an elastic joint without backlash, measured the motion of the wing. The digital signals generated by the encoder, which identify the sign, the increment and the zero crossing of $\phi(t)$, were conditioned by an electronic device consisting of an incremental counter and a 12 bit digital/analog converter.

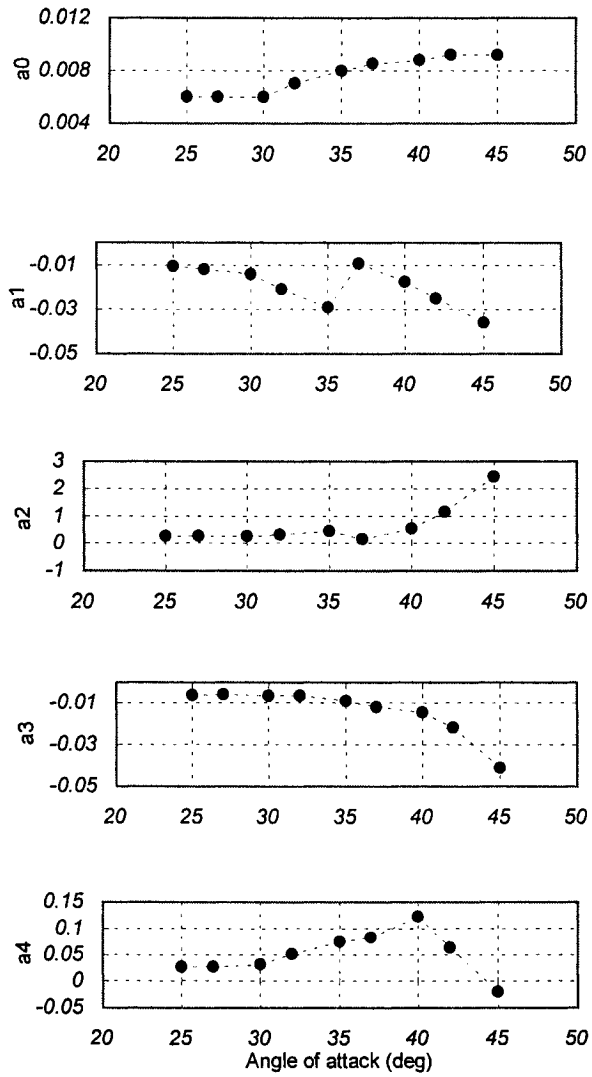

Figure 2.5 The coefficients a_i in Equation (2.9)

The differential equation describing wing rock in References [88-89] is given by

$$\ddot{\phi} + a_0\phi + a_1\dot{\phi} + a_2|\dot{\phi}|\dot{\phi} + a_3\phi^3 + a_4\phi^2\dot{\phi} = 0 \tag{2.9}$$

where a_i (i=0, 1, 2, 3, 4) are the parameters relative to free-to-roll experiment conditions. A typical set of coefficients a_i at Reynolds number =636000 is illustrated in Figure 2.5.

2.2. Simulations of Wing Rock Model

2.2.1 Fixed AOAs

Figure 2.6 illustrates the behavior of typical wing rock at AOA =32.5^0. Although given initial condition is very small, $\phi(0) = 0.1^0$ and $\dot{\phi}(0) = 0$, uncontrolled wing rock motion can still develop into LCOs with time. This implies that a very small disturbance is enough to cause wing rock motion. Similarly, Figure 2.7 shows the simulation results at the other fixed AOAs, that is, AOA =25^0, 27.5^0, 30^0, 35^0, 37.5^0, 40^0, 42.5^0, and 45^0, respectively, at the initial condition $\phi(0) = 1^0$ and $\dot{\phi}(0) = 0$.

2.2.2 Time-Varying AOAs

To structure a time-varying wing-rock model, we use a cubic interpolation functions to pass a smooth curve plotted in Figure 2.5 with AOA, which is a piecewise constant model with interpolation per 0.5^0. Figure 2.8 shows the numerical simulation results of the model with time-varying AOAs from 25^0 to 45^0 or with time from t=0 to t=2000 time steps at the initial condition $\phi(0) = 31^0$ and $\dot{\phi}(0) = 0$.

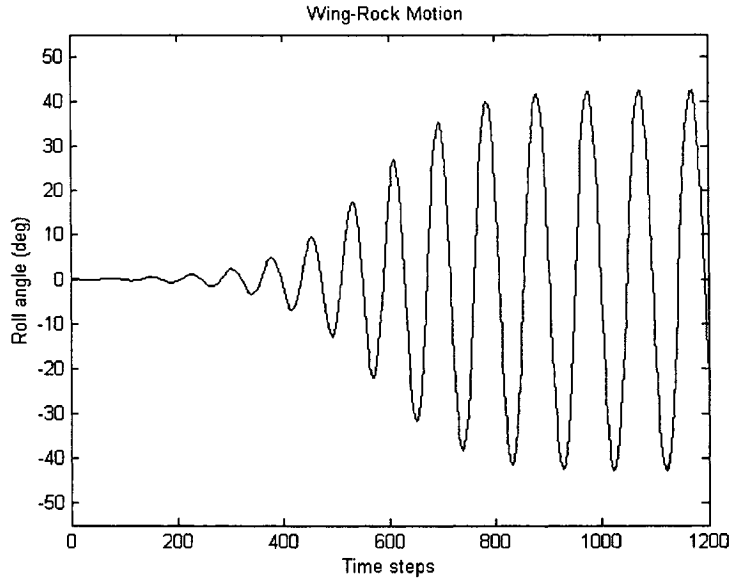

(a) Wing-rock time history

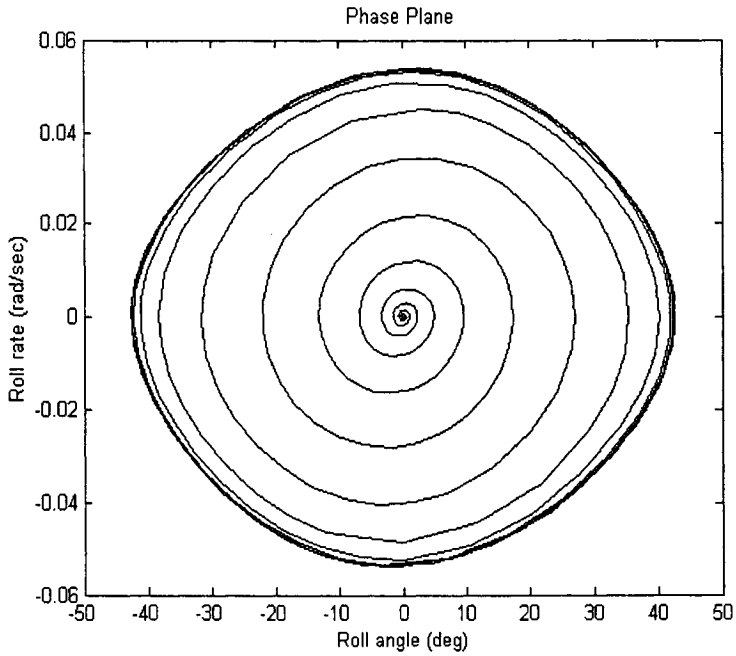

(b) Phase Plane

Figure 2.6 Wing-rock behavior at AOA=32.5^0

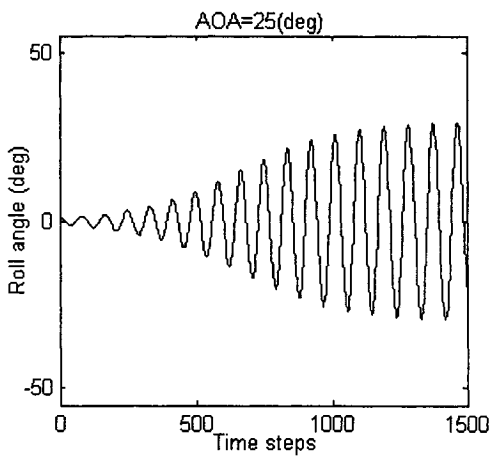
AOA=25(deg)
Roll angle (deg)
50
0
-50
0
500
1000
1500
Time steps

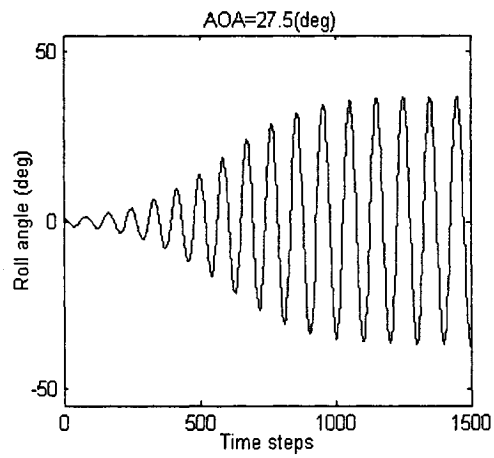
AOA=27.5(deg)
Roll angle (deg)
50
0
-50
0
500
1000
1500
Time steps

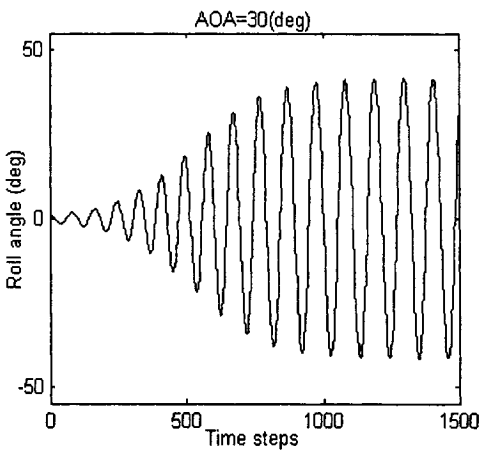
AOA=30(deg)
Roll angle (deg)
50
0
-50
0
500
1000
1500
Time steps

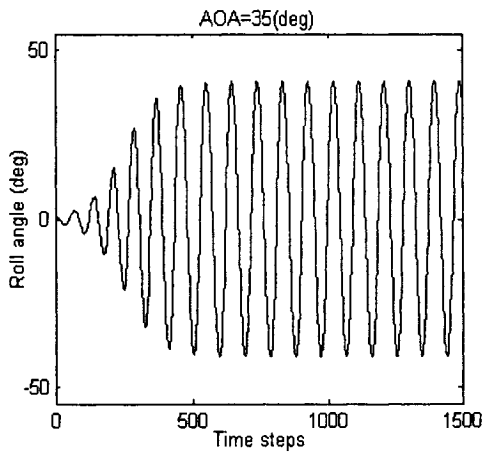
AOA=35(deg)
Roll angle (deg)
50
0
-50
0
500
1000
1500
Time steps

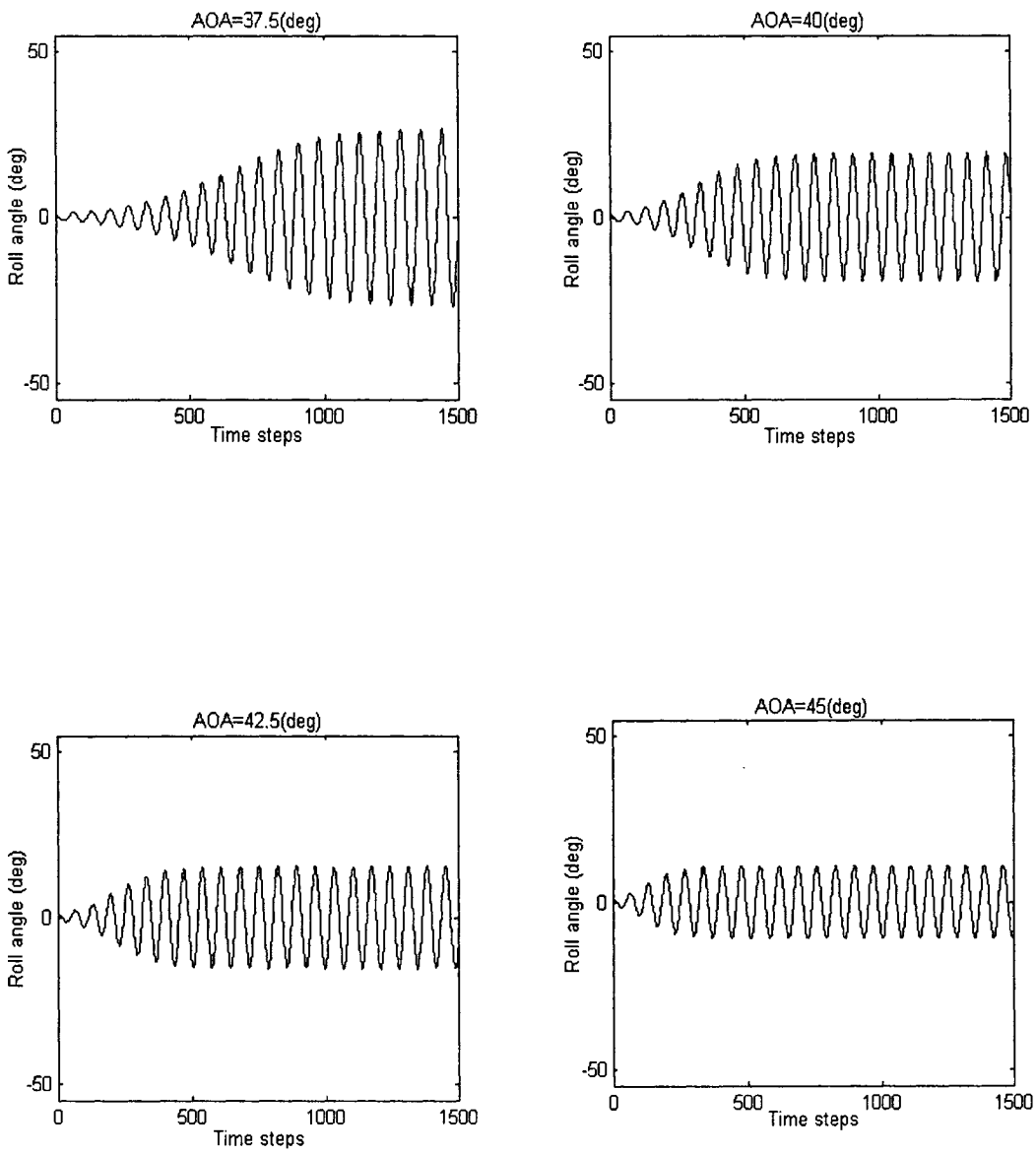

Figure 2.7 Wing-rock behavior at the other fixed AOAs

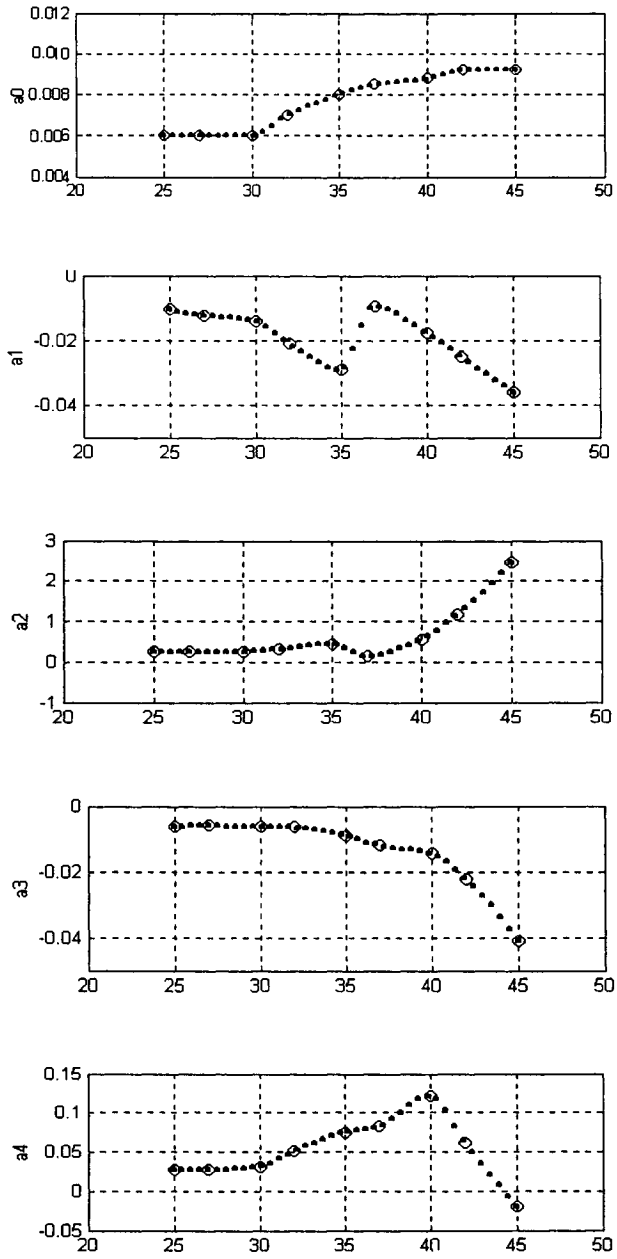

Figure 2.8 Coefficients of the time-varying wing-rock model

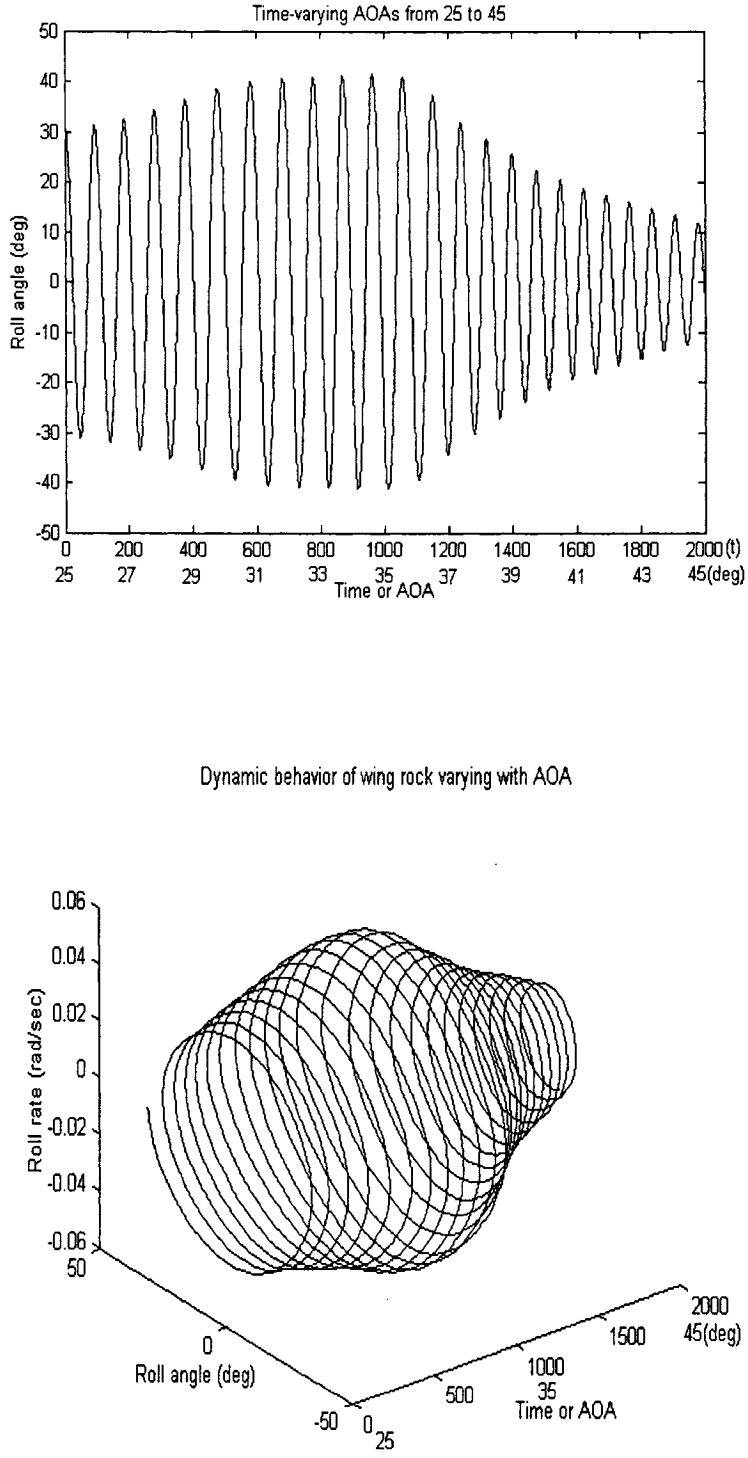

Figure 2.9 Time-varying wing-rock behavior

2.3. Summary

In this chapter, we have introduced the one-DOF wing rock models in the literature and then numerically simulated the wing rock behavior at fixed AOAs and with time-varying AOAs.

Chapter 3

Limit Cycle Analysis of Wing Rock Phenomenon

In this chapter, we will analyze the limit cycle characteristics of wing rock phenomenon. This chapter is organized as follows: We introduce the geometric method of obtaining general information about the behavior of a nonlinear system in Section 3.1 and the limit cycle analysis of the nonlinear system in Section 3.2. In Sections 3.3, we present the phase plane analysis of wing rock phenomenon and the corresponding graphic results. Section 3.4 summarizes this chapter.

3.1 Geometric Method

In this section, we briefly introduce a geometric method, as described in Reference [91].

1) Basic Notions

Because exact solutions of nonlinear equations of motion are generally unobtainable, the geometric method will be useful to study the fundamental qualitative characteristics of motion. The basic idea of the geometric method, which makes it possible to obtain general information about the behavior of a nonlinear system, is as follows:

$$\ddot{x}_i + F_i(x_1, \cdots, x_n, \dot{x}_1, \cdots, \dot{x}_n) = 0, \quad i = 1,2, \cdots, n$$

where $F_i(\cdots)$ satisfy the conditions of existence and uniqueness of a solution with prescribed initial conditions.

If we adopt a two-dimensional space defined by $x(t)$ and $\dot{x}(t)$, the point $\{x(t_i), \dot{x}(t_i)\}$ at any given time t_i will represent the state of the system. The point starts from $P_0 = \{x(t_i), \dot{x}(t_i)\}$ determined by the initial conditions and moves along a curve over time. These points form a path and a plane, referred to as a *trajectory* and a *phase plane* $\{x(t), \dot{x}(t)\}$, respectively. From the shape of the path and the direction of motion of the point over time, we can draw a conclusion on the qualitative characteristics of the nonlinear system.

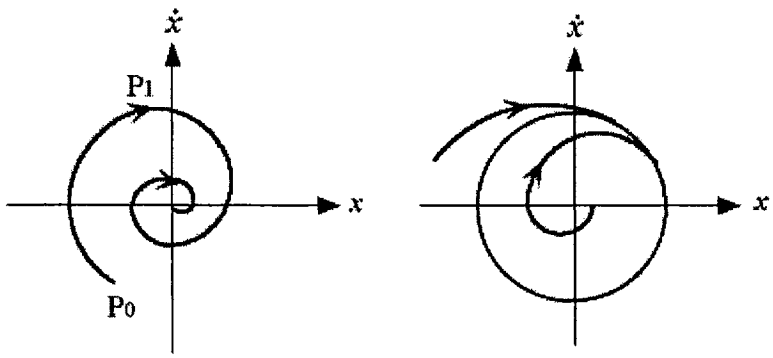

(a) (b)

Figure 3.1 Trajectories on phase plane

In fact, the phase portrait represents all possible solutions since it aggregates all trajectories. For example, Figure 3.1(a) illustrates that the motion of points $\{x(t), \dot{x}(t)\}$ is

oscillatory and that $x(t)$ and $\dot{x}(t)$ tend to zero with time, even though we do not have an explicit solution for $x(t)$. Figure 3.1(b) gives another example, where the closed trajectory shows that a periodic solution for $x(t)$ exists.

Moreover, the motion tendency of the point in the neighborhood of an equilibrium point ($x(t) = \dot{x}(t) = 0$) gives us our first intuitive view of stability problems. Let us take Figure 3.1 as an example. Since $x(t) \to 0$ and $\dot{x}(t) \to 0$ as $t \to \infty$ in Figure 3.1(a), the equilibrium point must be stable. We qualify this system as asymptotic stability. In Figure 3.1(b), because all neighboring trajectories approach the closed trajectory as $t \to \infty$, the corresponding periodic solution in this system is stable.

2) Singular Point

The singular point of a differential equation is fundamental in determining the properties of the equation solution. Through a study of singularity, we will have considerable insight into the qualitative aspect of the solution. In fact, a type of the singularity presents a picture in compact form of all the solutions that may exist. As usual, a study of singularity is a combination of analytical and graphical approaches to the problem.

Consider the more general autonomous system of the form

$$\begin{cases} \dot{x}_1 = f_1(x_1, x_2) \\ \dot{x}_2 = f_2(x_1, x_2) \end{cases} \tag{3.1}$$

where $f_1(x_1, x_2)$ and $f_2(x_1, x_1)$ are polynomials in terms of $x_1(t)$ and $x_2(t)$, and the initial condition $f_1(0,0) = f_2(0,0) = 0$ is satisfied.

We will examine the qualitative characteristics of this system by introducing the *state-plane* $\{x_1(t), x_2(t)\}$. In the case of Equation (3.1), if $x_1(t)$ and $x_2(t)$ are related to each other by $\dot{x}_1(t) = x_2(t)$, then the state-plane is referred to as *phase plane*.

Equation (3.1) can be rewritten as follows:

$$\frac{dx_2}{dx_1} = \frac{f_2(x_1, x_2)}{f_1(x_1, x_2)} \tag{3.2}$$

First, we consider a particular point on the state plane, the point satisfies the conditions

$$f_1(x_1(0), x_2(0)) = f_2(x_1(0), x_2(0)) = 0 \tag{3.3}$$

At this special point, the field direction is undefined, that is

$$\frac{dx_2}{dx_1} = \frac{0}{0}$$

In the case of Equation (3.1), this point coincides with the origin, $x_1(0) = x_2(0) = 0$. In mathematics, this particular point is called a *singular point*; on the other hand, in mechanical applications, we refer to it as an *equilibrium point*.

Next, if we separate the linear terms in functions $f_1(x_1, x_2)$ and $f_2(x_1, x_2)$, we can rewrite Equation (3.1) into the following form:

$$\begin{cases} \dot{x}_1 = a_{11}x_1 + a_{12}x_2 + g_1(x_1, x_2) \\ \dot{x}_2 = a_{21}x_1 + a_{22}x_2 + g_2(x_1, x_2) \end{cases} \tag{3.4}$$

where a_{ij} $(i, j = 1, 2)$ are constant coefficients, and $g_1(x_1, x_2)$ and $g_2(x_1, x_2)$ are high order polynomials higher than the first. It has been shown by Poincare that Equation (3.4) has the singularities same as those of the simplified linear equation. In other words, the

linear terms of Equation (3.4) will play a predominant role for small values of $x_1(t)$ and $x_2(t)$.

$$\begin{cases} \dot{x}_1 = a_{11}x_1 + a_{12}x_2 \\ \dot{x}_2 = a_{21}x_1 + a_{22}x_2 \end{cases} \tag{3.5}$$

For this linear system, we can write a particular solution in explicit form

$$x_1 = A_1 e^{\lambda t}, \quad x_2 = A_2 e^{\lambda t} \tag{3.6}$$

Substituting Equation (3.6) into Equation (3.5), we obtain the homogeneous algebraic equations for A_1 and A_2:

$$\begin{cases} A_1(a_{11} - \lambda) + A_2 a_{12} = 0 \\ A_1 a_{21} + A_2(a_{22} - \lambda) = 0 \end{cases} \tag{3.7}$$

To assure nonzero solutions for A_1 and A_2, we set the characteristic determinant of Equation (3.7) equal to zero:

$$\Delta = \begin{vmatrix} a_{11} - \lambda & a_{12} \\ a_{21} & a_{22} - \lambda \end{vmatrix} = 0 \tag{3.8}$$

and obtain a second order polynomial for λ:

$$\lambda^2 - \lambda(a_{11} + a_{22}) + a_{11}a_{22} - a_{12}a_{21} = 0 \tag{3.9}$$

Equation (3.9) yields the desired exponent:

$$\lambda = \frac{a_{12} + a_{22}}{2} \pm \sqrt{\tfrac{1}{4}(a_{11} + a_{22})^2 - a_{11}a_{22} + a_{12}a_{21}} \tag{3.10}$$

Finally, we discuss the three types of singular points relative to wing rock analysis.

(a) The singular point is called a *saddle point* if both characteristic roots λ_1, λ_2 are real but have opposite signs. The behavior of trajectories around a saddle point in Figure 3.2(a) shows an unstable singular point.

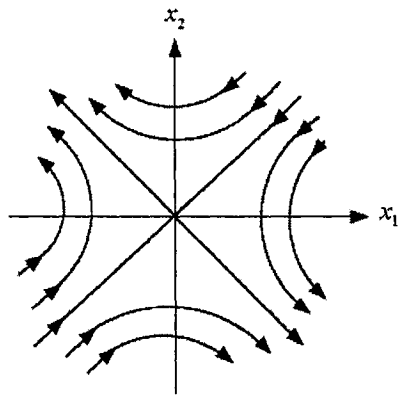

(c) Singular Points on the state-planes – a saddle point

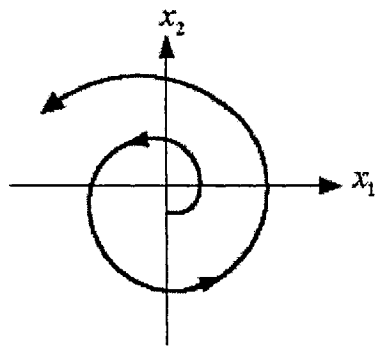

(b) Singular points on the state-plane – an unstable focus

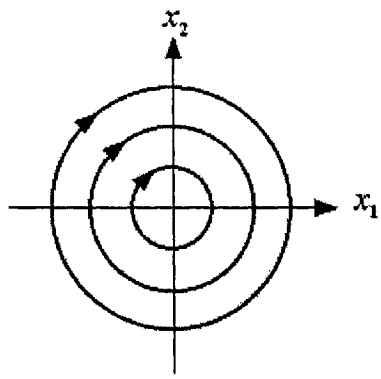

(c) Singular point on the state-plane – a center

Figure 3.2 Examples of singular points

(b) The singular point is called a *focal point* if both roots λ_1, λ_2 are complex-conjugates ($\lambda_{1,2} = \alpha \pm i\omega, \alpha \neq 0, \omega \neq 0$). If $\alpha < 0$, the trajectories in Figure 3.1(a) approach the singular point; if $\alpha > 0$, they moves away it, as shown in Figure 3.2 (b). Therefore, the focal point can be either asymptotically stable or unstable depending on the sign of the real part of the characteristic roots.

(c) The singular point is called a *center* if the two characteristic roots λ_1, λ_2 are purely imaginary, as shown in Figure 3.2(c), where the points on the state plane neither depart from nor approach the origin. If they start in its neighborhood, they will remain close to the origin. Thus the center is merely stable, not asymptotically stable.

3.2 Limit Cycle Analysis

3.2.1 Limit Cycle

As illustrated in Figure 3.1(b), the phase portrait shows a closed curve on phase plan. Trajectories inside the cure and those outside the curve all tend to the curve while a motion started on this curve will stay on it forever, circling periodically around the origin. This curve is an instance of the so-called "limit cycle" phenomenon, which is a unique feature of nonlinear systems.

A limit cycle can be stable or unstable, depending on whether the paths in the neighborhood of the limit cycle converge toward it or diverge away from it. They can result from either soft or hard self-excitation. Figure 3.3 illustrates an example of soft-

excitation. Physically, this phase portrait may represent a system that has excessive gain for the small signals and the output builds up in an unstable manner. With large signals, the output also approaches the stable limit cycle from the outside, as discussed in Reference [94].

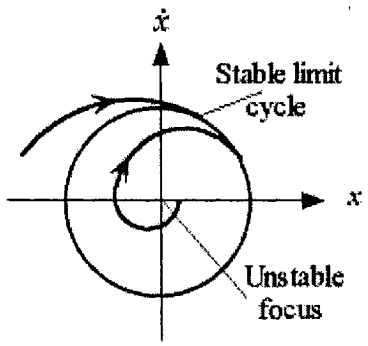

Figure 3.3 Phase portrait of soft self-excitation

3.2.2 Limit Cycle Existence

We now discuss the existence of limit cycles of the system described in Equation (3.4). To avoid solving this equation, we may seek help from the energy equation *dE/dt*. The only information we do have concerning energy is that the exchange of energy during one cycle is equal to zero:

$$\oint dE = 0 \tag{3.11}$$

where $\oint$ denotes integration along the closed trajectory. Unfortunately, Equation (3.11) is of no benefit in our effort to establish the existence of limit cycles.

Here, we give a famous *Poincare-Bendixon theorem*:

If a half-trajectory (for $t > t_0$ *or* $t < t_0$) remains in a finite domain D without approaching a singular point, then C is either a closed trajectory or approaches such a trajectory.

In the case of a ring-shaped domain D_1 bounded by two concentric circles C_1 and C_2 in Figure 3.4, sufficient conditions for the existence of at least one closed trajectory are:

(a) Those trajectories enter D_1 through every point on C_1 and C_2.

(b) There are no singular points either in D_1 or on C_1 and C_2.

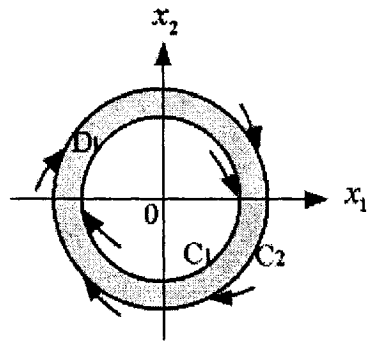

Figure 3.4 The shaded domain D_1 assures existence of at least one closed trajectory

3.3 Phase Plane Analysis of Wing Rock Phenomenon

Note that it is possible for a system trajectory to correspond to only a single point. Such a point is called an equilibrium point. As we shall see later, many stability problems are naturally formulated with respect to equilibrium points.

Definition: A state **x** is an equilibrium point of the system if once **x**(t) is equal to **x**, it remains equal to **x** for all future time.

Mathematically, this means that the constant vector $\boldsymbol{x}$ satisfies $f(\mathbf{x}) = \mathbf{0}$. Equilibrium points can be found by solving the nonlinear algebraic equations above. A nonlinear system usually has several (or infinitely many) isolated equilibrium points.

In discussing the phase plane analysis of wing rock phenomenon, two points should be kept in mind. Phase plane analysis of nonlinear systems is related to that of linear systems because the local behavior of a nonlinear system can be approximated by the behavior of a linear system. However, nonlinear systems can display much more complicated patterns on phase plane, such as multiple equilibrium points and limit cycles. The following is the detail discussions about the phase plane analysis of wing rock.

Let $x_1(t) = \phi(t)$ and $x_2(t) = \dot{\phi}(t)$; we first rewrite Equation (2.9) as a system of two first-order equations:

$$\begin{cases} \dot{x}_1 = x_2 \\ \dot{x}_2 = -a_0 x_1 - a_1 x_2 - a_2 |x_2| x_2 - a_3 x_1^3 - a_4 x_1^2 x_2 \end{cases} \tag{3.12}$$

To find the equilibrium points, we put

$$\dot{x}_1 = x_2 = 0 \tag{3.13}$$

It follows that

$$x_1 = 0, \quad \pm\sqrt{-a_0/a_3} \tag{3.14}$$

The nonzero solution exists only when $a_0/a_3 < 0$. From Figure 2.5, we know it is true for the AOA from 25^0 to 45^0 because of $a_0 > 0$ and $a_3 < 0$. We use the data in Figure 2.5 to calculate the two equilibrium points, $\pm\sqrt{-a_0/a_3}$, at different AOAs. With the AOA

increasing from 25^0 to 45^0, the points move toward the origin ($x_1 = 0.9837 \rightarrow 0.4737$).

To determine the character of the motion in a small neighborhood of these equilibrium positions, we introduce the following small perturbations, as introduced in Reference [92].

$$\begin{cases} x_1 = x_{10} + u_1 \\ x_2 = u_2 \end{cases} \tag{3.15}$$

where x_{10} is the coordinate of an equilibrium position (x_{20} =0 at all equilibrium points).

Substituting Equation (3.15) into Equation (3.12) and retaining only linear terms in $u_1(t)$ and $u_2(t)$ in the result, we have

$$\begin{cases} \dot{u}_1 = u_2 \\ \dot{u}_2 = -(a_0 + 3a_3 x_{10}^2)u_1 - (a_1 + a_4 x_{10}^2)u_2 \end{cases} \tag{3.16}$$

or the form of matrix

$$\begin{Bmatrix} \dot{u}_1 \\ \dot{u}_2 \end{Bmatrix} = \begin{bmatrix} 0 & 1 \\ -(a_0 + 3a_3 x_{10}^2) & -(a_1 + a_4 x_{10}^2) \end{bmatrix} \begin{Bmatrix} u_1 \\ u_2 \end{Bmatrix} \tag{3.17}$$

The eigenvalues of this system are

$$\lambda_1, \lambda_2 = \tfrac{1}{2}[-(a_1 + a_4 x_{10}^2) \pm \sqrt{(a_1 + a_4 x_{10}^2)^2 - 4(a_0 + 3a_3 x_{10}^2)}\,] \tag{3.18}$$

At the origin (x_{10} = 0), Equation (3.18) reduces to

$$\lambda_1, \lambda_2 = \tfrac{1}{2}(-a_1 \pm i\sqrt{4a_0 - a_1^2}\,) \tag{3.19}$$

Using the data in Figure 2.5, we find that $a_1 < 0$ and $4a_0 > a_1^2$ for the AOA from 25^0 to 45^0, and λ_1 and λ_2 are complex conjugates. Therefore, the origin of wing rock motion is an *unstable focus*.

Likewise, we can determine the character of the motion in a small neighborhood of the nonzero equilibrium points ($x_1 = \pm\sqrt{-a_0/a_3}$). Substituting $x_1 = x_{10} = \pm\sqrt{-a_0/a_3}$ into Equation (3.18), we obtain

$$\lambda_1, \lambda_2 = \frac{1}{2}[(\frac{a_0 a_4}{a_3} - a_1) \pm \sqrt{8a_0 + (a_1 - \frac{a_0 a_4}{a_3})^2}\ ] \tag{3.20}$$

Regardless of the sign of $a_1 - a_0 a_4 / a_3$, both eigenvalues are real, one is positive and the other is negative, which means the two equilibrium points away from the origin. Thus, whenever nonzero equilibrium points exist, they are always saddle points.

The above results obtained at AOA = 32.5^0 are illustrated in Figure 3.5, where the entire phase plane is constructed by numerically integrated Equation (3.12), as introduced in Reference [93]. First, there are three equilibrium points marked as s1, s2, and s3 in Figure 3.5 (a). With Equation (3.14) and the data in Figure 2.5, the three points are

$$x_{10} = 0, \quad \pm 59.46^0 \tag{3.21}$$

Next, we have observed that any motion initiated at a point in the shaded region will diverge, not oscillate, which means that the wing will continuously execute complete revolution. We have also observed that any motion initiated at a point in the unshaded region will converge onto the limit cycle, which means that small-amplitude initial conditions lead to motions that grow to the stable limit cycle and large-amplitude initial conditions lead to motions that decay to the limit cycle. Finally, we have provided the added trajectories for many different initial conditions in Figure 3.5(b).

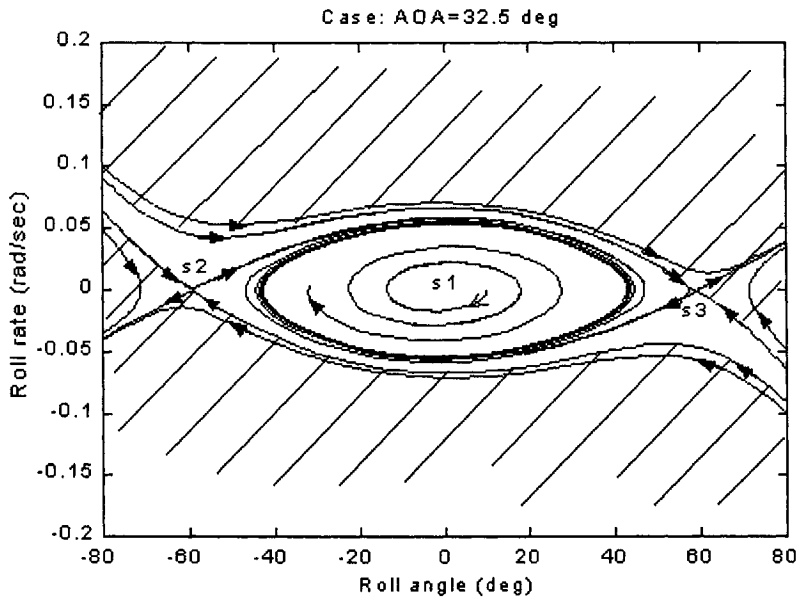

(a) The trajectories initiated in the shaded region diverge

and all the others approach the stable limit cycle

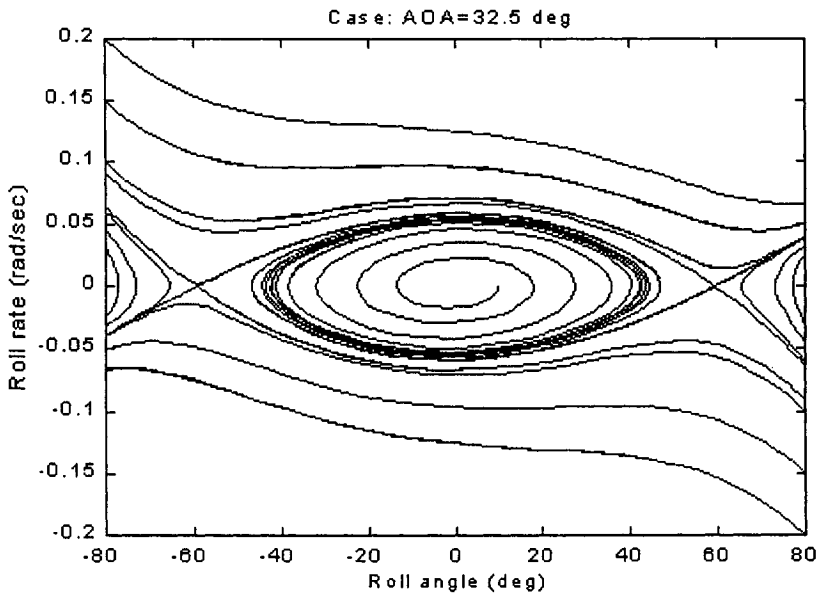

(b) Many trajectories on phase plane

Figure 3.5 Phase planes obtained by numerical integration at $AOA = 32.5^0$

If we compare Figure 3.5(a) with Figure 3.3, we can conclude that wing rock phenomenon is a typical nonlinear system with soft self-excitation.

On the other hand, we introduce the free-to-roll test results of wing rock on 80^0 swept delta wing models reported in Reference [89]. The effect of initial conditions on model time domain response is depictured in Figure 3.6. The mathematical model predicts roll divergence for initial release roll angles $\phi(0) > 60^0$ that is not consistent with the

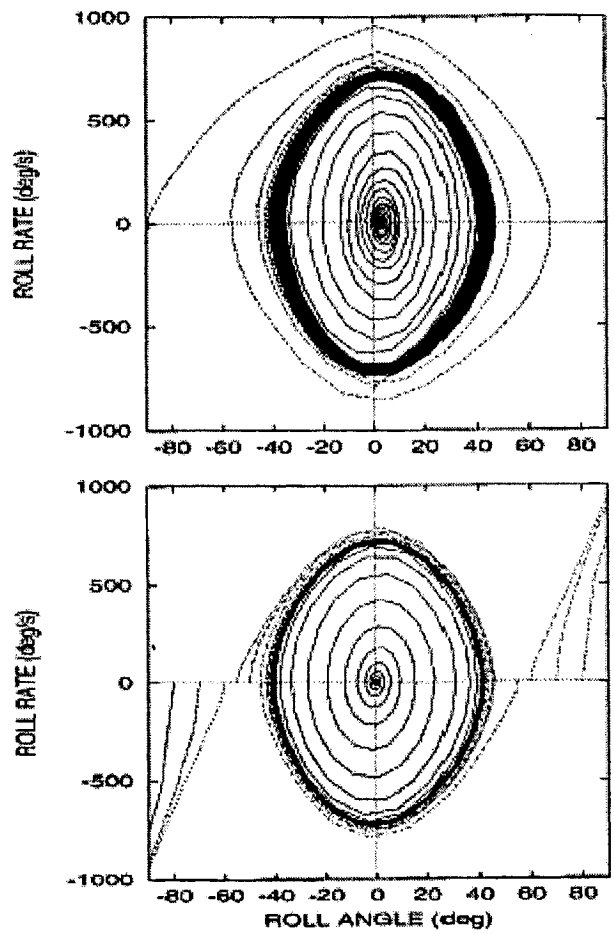

Figure 3.6 The phase plane plot for different initial conditions: comparison of experimental (top) and analytical (bottom) results at AOA =32.5^0 [89]

available test results. This discrepancy can be related with the divergence of the restoring moment due to the softening term $a_3\phi^3$ in Equation (2.9) that underestimates the wing dihedral stability for larger roll displacements. Anyway, limit cycle characteristics and build-up dynamics are accurately predicted for realistic release roll angles $\phi(0) < 60^0$. From this point of view, we can say that the analytical and graphical results are in agreement with the test results.

3.4 Summary

In this chapter, we have introduced phase plane analysis, which is a graphical method used to study second-order nonlinear dynamic systems and allows us visual examination of the global behavior of systems. We have also illustrated an example of soft self-excitation and discussed the existence of limit cycles. Finally, we have obtained the entire phase plane of wing rock phenomenon, based on perturbation techniques and numerical simulations. If $\phi(0) < 60^0$, we can conclude that the analytical results are in agreement with the test results.

Chapter 4

Hysteresis Mechanism Analysis of Wing Rock Phenomenon

In this chapter, we will theoretically analyze the hysteresis mechanism of wing rock phenomenon. This chapter is organized as follows: Section 4.1 is an introduction. In Sections 4.2, we briefly introduce Lyapunov's stability theory. In Section 4.3, we analyze the relationship between wing rock energy variation and wing rock hysteresis and then present some numerical simulation results for the cases of fixed AOA and time-varying AOA. In Section 4.4, we also presented some test results of wing rock phenomenon in the literature. Section 4.5 summarizes this chapter.

4.1 Introduction

Many modern combat aircraft often operate at subsonic speeds and high angles of attack. At a sufficiently high AOA, these aircraft become unstable and enter into an LCO, mainly rolling motion known as wing rock in References [4, 75, 78, 88]. In practice, high-speed civil transport and combat aircraft can fly in conditions where this self-

induced oscillatory rolling motion is observed. More importantly, wing rock phenomenon can be highly annoying to the pilot and may pose serious limitations to the combat effectiveness of the aircraft. Therefore, the control of wing rock phenomenon of aircraft is an important issue.

Considerable research has been conducted on the motion of 80^0 swept delta wing to help understand the fundamental mechanisms causing wing rock, as shown in References [4, 78-80, 82, 84-86, 88-89]. Free-to-roll tests are usually used to determine build-up and limit-cycle characteristics of wing rock. These test results reveal the magnitude of limit cycles of wing rock varying with AOA, as depicted in Figure 1.3. In addition, the tracking tests of the primary vortex positions in the cross-flow plane in References [78-80, 82, 84-86, 88-89] provided the data to understand the driving mechanism of wing rock. These authors found that hysteresis existing between the roll angle and the rolling moment provides clues that help us explain wing rock phenomenon. The researchers in References [4, 79, 82, 84-86, 88-89] *observed* this hysteresis, noticed the three loops during one cycle, and explained this observation. The work done by the rolling motion is driving the oscillation during the central loop since the aerodynamic motion acts in the direction of the wing rolling motion, whereas the oscillation is being damped during the two reverse outer loops.

In this chapter, we will use Lyapunov's direct method theoretically to analyze the hysteresis mechanism of wing rock phenomenon instead of physical insight.

4.2 Lyapunov's Stability Theory

4.2.1 The Basics of Lyapunov's Theories

The most useful and general approach for studying the stability of nonlinear systems is Lyapunov's theory. The theory mainly addresses the question of stability of any system, linear or nonlinear systems. It is well known that for any stable system, there is always a point where the motion of such a system will converge after some disturbance, whereas there is none for an unstable one, thus resulting in motion divergence even under very slight disturbances. In dealing with stability problems, Lyapunov's stability theory appears in two versions, the Lyapunov linearization method (first method) and the Lyapunov's direct method (second method). Lyapunov's direct method gets more application in nonlinear systems because it is the most important tool for nonlinear system analysis and design.

Since nonlinear systems may have much more complex and exotic behavior than linear systems, the mere notion of stability is not enough to describe the essential features of their motions. A number of more refined stability concepts such as asymptotic stability, exponential stability, and globally asymptotic stability are needed. We introduce these stability concepts formally and explain their practical meanings below. Let us first introduce the basic concepts of stability and instability.

Definition 4.1: The equilibrium state $\mathbf{x} = 0$ is said to be stable if, for any $R = 0$, there exists $r > 0$, such that if $\|\mathbf{x}(0)\| < r$, then $\|\mathbf{x}(0)\| < R$ for all $t \geq 0$. Otherwise, the equilibrium point is unstable.

Essentially, the definition states that the origin is stable, if, given that we do not want the state trajectory $x(0)$ to get out of a ball of arbitrarily specified radius S_R, a value can be found such that starting the state from within the ball S_r at time $t = 0$ guarantees that the state will stay within stay within the ball S_R thereafter. The geometrical implication of stability is indicated by curve 2 in Figure 4.1.

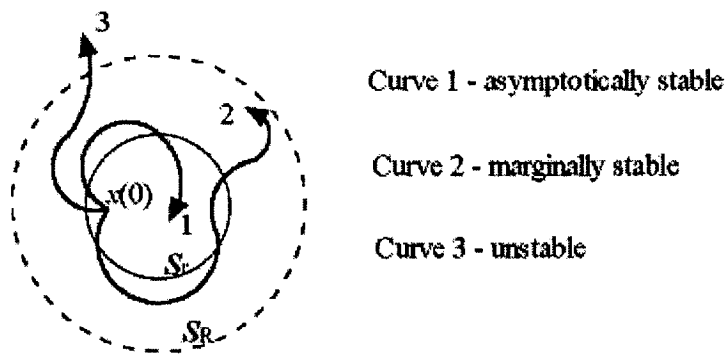

Figure 4.1 Concepts of stability

In practice, Lyapunov stability is not enough. We need to check the asymptotically stable.

Definition 4.2: An equilibrium point **0** is asymptotically stable if it is stable, and if it addition there exist some $r > 0$ such that $\|\mathbf{x}(0)\| < r$ implies that $\mathbf{x}(t) \to 0$ as $t \to \infty$.

Definition 4.3: If asymptotic (or exponential) stability holds for any initial states, the equilibrium point is said to be asymptotically (or exponentially) stable in the large. It is also called globally asymptotically (or exponentially) stable.

4.2.2 Lyapunov's Direct Method

The basic philosophy of Lyapunov's direct method in Reference [95] is the mathematical extension of a fundamental physical observation. If the total energy of a mechanical system is continuously dissipated, then the system, whether linear or nonlinear, must eventually settle down to an equilibrium point. Therefore, we may conclude the stability of a system by examining the variation of a single scalar function.

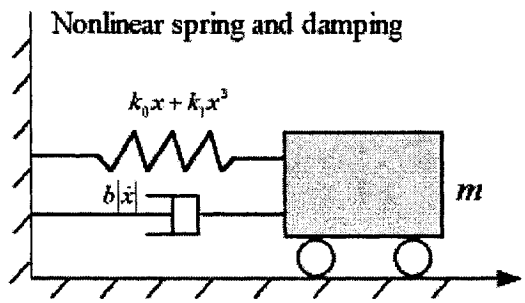

Figure 4.2 A nonlinear mass-damping-spring system

Let us take an example from Reference [96] to illustrate this method. Figure 4.2 shows a nonlinear mass-damping-spring system, and the dynamic equation of this system is

$$m\ddot{x} + b|\dot{x}|\dot{x} + k_0x + k_1x^3 = 0 \tag{4.1}$$

where $b|\dot{x}|$ is nonlinear damping, and $k_0x + k_1x^3$ is a nonlinear spring term.

The total mechanical energy of the system is the sum of its kinetic energy and its potential energy.

$$V(\mathbf{x}) = \frac{1}{2}m\dot{x}^2 + \int_0^x (k_0x + k_1x^3)dx = \frac{1}{2}m\dot{x}^2 + \frac{1}{2}k_0x^2 + \frac{1}{4}k_1x^4 \tag{4.2}$$

Comparing the definitions of stability and mechanical energy, we can easily see some

relations:

(a) Zero energy corresponds to the equilibrium point ($\mathbf{x}(t) = 0$, $\dot{\mathbf{x}}(t) = 0$).

(b) Asymptotical stability implies the convergence of mechanical energy to zero.

(c) Instability is related to the growth of mechanical energy.

These relations indicate that the stability properties of the system can be characterized by the variation of the mechanical energy of the system.

The rate of energy variation of the system is obtained by differentiating Equation (4.2) with Equation (4.1)

$$\dot{V}(\mathbf{x}) = m\dot{x}\ddot{x} + (k_0 x + k_1 x^3)\dot{x} = \dot{x}(-b\dot{x}|\dot{x}|) = -b|\dot{x}|^3 \tag{4.3}$$

Equation (4.3) implies that the energy of the system, starting from some initial value, is continuously dissipated by the damper until the mass settles down, that is, until $\dot{x}(t) = 0$.

Lyapunov's direct method is based on a generalization of the concepts in the above mass-spring-damper system to more complex systems. Faced with a set of nonlinear differential equations, the basic procedure of Lyapunov's direct method is to generate a scalar "energy-like" function for the dynamic system and to examine its time variation. In this way, conclusions may be drawn on the stability of the set of differential equations without using the stability definitions or requiring explicit knowledge of solutions.

4.2.3 Lyapunov Function and Theorem

The energy function in Equation (4.2) has two properties:

(a) It is strictly positive unless state variables $x(t)$ and $\dot{x}(t)$ are zero.

(b) The function is monotonically decreasing when the variables $x(t)$ and $\dot{x}(t)$ vary according to Equation (4.1).

In Lyapunov's direct method, the notions of positive definite function and Lyapunov function formalize above two properties, respectively.

Definition 4.4: A scalar continuous function $V(\mathbf{x})$ is said to be locally positive definite if $V(\mathbf{0}) = 0$ and, in a ball $\mathbf{S}_{R0}$, $\mathbf{x} \neq \mathbf{0}$, then $V(\mathbf{x}) > 0$. If $V(\mathbf{0}) = 0$ and the above property holds over the whole state space, then $V(\mathbf{x})$ is said to be globally positive definite.

Definition 4.5: The nonlinear system, $\dot{\mathbf{x}} = \mathbf{f}(\mathbf{x},t)$, is said to be autonomous if $\mathbf{f}$ does not depend explicitly on time, that is, if the system's state equation can be written

$$\dot{\mathbf{x}} = \mathbf{f}(\mathbf{x}) \tag{4.4}$$

Otherwise, the system is called non-autonomous.

Definition 4.6: If, in a ball $\mathbf{B}_{R0}$, the function $V(\mathbf{x})$ is positive definite and has continuous partial derivatives, and if its time derivative along any state trajectory of system (4.4) is negative semi-definite, that is, $\dot{V}(\mathbf{x}) \leq 0$, then $V(\mathbf{x})$ is said to be a Lyapunov function for the system (4.4).

Liapunov's direct method relies on a test function, called the Liapunov function, to determine the stability characteristics of the system. Liapunov stability theorems usually have local and global versions.

Theorem 4.7: (Local stability) if, in a ball $\mathbf{B}_R$, there exists a scalar function $V(\mathbf{x})$ with continuous first partial derivative such that

(a) $V(\mathbf{x})$ is positive definite (locally in $\mathbf{B}_{R0}$) and

(b) $\dot{V}(\mathbf{x})$ is negative semi-definite (locally in $\mathbf{B}_{R0}$),

then the equilibrium point $\mathbf{0}$ is stable. If, actually, the derivative $\dot{V}(\mathbf{x})$ is locally negative definite in $\mathbf{S}_{R0}$, then the stability is asymptotic.

Theorem 4.8: (Global stability) Assume that there exists a scalar function V of the state $\mathbf{x}(t)$, with continuous first order derivatives such that

(a) $V(\mathbf{x})$ is positive definite

(b) $\dot{V}(\mathbf{x})$ is negative semi-definite (locally in $\mathbf{B}_{R0}$)

(c) $V(\mathbf{x}) \to \infty$ as $\|\mathbf{x}\| \to \infty$.

then the equilibrium point at the origin is globally asymptotically stable.

4.3 Hysteresis Mechanism of Wing Rock Phenomenon

In this section, we use the above theories and analytical methods to study wing-rock hysteresis mechanism and then show the numerical results.

First, the wing-rock model in Equation (2.9) can be written in the following form:

$$\ddot{\phi} + (a_1 + a_2|\dot{\phi}| + a_4\phi^2)\dot{\phi} + (a_0\phi + a_3\phi^3) = 0 \tag{4.5}$$

Let $x_1(t) = \phi(t)$ and $x_2(t) = \dot{\phi}(t)$ and rewrite Equation (4.5) in a state-variable form:

$$\begin{cases} \dot{x}_1 = x_2 \\ \dot{x}_2 = -(a_1 + a_2|x_2| + a_4 x_1^2)x_2 - (a_0 x_1 + a_3 x_1^3) \end{cases} \tag{4.6}$$

Equation (4.6) is further expressed in the phase-trajectory equation:

$$\frac{dx_2}{dx_1} = \frac{-(a_1 + a_2|x_2| + a_4 x_1^2)x_2 - (a_0 x_1 + a_3 x_1^3)}{x_2} \tag{4.7}$$

By integrating Equation (4.7) and substituting $x_2(t) = \dot{x}_1(t)$, we have

$$\tfrac{1}{2}x_2^2 + U(x_1) = C - \int_0^t (a_1 + a_2|x_2| + a_4 x_1^2)x_2^2 dt \tag{4.8}$$

where $U(x_1) = \int (a_0 x_1 + a_3 x_1^3)dx_1$ is the potential energy and C is an integral constant.

As discussed in References [91, 96], we define $E(t)$ as the total mechanical energy of the system:

$$E = \tfrac{1}{2}x_2^2 + U(x_1) \tag{4.9}$$

By differentiating Equation (4.8), we obtain the rate of change of the total energy $E(t)$:

$$\frac{dE}{dt} = -(a_1 + a_2|x_2| + a_4 x_1^2)x_2^2 \tag{4.10}$$

Equation (4.10) shows that the total energy $E(t)$ is not a constant, and increases or decreases according to the sign of $(a_1 + a_2|x_2| + a_4 x_1^2)x_2^2$.

Next, we turn our attention to the hysteresis of wing rock. Substituting Equation (4.5) into Equation (2.1) and taking $D = 0$, we obtain a $C_l - \phi$ relationship to described the hysteresis

$$C_l = -(a_0\phi + a_1\dot{\phi} + a_2|\dot{\phi}|\dot{\phi} + a_3\phi^3 + a_4\phi^2\dot{\phi})/k \tag{4.11}$$

where $k = \frac{\rho U_\infty^2 Sb}{2I_{xx}}$; these parameters are defined in Equation (2.1).

To illustrate the behavior of hysteresis, we simulate the build-up phase of hysteresis in Figure 4.3(e) and the full hysteresis in Figure 4.3(f), and draw arrows indicating the developing direction of hysteresis over time. Note that Figure 4.3 is simulated at $AOA = 32.5^0$, in the initial conditions $\phi(0) = 0.1^0$ and $\dot{\phi}(0) = 0$, and with $k \approx 1/30$.

Finally, we analyze the relationship between the *dE/dt* and the hysteresis of wing rock. Note that $a_1 < 0$, $a_2 > 0$, and $a_4 > 0$ (except $AOA = 45^0$) in Figure 2.5.

(a) If $x_2 \neq 0$ and $dE/dt = 0$, then $x_1 = \pm X_c$. We define this roll angle X_c as a *critical angle*, marking X_c in Figure 4.3(b) and B and C in Figure 4.3(f), which lies on the boundary between increasing energy and decreasing energy and is an important parameter to design variable phase control described in the next chapter. If $x_2 = 0$ and $dE/dt = 0$, then $x_1 = \pm\phi_{\max}$, we mark them as A and D in Figure 4.3(f).

(b) If $x_2 \neq 0$ and $|x_1| < X_c$, then $dE/dt > 0$; this means that the wing-rock motion is absorbing energy and developing a single-loop hysteresis in a clockwise direction, as shown in Figures 4.3(e) and in the center loop BC of Figure 4.3(f). If $x_2 \neq 0$ and $|x_1| > X_c$, then $dE/dt < 0$; this implies that the motion dissipates energy and develops two additional outer-loop hysteresis, as shown in the outer loops AB and CD of Figure 4.3(f) where the direction of the motion is anticlockwise,

(c) Similarly, the role of x_2 can be analyzed because the relationship of x_1 and x_2 is constrained by wing rock to limit cycles, as shown in Figure 4.3(b). If $|x_2| > -(a_1 + a_4 x_1^2)/a_2$ or $|x_2| < -(a_1 + a_4 x_1^2)/a_2$, then $dE/dt > 0$ or $dE/dt < 0$, respectively. With Equation (4.5), it is easy to see that in this case a roll damping has a variable sign.

We now explain wing-rock mechanism by the limit-cycle energy analysis:

(a) During the wing-rock build-up phase, the oscillation is unstable and energy flows into the system ($dE/dt > 0$) as in Figure 4.3(e). The aerodynamic moment acts on the direction of the wing rolling motion. Wing rock exhibits the central-loop hysteresis in a clockwise direction.

(b) After the build-up phase, wing rock exhibits another two outer loops hysteresis. The direction of the motion is anticlockwise as in Figure 4.3(e), which means that the energy is being dissipated ($dE/dt < 0$), and the system tends to stable.

(c) During the limit-cycle phase, the balance of the energy exchanged by the system over an oscillation period confirms that wing-rock limit cycle is dynamically stable ($\oint dE = 0$).

As for the time-varying wing-rock case, we simulate this in the same conditions as we mentioned in Section 2.2.2. Figure 4.4 shows time-varying wing-rock behavior.

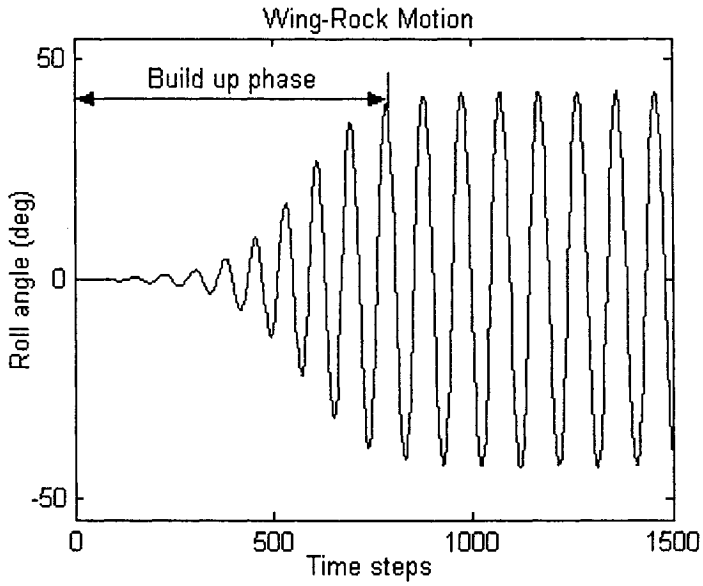

(a) Wing-rock time history

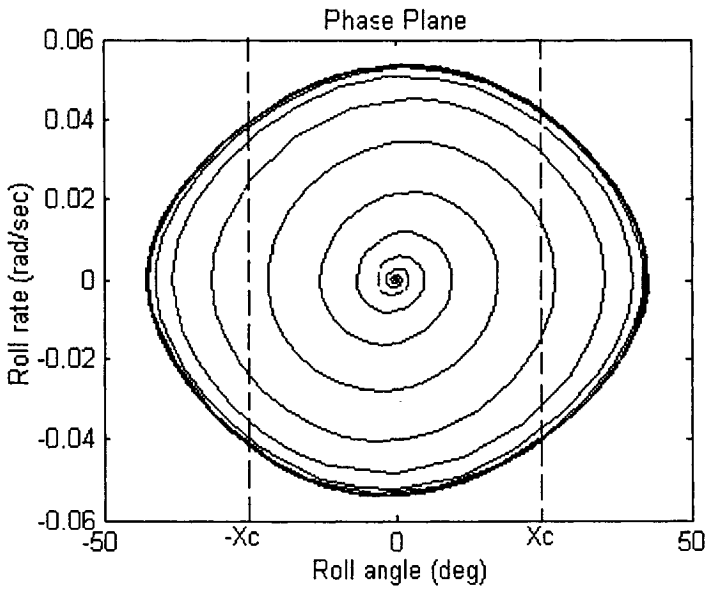

(b) Phase plane

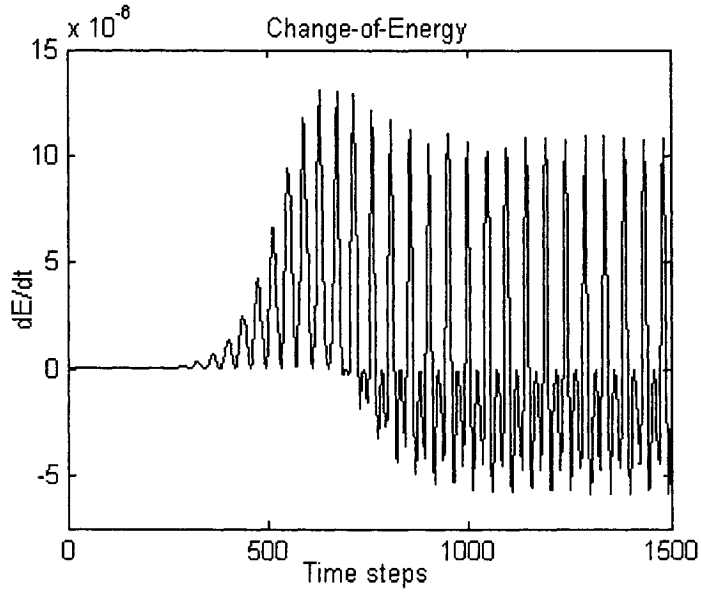

(c) *dE/dt* versus time steps

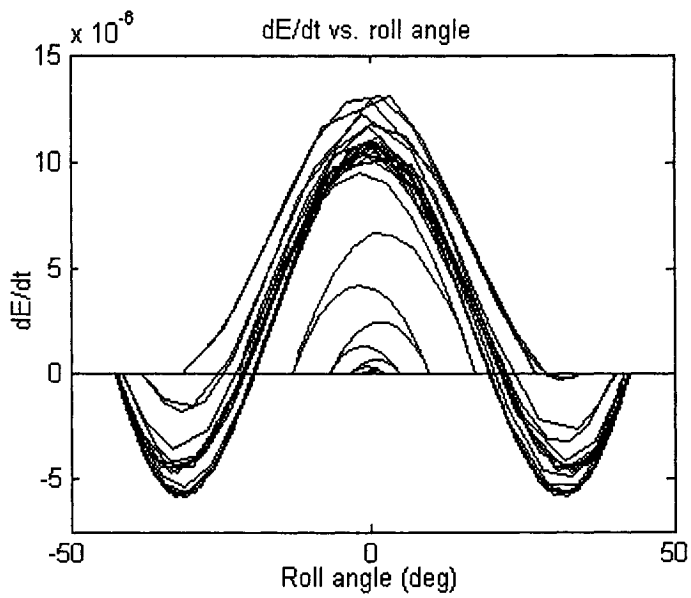

(d) *dE/dt* versus roll angle $\phi(t)$

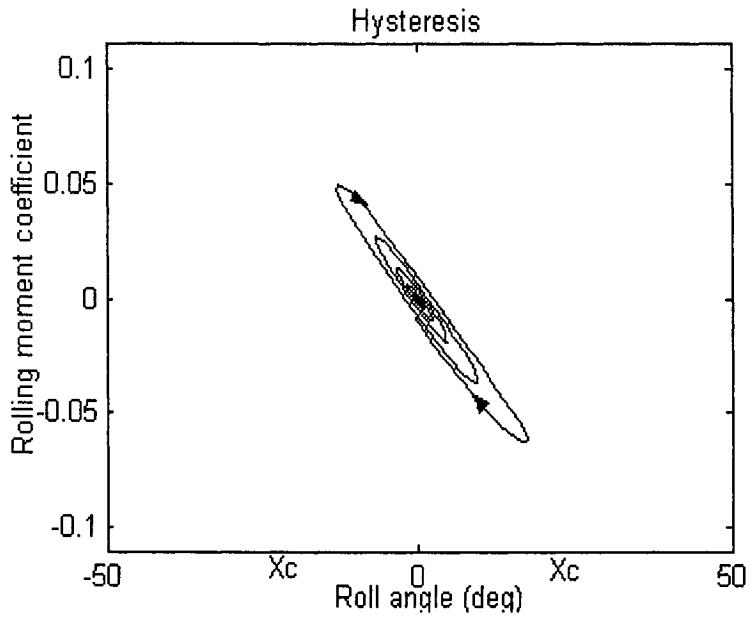

(e) Wing-rock build-up phase

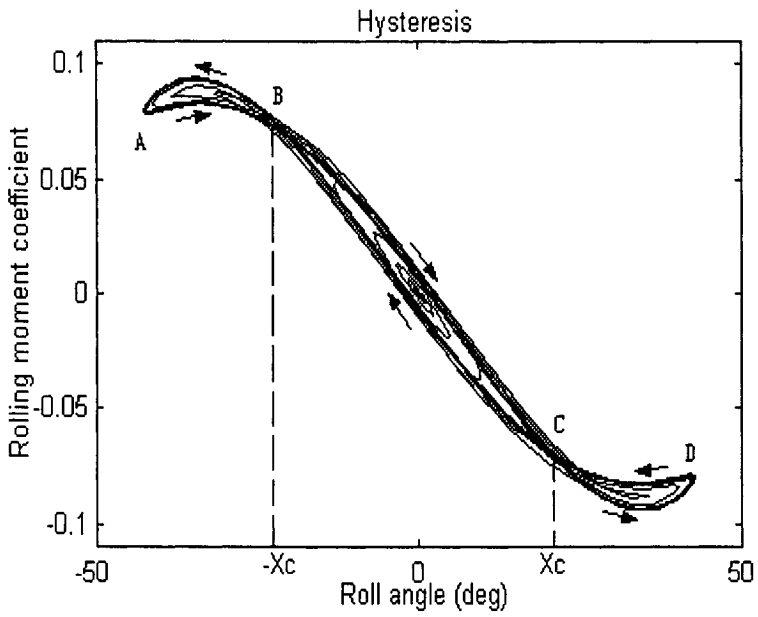

(f) Wing-rock limit-cycle phase

Figure 4.3 Wing rock behavior

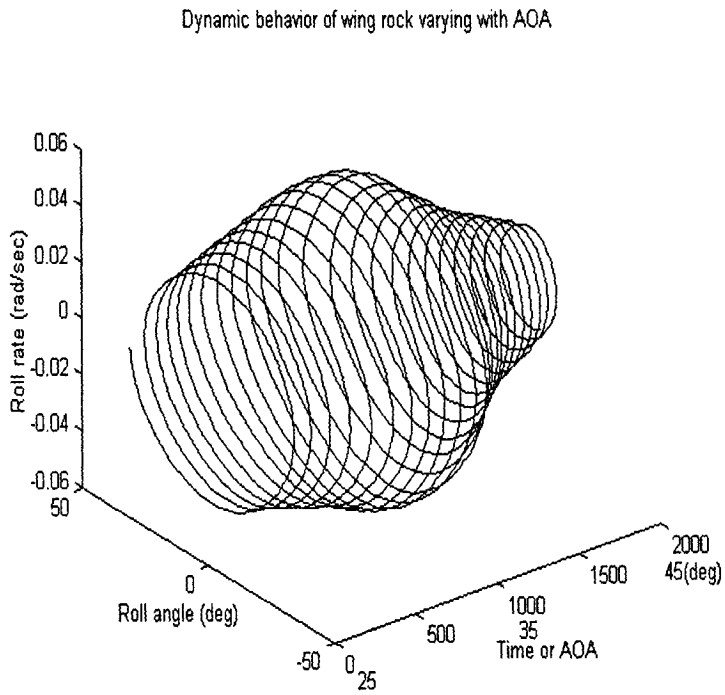

(a) Phase plane

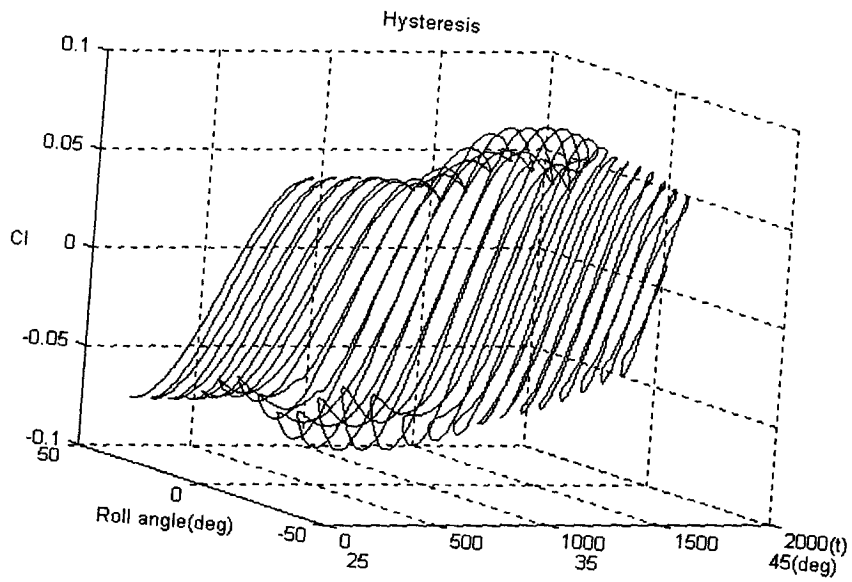

(b) Hysteresis developing

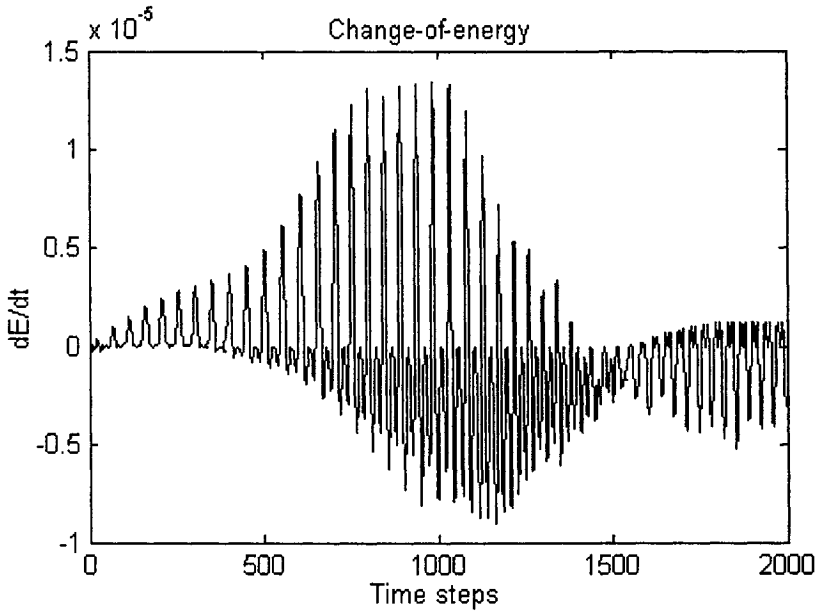

(c) *dE/dt* versus time steps

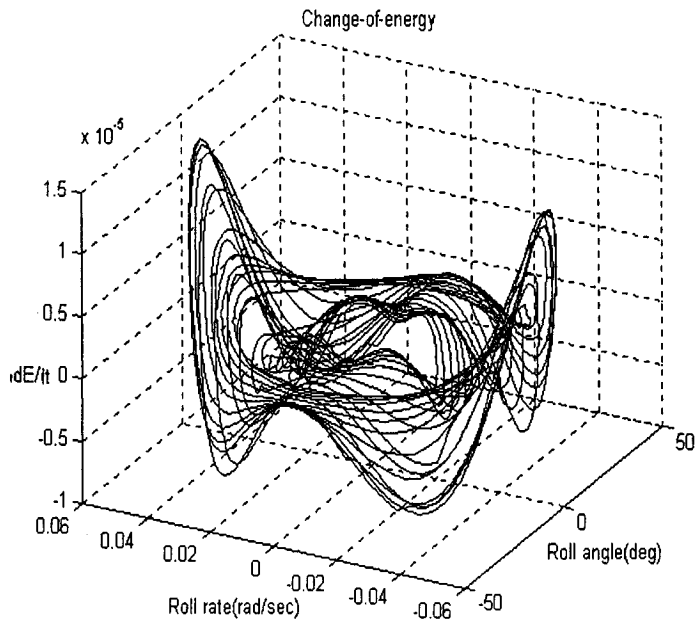

(d) *dE/dt* versus roll angle $\phi(t)$ and roll rate $\dot{\phi}(t)$

Figure 4.4 Time-varying wing-rock behavior

From above Figures 4.3 and 4.4, we have observed some difference. The following discussion is based on comparison between wing rock with time-varying AOA and wing rock with fixed AOA.

(a) In Figure 4.4(a), the boundary curve of the roll angle varies with AOA, which is different from the results shown in Figure 1.3, where the boundary curve of the roll angle obtained from each fixed AOA.

(b) The shape of wing-rock hysteresis in Figure 4.4(b) varies with time. First it shows single loops, next bigger three loops, and then smaller three loops. The hysteresis in Figure 4.3(f) is formed first with single loop and then with stable three loops.

(c) Some differences in *dE/dt* can be observed. In Figure 4.4(c), the system absorbs and increases energy from $t = 0$ to $t = 1000$ time steps. After $t > 1000$ time steps, the rate of energy change is decreasing until about $t = 1500$ time steps. When $t > 1600$ time steps, the rate increases again. By comparison, in Figure 4.3(c) the system absorbs the energy during $0 < t < 750$ and then it shows the constant rate of energy change and keeps stable LCOs.

Finally, we exhibit all the shapes of wing rock hysteresis at other fixed AOAs like Figure 4.3(f). In Reference [100], we have simulated the hysteresis at nine different AOAs, AOA=25^0, 27.5^0, 30^0, 32.5^0, 35^0, 37.5^0, 40^0, 42.5^0, and 45^0, in the initial conditions $\phi(0) = 0.1^0$ and $\dot{\phi}(0) = 0$, as shown in Figure 4.5. We have observed that wing rock hysteresis all shows the three loops: a center loop and two reverse outer loops, even though some loops are very small.

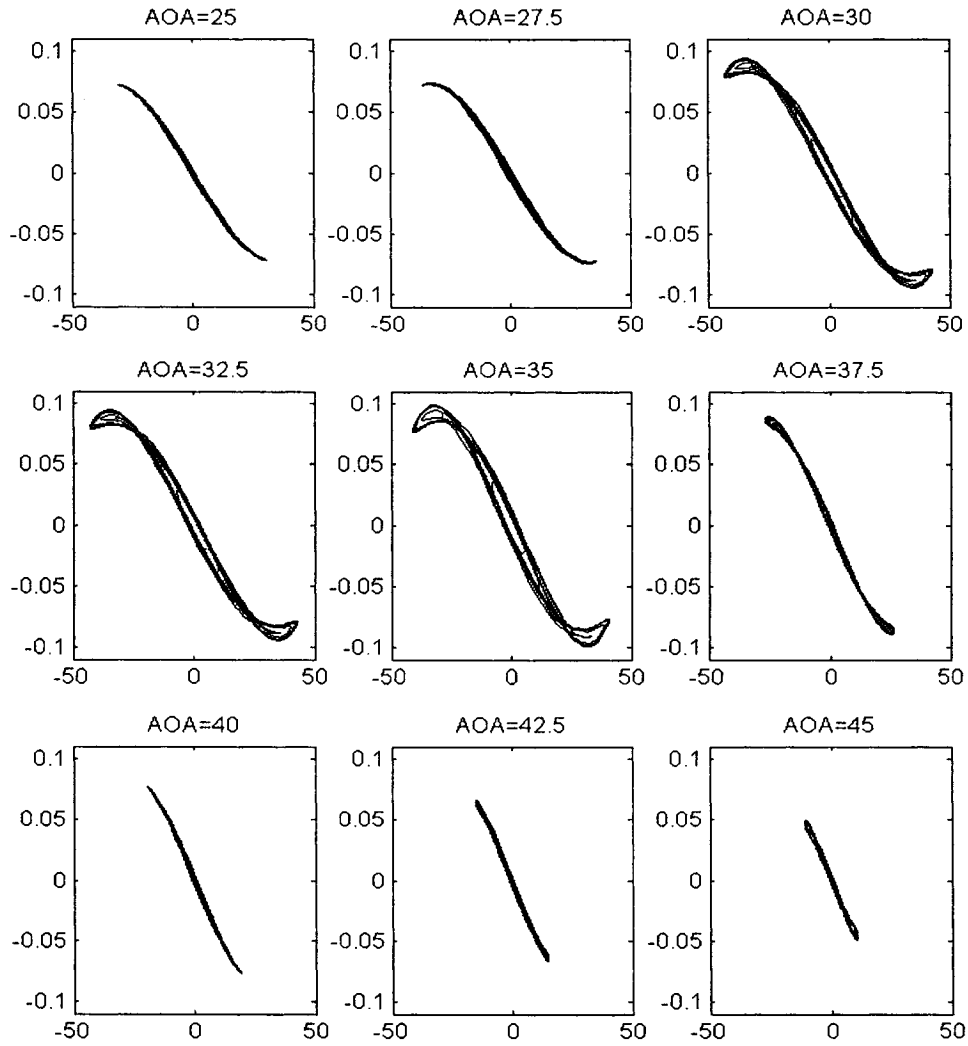

Rolling moment coefficient C_l versus roll angle $\phi(t)$ (deg)

Figure 4.5 Wing rock hysteresis at the nine different AOAs

4.4 Test Results of Wing Rock Phenomenon

In Section 4.3, we have analyzed the relationship of the energy variation and hysteresis of wing rock and presented some numerical simulation results. In this section, we further present some test results of wing rock in the literature.

Katz and Levin in Reference [82] presented the histogram of the normal force coefficient versus roll angle during wing rock limit cycles of a $\Lambda = 76^0$ delta wing with a small $\Lambda = 80^0$ canard, as shown in Figures 4.6. In this particular experiment, the sting balance was stationary while the wing was undergoing limit cycle roll oscillations. The data in Figure 4.6 show that the dynamic normal force is less than its steady state value multiplied by $\cos\phi$, implying a loss of lift during the limit cycle.

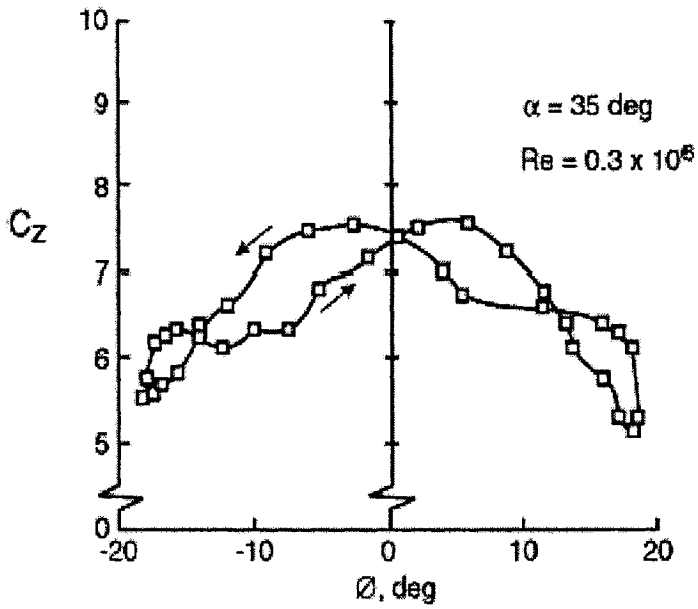

Figure 4.6 Histogram of the normal force coefficient during the wing rock limit cycle [82]

The hysteresis loop of the side force during the same experiment is presented in Figure 4.7, which shows a slight increase toward the side of the downward rolling wing. Both figures demonstrate a significant hysteresis loop, which changes direction at the larger rolling angles, creating additional 'outer loops'.

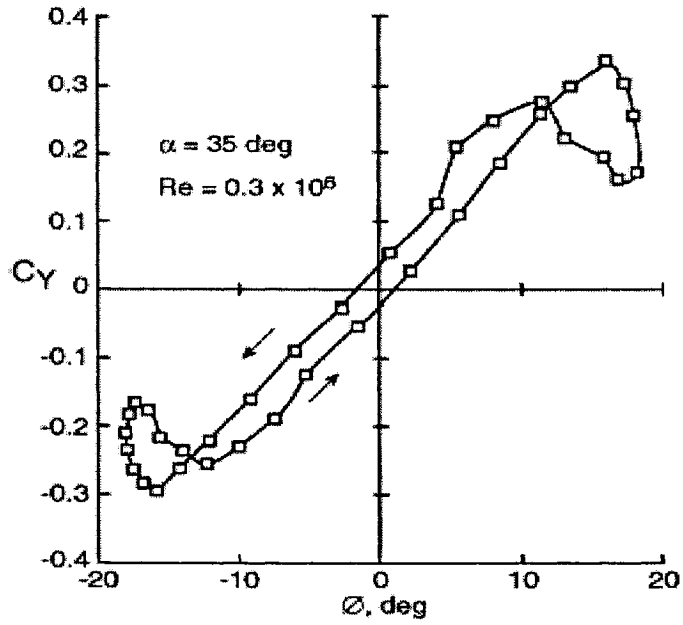

Figure 4.7 Histogram of the side force coefficient during the wing rock limit cycle [82]

Also, this trend can be demonstrated in Figure 4.8 from Reference [85] by calculating the roll acceleration during the roll limit cycle for an 80^0 delta wing. The authors indicated that the inner loop encloses the area in a clockwise sense and the loop traverses in the direction of increasing time. The positive area corresponds to the addition of energy to the system, and the negative area implies extraction of energy from the system. Therefore, the positive loop for $|\phi(t)| \leq 20^0$ is destabilizing, and the outer lobes for $20^0 < |\phi(t)| < 55^0$ are stabilizing. If the net area in Figure 4.7 is positive, the amplitude of the oscillatory motion increases and leads to a divergence. If the net area is negative, the oscillatory motion decays gradually (damped oscillation). If the net area is zero, it is a case of constant amplitude or limit cycle motion. It may be observed that the net area of the histogram is close to zero, confirming that the wing rock is an example of LCO.

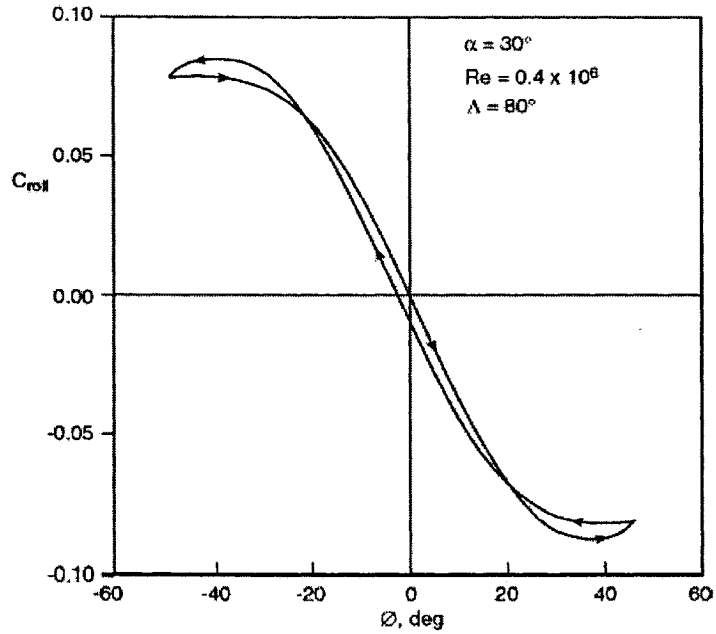

Figure 4.8 Typical wing rock hysteresis [85]

4.5 Summary

In this chapter, after introducing the Lyapunov's stability theory, we have proposed the energy analysis approach to analyze the hysteresis mechanism of driving wing rock phenomenon. First, the rate of energy change of wing rock phenomenon is derived. The hysteresis loops, based on a defined critical angle, are divided into two parts: a center loop ($dE/dt > 0$) and two reverse outer loops ($dE/dt < 0$). Then we have presented the simulation results and test results of wing rock hysteresis. The analytical results are in agreement with the observation of free-to-roll tests.

Chapter 5

Variable Phase Control of Wing Rock Phenomenon

In this chapter, we want to use the analytical results of Chapter 4 to suppress wing rock. Variable phase control issues of wing rock will be addressed. This chapter is organized as follows: Section 5.1 is the introduction, the variable phase control scheme is designed in Section 5.2, the simulation results of wing rock suppression is presented in Section 5.3, and Section 5.4 summarizes this chapter.

5.1 Introduction

Recently, considerable research has been conducted on the motion of 80^0 swept delta wing to help understand the fundamental mechanisms causing wing rock. The researchers in References [4, 79, 82, 84-86, 88-89] have *observed* that the hysteresis existing between the roll angle and the rolling moment provides clues for explaining wing rock mechanism. In addition, we have theoretically analyzed the hysteresis mechanism of wing rock in Chapter 4. Wing rock phenomena indicate the three-loop hysteresis during one cycle. Based on a defined critical angle, the three loops are divided into two parts: in a center

loop the energy flows into the system ($dE/dt > 0$) and in two reverse outer loops the energy is being dissipated ($dE/dt < 0$). On the boundary between increasing energy and decreasing energy, $dE/dt = 0$.

Now, the question is how to use these research results in the literature to control wing rock. The natural way of controlling wing rock phenomenon is directly to apply a hysteresis compensation approach to remove wing rock hysteresis effects.

In this chapter, a variable phase control (VPC) scheme is first proposed to suppress wing rock with hysteresis, inspired by the hysteresis mechanism of driving wing-rock motion studied in Chapter 4. The conception of the *phaser* proposed by Cruz-Hernandez in References [97-98] is adopted to design the variable phase control scheme.

The main objective of this chapter is to investigate the variable phase control to suppress wing rock with hysteresis. We will develop a variable phase control scheme to compensate the hysteresis effects of wing rock. To suppress wing rock completely, both the phase and the magnitude of hysteresis should be compensated. The suppression of wing rock with hysteresis will be demonstrated in six cases in order to verify the effectiveness and robustness of the proposed method.

5.2 Variable Phase Control

5.2.1 Phase Control

In general, the effects of hysteresis can be seen as a phase lag between a periodic input and a corresponding output. The natural way of correcting this lag is to reverse its effect. When a periodic input signal with period T is applied to a system with hysteresis, the output signal generally has the same period T as the input signal does but is shifted in some phase. In our wing-rock case, the output signal of wing-rock motion is complex and can be approximated by $y(\omega t - \varphi) = a_0 + \sum_{k=1}^{\infty}[a_k \cos(k\omega t) + b_k \sin(k\omega t)]$. If this signal is referenced to the input $u(t)$, all the components of $y(t)$ are shifted by some angle. It is possible to speak of phase shift between the input signal and the output signal. First of all, we introduce the concept of the *phaser* in References [97-98].

Definition: A *phaser* L_{ph} is an operator that shifts a periodic input signal by a constant angle $\varphi \geq 0$ and has unity gain.

In the frequency domain, the *phaser* can be expressed as

$$L_{ph}(j\omega) = a + jb, \quad \left|L_{ph}(j\omega)\right| = 1, \quad and \ \angle L_{ph}(j\omega) = \varphi \tag{5.1}$$

The basic idea of phase control can be explained with Figure 5.1, where a *phaser* L_{ph} is connected in series with a plant. If the plant is with hysteresis, the phase of the output signal $y(t)$ will be shifted by $-\varphi_s < 0$ with respect to the control input signal $u(t)$; if the *phaser* is used as a controller, then the phase of the control input signal $u(t)$ will be shifted by $\varphi > 0$ with respect to the input signal $r(t)$. If we design this *phaser* to make with $\varphi = \varphi_s$, the compensation can be obtained because one block cancels the other.

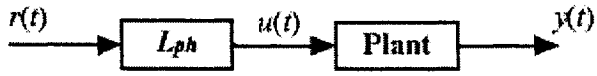

Figure 5.1 Hysteresis compensation

5.2.2 Variable Phase Compensation

In Figure 4.3, we have observed that when the wing rock develops into an LCO, it will exhibit three loops of hysteresis: a center loop and two reverse outer loops. The loop in the center resembles single-loop hysteresis with saturation; the two outer loops are symmetric but have a reverse phase angle. Therefore, the overall hysteresis compensation involves two types of *phasers*: a positive angle $\varphi_1 > 0$ for the center loop and a negative angle $\varphi_2 < 0$ for the outer loops. These angles can be obtained considering each loop independently from the other.

A variable *phaser* controller, based on the input signal $|r(t)|$ to switch from one *phaser* to the other, is given by

$$u(j\omega) = \begin{cases} L_{ph1}(j\omega)r(j\omega) & if\ |r| \le X_c \\ L_{ph2}(j\omega)r(j\omega) & if\ |r| > X_c \end{cases} \tag{5.2}$$

where $\angle L_{ph1}(j\omega) = \varphi_1 > 0$, $\angle L_{ph2}(j\omega) = \varphi_2 < 0$, and X_c is the *critical angle* defined in Section 4.3, where a change in the orientation of the loop occurs. It should be noted that when $|r(t)| > X_c$, the *phaser* $L_{ph2}(j\omega)$ is introduced in order to speed the oscillation attenuation, even if in this situation $dE/dt < 0$.

Obviously, the single-loop hysteresis during the build-up phase of wing rock like in Figure 4.3(e) is a special case, which means $\angle L_{ph2}(j\omega) = 0$.

5.2.3 Variable Phase Implementation

The *phaser* defined in Equation (5.1) is an ideal *phaser*. But we can approximately implement it by applying two important properties of the *phaser* described in References [97-98]: superposition and noncausality. Superposition follows from linearity. Noncausality prevents direct online implementation. Thus two linear filters are adopted to approximate the two *phasers* as

$$\begin{cases} L_{ph1}(s) = \dfrac{s^n + p_{1,n-1}s^{n-1} + \ldots + p_{1,1}s + p_{1,0}}{s^n + q_{1,n-1}s^{n-1} + \ldots + q_{1,1}s + q_{1,0}} & for\ \varphi_1 > 0 \\ L_{ph2}(s) = \dfrac{s^n + p_{2,n-1}s^{n-1} + \ldots + p_{2,1}s + p_{2,0}}{s^n + q_{2,n-1}s^{n-1} + \ldots + q_{2,1}s + q_{2,0}} & for\ \varphi_2 < 0 \end{cases} \tag{5.3}$$

where the coefficients $p_{i,n}$ and $q_{i,n}$ are determined such that the phase of the filters is almost constant around the design parameters φ_1 and φ_2 within the input signal frequency range $\omega = [\omega_1\ \omega_2]$. In other words, if we know the phase angles φ_1 and φ_2, we can calculate all the coefficients of Equation (5.3), which is described in detail in the Appendix A.

To design the *phaser*, the angle φ is the *sole* parameter we need to know. In a close-loop nonlinear system, it is difficult to find this angle. In general, the bigger the angle φ is, the faster will the system response be, but a too large value of φ can cause instability. If a small φ is chosen, wing rock motion will develop into some small LCOs. One simple

method is to choose a big φ and then to adjust this angle by evaluating control performance. As for the frequency range $\omega = [\omega_1 \ \omega_2]$ of compensation, because lower harmonic components usually have bigger coefficients, a low frequency range should be selected in order to obtain a better phase compensation.

In this study, we choose a six-order linear approximation for *phaser* $\varphi_1 = 36^0$ in the frequency range $[\omega_1 \ \omega_2] = [0.01 \quad 1]$ and design it as

$$L_{ph1}(s) = \frac{s^6 + 1.652s^5 + 0.7709s^4 + 0.1259s^3 + 0.00745s^2 + 0.00015s + 0.00000075}{s^6 + 3.017s^5 + 2.32s^4 + 0.5477s^3 + 0.05108s^2 + 0.0015s + 0.00001579} \tag{5.4}$$

The Bode Diagrams of *phaser* 36° in the frequency range $[\omega_1 \ \omega_2] = [0.01 \quad 1]$ are plotted in Figure 5.2.

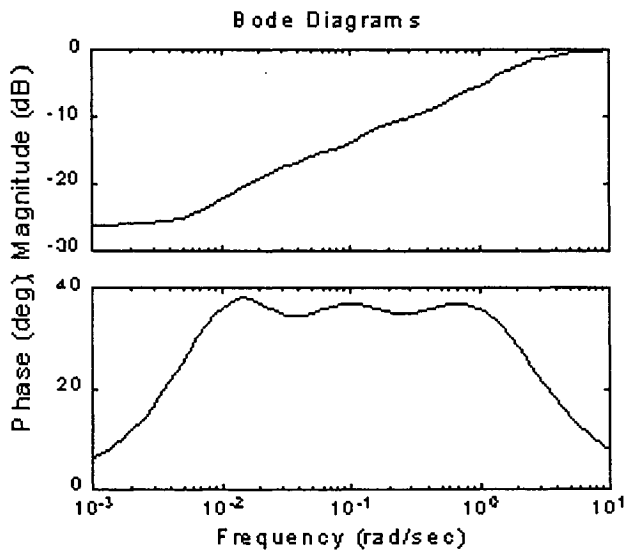

Figure 5.2 Bode Diagrams of *phaser* $\varphi_1 = 36^0$ in the frequency $[\omega_1 \ \omega_2] = [0.01 \ 1]$

For the *phaser* φ_2, for simplicity, let the *phaser* $\varphi_2 = -\varphi_1 = -36^0$; similarly, we have

$$L_{ph2}(s) = \frac{s^6 + 1.652s^5 + 0.7709s^4 + 0.1259s^3 + 0.00745s^2 + 0.00015s + 0.00000075}{s^6 + 0.7665s^5 + 0.2658s^4 + 0.02618s^3 + 0.001122s^2 + 0.000012s + 0.00000004} \tag{5.5}$$

Note that the different *phasers* have only the different values of q_i's in the denominator.

We should point out that the order of linear approximation usually depends on the value of *phaser* φ. If φ is big, we need a high order linear approximation; otherwise, it will affect the compensation effect. Besides, the method of variable phase control we consider above focuses on the phase shift or compensation of the output signal, whereas ignoring the magnitude compensation of the signal. The magnitude compensation will be discussed in the next section.

5.2.4 Implementation of Variable Phase Control

Before implementing the variable phase control scheme to suppress wing rock with hysteresis, we need to address two issues: the input signal of the *phaser* and the magnitude compensation of the *phaser*.

Input signal of the phaser: The wing rock hysteresis in Figure 4.3 is seen as the phase shift between the rolling moment coefficients and the roll angle, that is, $C_l = f(\phi, \dot{\phi})$. However, it is not the input-output relationship of the wing rock model given in Equation (2.9). We cannot directly use the variable phase control technique without the rolling moment information. Fortunately, we could obtain the term kC_l from Equation (4.11) as

the input signal of the *phaser*.

The magnitude compensation of the phaser: As mentioned earlier, the *phaser* only corrects the phase distortion of the system while ignoring the magnitude distortion. To suppress wing rock completely, both the phase and the magnitude need to be compensated. For this purpose, a *phaser* gain, $k_p \geq 1$, is applied in the control system. In general, the bigger the *phaser* gain k_p is, the faster will the system response be, but a too large value of k_p can cause overshoot, or even instability. In addition, we have observed that the system with a big k_p is more sensitive to the output measurement noise than the system with a small k_p.

Control structure: In Figure 5.1, the *phaser* is connected in series with the plant, which forms an open-loop control system. To suppress wing rock, we need the closed-loop control system and then propose the variable phase control scheme of wing rock, as shown in Figure 5.3. In this control structure, *phasers* $L_{ph1}(s)$ and $L_{ph2}(s)$ are switched

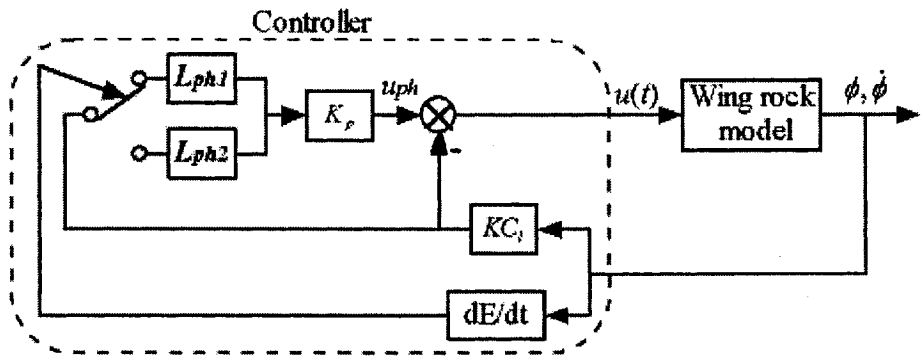

Figure 5.3 The variable phase wing rock control diagram

depending on the sign of *dE/dt*, k_p is the *phaser* gain, and kC_l is the input signal of the *phaser*. The overall control law in Figure 5.3 can be expressed by the sum of two terms: $u = -kC_l + u_{ph}$, the linearizing control law and the *phaser* control law with magnitude compensation.

5.2.5 Wing Rock Control Model

The differential equation of describing wing rock control in References [46-47, 49] is given by

$$\ddot{\phi} = (\rho U_\infty^2 Sb / 2I_{xx})C_l + u \tag{5.6}$$

where $\phi(t)$ is the roll angle, ρ is the density of air, U_∞ is the freestream velocity, S is the wing reference area, b is the chord, I_{xx} is the mass moment of inertia, $u(t)$ is the control input, and C_l is the rolling moment coefficients written as

$$C_l = b_0 + b_1\phi + b_2\dot{\phi} + b_3|\dot{\phi}|\dot{\phi} + b_4\phi^3 + b_5\phi^2\dot{\phi} \tag{5.7}$$

where the aerodynamic parameters b_i (i =0,1,2,3,4) are the time-varying functions of AOA.

Substituting Equation (5.7) into Equation (5.6), we have

$$\ddot{\phi} + a_0\phi + a_1\dot{\phi} + a_2|\dot{\phi}|\dot{\phi} + a_3\phi^3 + a_4\phi^2\dot{\phi} = u \tag{5.8}$$

where a_i (i =0, 1, 2, 3, 4) are the parameters relative to free-to-roll experiment conditions given in References [88-89]. A typical set of coefficients a_i is depicted in Figure 2.5. The other set of coefficients a_i can be found in References [88-89].

5.3 Simulation Results

The control objective is to suppress wing rock. This means to achieve the roll angle $\phi(t) = 0$ and the roll rate $\dot{\phi}(t) = 0$ when wing rock phenomenon occurs and commanded signal is $\phi = \dot{\phi} = 0$. Besides, the numerical simulations of wing rock control are implemented in Matlab and Simulink environments. Figure 5.4 shows the corresponding Simulink block diagram.

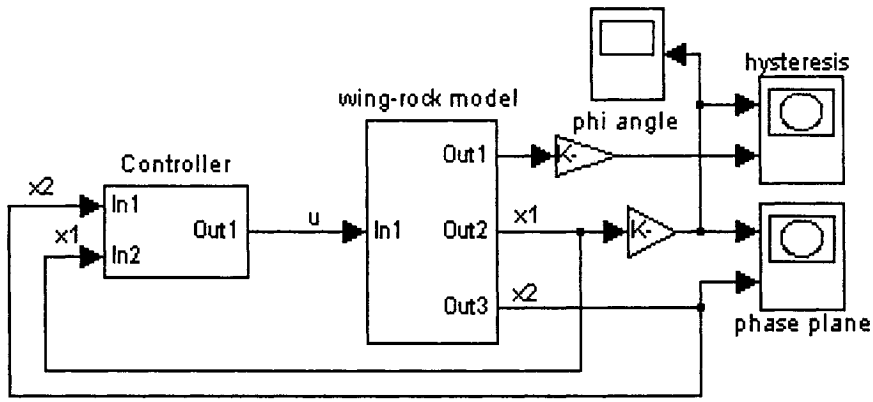

(a) The control system block diagram

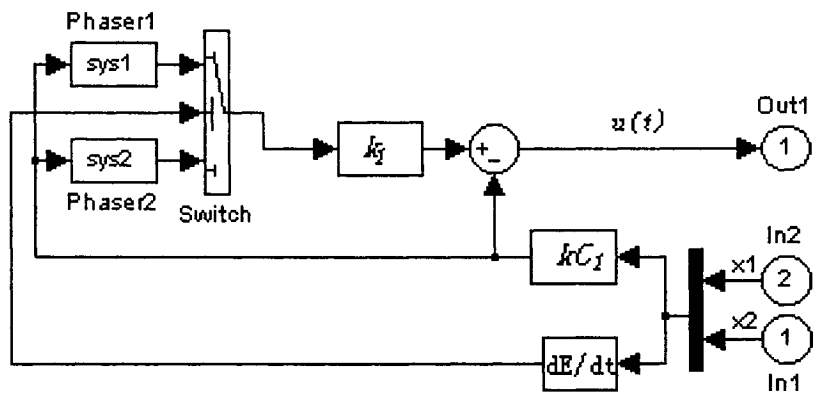

(b) The controller block diagram

Figure 5.4 Block diagrams of wing-rock control scheme in Simulink

The following six cases are used to verify the proposed variable phase control scheme, as shown in Reference [101].

Case 1: $AOA = 32.5^0$, k_1=1, $\varphi_1 = -\varphi_2 = 36^0$

To compare the performances achieved with the linearizing control law $u(t) = -kC_l$ and the overall control law $u(t) = -kC_l + u_{ph}$, the uncontrolled wing-rock motion is allowed to exhibit some LCOs, and then the controller is activated to suppress wing rock phenomenon, as shown in Figure 5.5. From this simulation, we have observed that if the system is with the control law $u(t) = -kC_l$, it is unstable; if the system is with the control law $u(t) = -kC_l + u_{ph}$, it is stable and can suppress wing rock quickly.

Case 2: The same as Case 1 except k_1 =6

When we simulated Figure 5.5(b) in *Case 1*, we observed that the control system is unstable in some initial conditions where they imply $dE/dt > 0$, for example, $\phi(0)$ =0 and $\dot{\phi}(0) = \dot{\phi}_{-\max}(t)$, as illustrated in Figure 5.6(b). If we modify the *phaser* gain from k_1 =1 to k_1 =6, then the proposed scheme can guarantee the control system stability and the system states tend towards zero with time, as shown in Figures 5.6(a) and 5.6(b). Figure 5.6(c) shows the corresponding *dE/dt* decreasing to zero over time, which reveals that the variable phase control essentially makes the system energy dissipative. Figure 5.6(d) displays the corresponding control input $u(t)$. If we compare this $u(t)$ with the $u_{\max}(t)$ ≈ -0.9 of Reference [102], we draw a conclusion that the proposed control scheme needs only a very small control input, which is important for aircraft control at a high AOA.

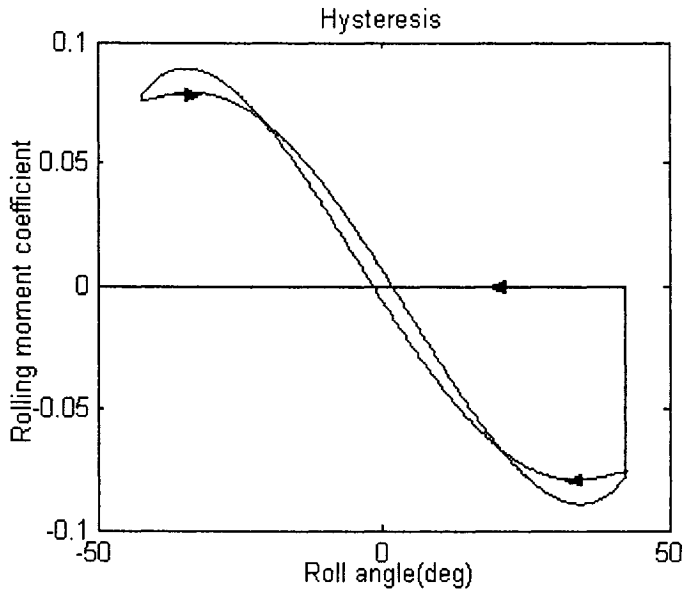

(a) Responses with the control law $u(t) = -kC_l$

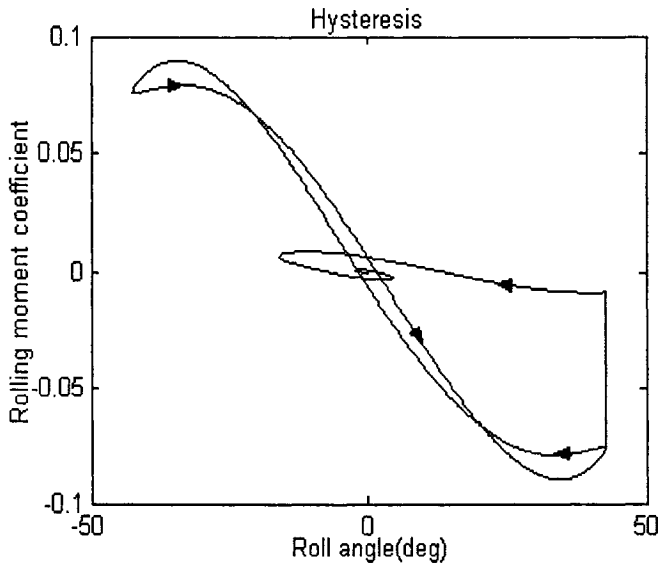

(b) Responses with the control law $u(t) = -kC_l + u_{ph}$

Figure 5.5 The performance comparison of the different control laws

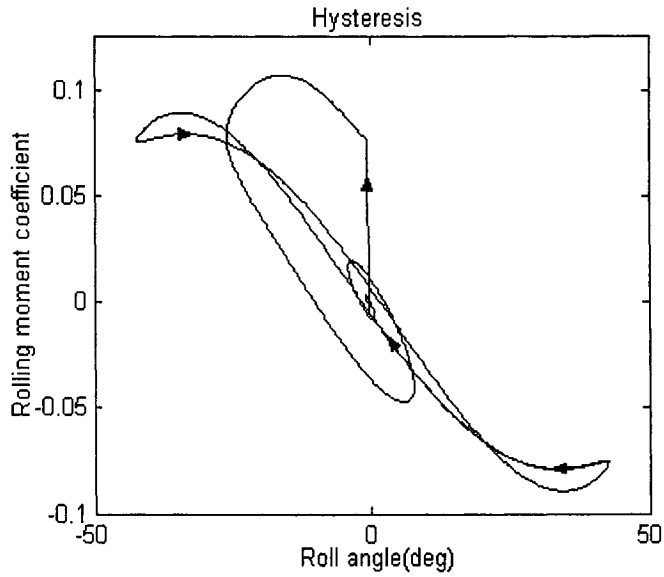

(a) Responses in hysteresis

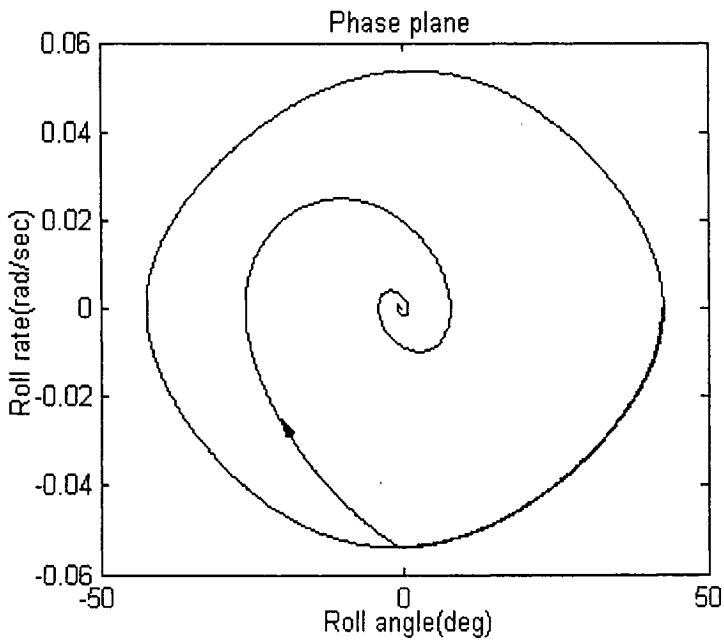

(b) Responses on phase plane

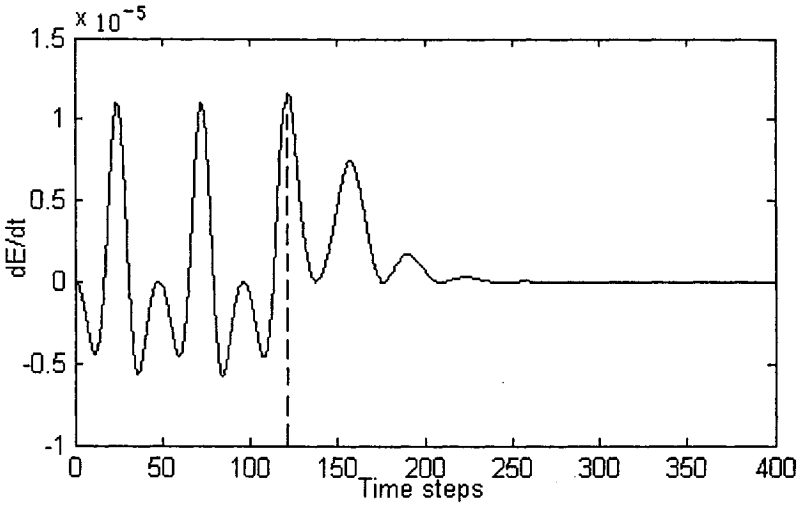

(c) The rate of change of energy

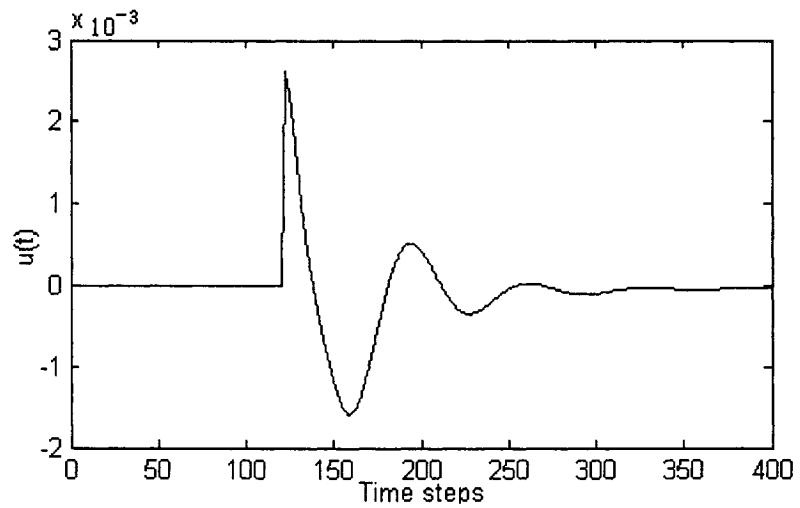

(d) Control input

Figure 5.6 Variable phase controls for *Case 2*

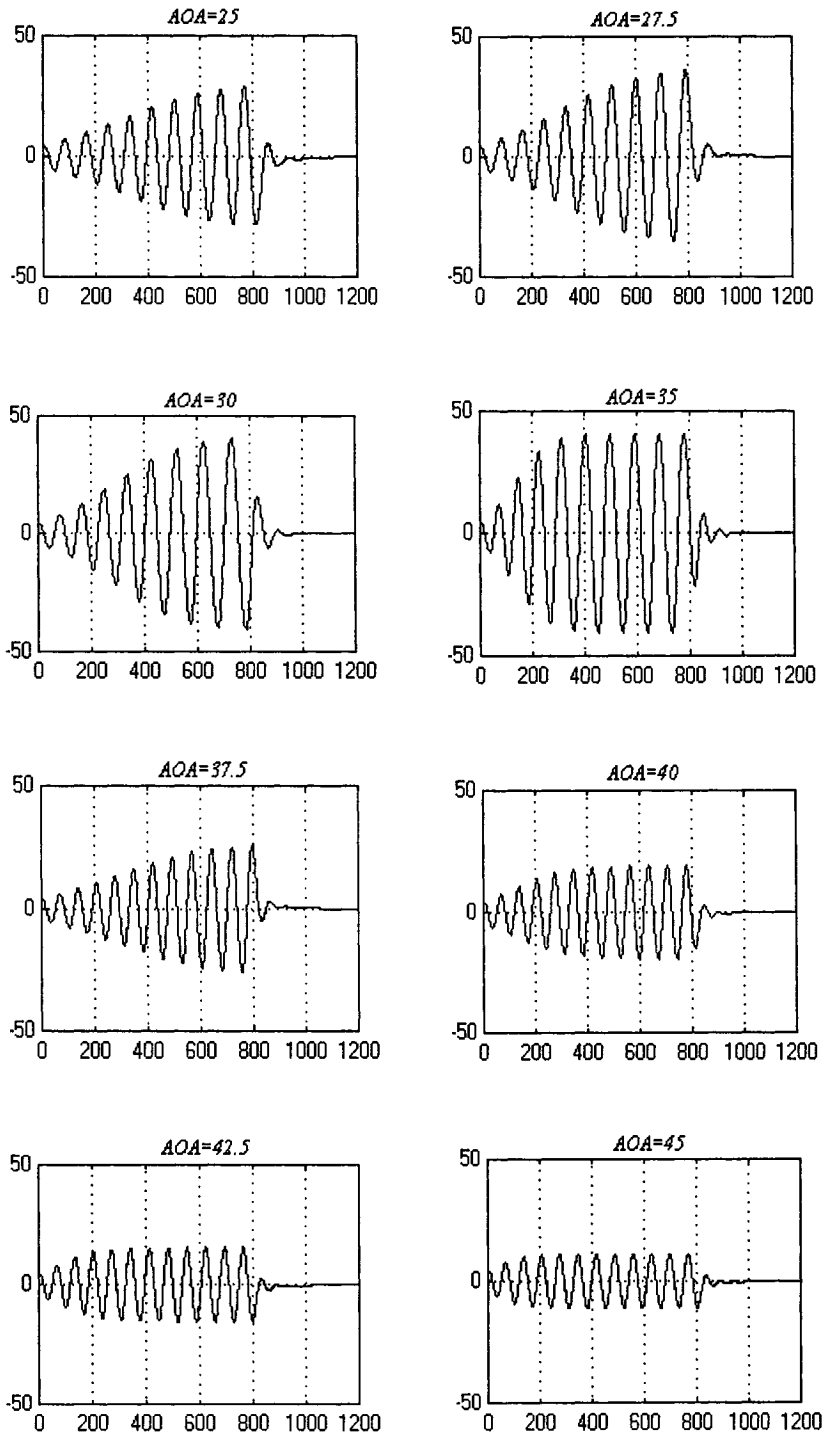

Figure 5.7 Output responses at the other fixed AOAs

Case 3: The same as Case 2 except AOAs

This case will verify the robustness of the proposed variable phase control method. Assume the initial condition of wing rock to be $\phi(0) = 5^0$ and $\dot{\phi}(0) = 0$. The controller can be activated at any time, say at t =800 time steps. Although the controller parameters remain the same as *Case 2,* the proposed control scheme can suppress the different wing rock motions at other fixed AOAs, that is, $AOA = 25^0, 27.5^0, 30^0, 35^0, 37.5^0, 40^0,$ 42.5^0, *or* 45^0, as shown in Figure 5.7.

Case 4: Single-phaser control ($AOA = 32.5^0$, k_1 =6, $\varphi_1 = 36^0$)

This simulation demonstrates a special case. We hope to suppress wing rock at the beginning of wing rock motion. In fact, single *phaser* $\varphi_1 = 36^0$ can easily achieve this aim because the wing rock motion during this time exhibits a single-loop hysteresis, as illustrated in Figure 4.3(e). If the *phaser* is activated at $t = 600$ time steps, Figure 5.8(a) shows the comparison outputs between the control system and the uncontrolled system, and Figure 5.8(b) indicates the corresponding change of *dE/dt*. From Figure 5.8(c), we have observed that once the *phaser* is activated, the direction of hysteresis loops will change from clockwise (the system absorbing energy) to anticlockwise (the system dissipating energy). We mark S as a starting point and draw arrows indicating its direction. Similarly, in Figures 5.5(b) and 5.6(a), regardless of the starting point at the outer loops or the center loop of hysteresis, the hysteresis development in all cases is forced to move in anticlockwise direction until the wing rock is completely suppressed.

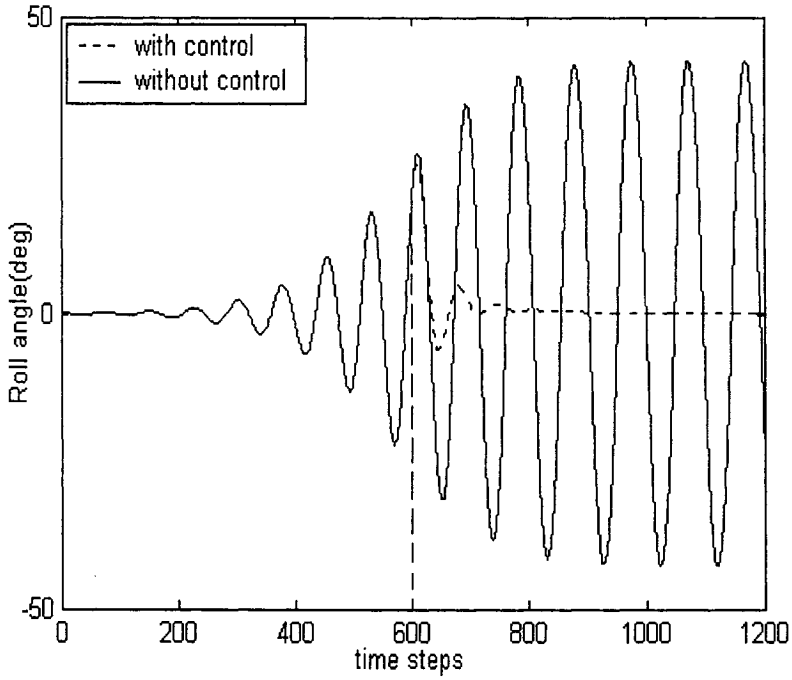

(a) Comparison of output responses

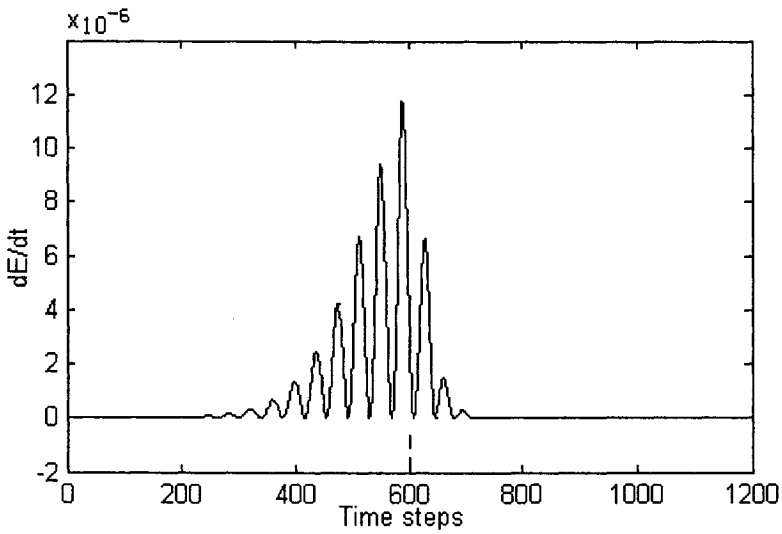

(b) The rate of change of energy

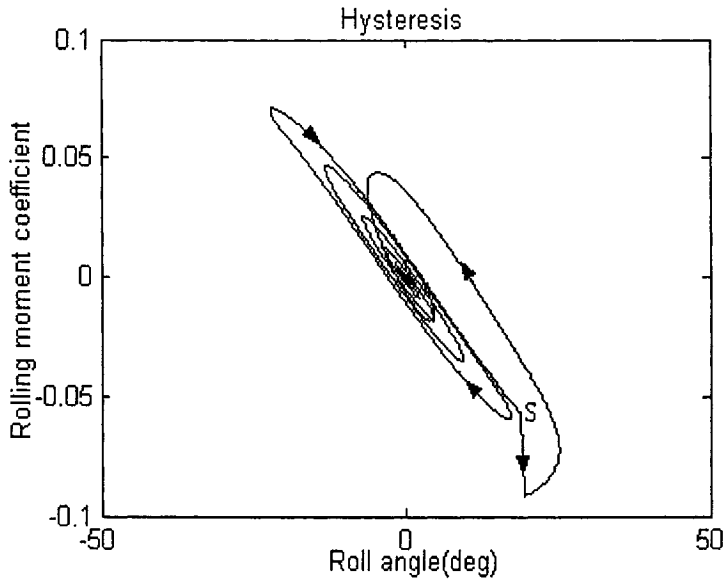

(c) Responses in hysteresis

Figure 5.8 Wing rock phase control for *Case 4*

Case 5: Comparison of different order phasers ($AOA = 32.5^0$, $k_p = 1$, $\varphi_1 = -\varphi_2 = 36^0$)

In this case, we compare the compensation performance of different order *phasers.* We take an example of the six-order *phaser* approximation in Equations (5.4) and (5.5) and a one-order *phaser* approximation designed as $L_{ph1}(s) = (s + 0.0075)/(s + 0.0285)$ for *phaser* $\varphi_1 = 36^0$ and $L_{ph2}(s) = (s + 0.0075)/(s + 0.00195)$ for *phaser* $\varphi_2 = -36^0$. Assume the initial condition is $\phi(0) = 42^0$ and $\dot{\phi}(0) = 0$. We have simulated the wing rock suppression with above two kinds of *phaser* approximations and observed that the response of the system with the one-order approximation is much slower than the response of the system with the six-order approximation, as shown in Figures 5.9(a) and 5.9(b), respectively.

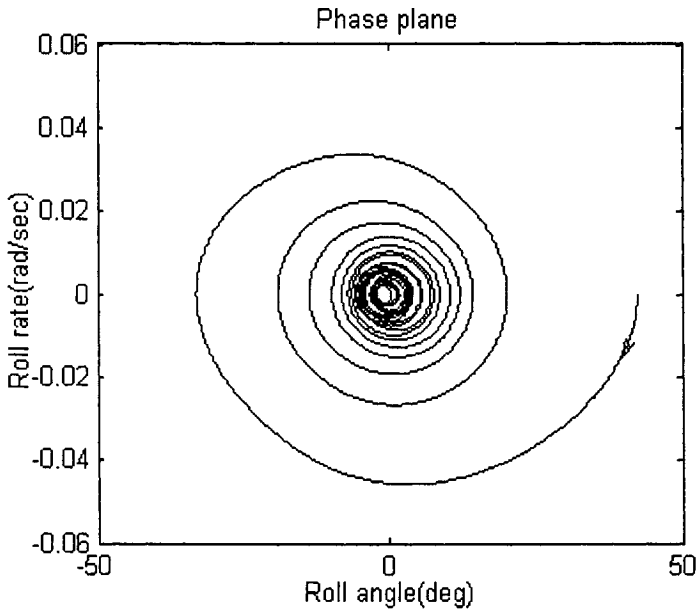

(a) Responses with the first-order *phaser* approximations

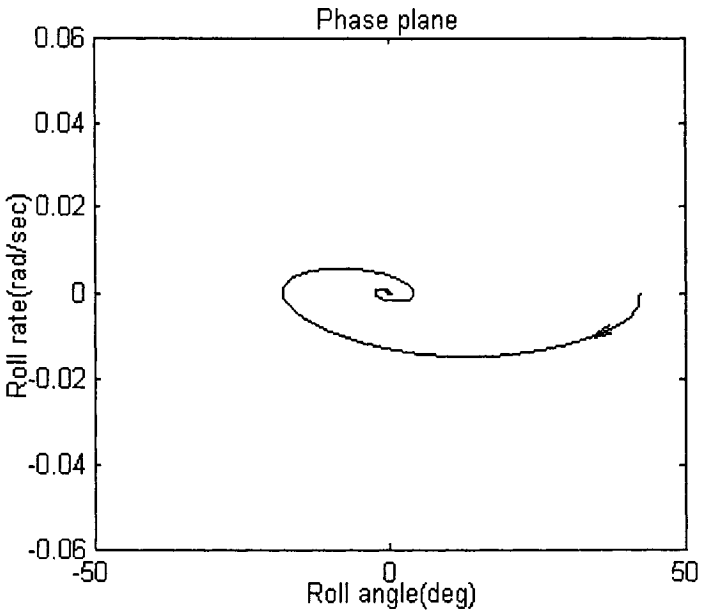

(b) Responses with the six-order *phaser* approximations

Figure 5.9 Response comparisons of different order phaser approximations

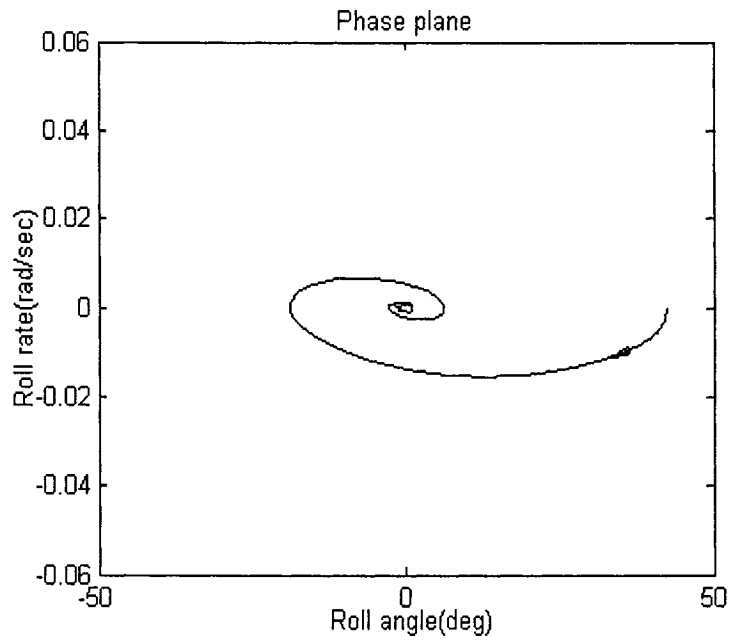

Figure 5.10 Wing rock suppression with the measurement noise

Case 6: System output with the measurement noise

Lastly, we illustrate a case of the variable phase control with the output measurement noise. Aassume a band limited white noise disturbance to be added to the system output variables, for example, $\phi(t)$ with the noise (its power is 10^{-4}, sample time is 0.05, and seed is 23341) and $\dot{\phi}(t)$ with the noise (its power is 10^{-6}, sample time is 0.05, and seed is 23341). The other parameters are the same as we simulate Figure 5.9(b). Figure 5.10 shows that the response of the control system is almost the same as Figure 5.9(b) except the small error at the equilibrium because the rate of signal and noise is lower. This result implies that the control system can work well with the measurement noise.

5.4 Summary

In this chapter, a variable phase control scheme has been developed to suppress wing rock with hysteresis at various AOAs and any initial conditions. After discussing the phase control scheme, we have designed the variable phase control scheme of wing rock suppression to compensate the phase and the magnitude for each part of the hysteresis. Simulation results show that the proposed control scheme, in nature, can guarantee wing-rock motion always to dissipate energy such that wing rock phenomena can be suppressed. The main advantages of proposed method are simple design and calculation, small control power need, and robustness. Therefore, the proposed control scheme may be an effective approach for wing rock suppression.

Part II

Intelligent Control Schemes of Wing Rock phenomenon with Unknown Disturbances

In Part I, we have presented wing rock models, investigated wing rock phenomena on phase plane, analyzed the energy mechanism of wing rock hysteresis, and then proposed the variable phase control scheme to suppress wing rock phenomenon with hysteresis. In Part II, we will devote to the problem of nonlinear controls of wing rock phenomenon with unknown disturbances. In the following Chapters 6-8, we will detail two types of fuzzy control schemes, the NDOFEL scheme, and reinforcement adaptive fuzzy control scheme. In this introduction section, we will discuss some general issues involved in nonlinear controls, emphasizing the intelligent control schemes of nonlinear systems with disturbances.

Generally, *the objective of control design* can be stated as:

Given a physical system to be controlled and the specifications of its desired behavior, construct a feed back control law to make the closed-loop system display the desired behavior.

In accordance with this design objective, we consider some key issues. First, we define two basic types of nonlinear control problems: suppressing and tracking. Next, we discuss the specifications of the desired behavior of nonlinear control systems. Finally, we briefly recall and remark the involved major methods of nonlinear controls.

1. Nonlinear Control Problems

When aircraft fly in a high AOA region where the aerodynamics is unstable, nonlinear effects in aircraft flight dynamics are significant. Therefore, nonlinear control schemes are necessary to achieve the desired performance of aircraft in a large flight envelope.

Generally, the tasks of control systems can be divided into two categories [94]: suppressing (or regulation, or stabilization) and tracking (or servo). In suppressing control problems, a control system, called a regulator (or a stabilizer), is to be designed so that the state of the closed-loop system will be suppressed around an equilibrium point. The control of wing rock suppression belongs to this type of problem.

The design objective of tracking control problems is to construct a controller so that the system output tracks a given time-varying trajectory. The tracking controls of wing rock try to make an aircraft fly along a specified roll path. To facilitate the analytic study of suppressing and tracking control design in this thesis, let us provide some formal definitions of suppressing and tracking problems.

Asymptotic Suppressing Problem: Given a nonlinear dynamic system described by

$$\dot{\mathbf{x}} = \mathbf{f}(\mathbf{x}, \mathbf{u}, t)$$

find a control law $\mathbf{u}(t)$ such that, starting from anywhere in a region in D, the state $\mathbf{x}(t)$ tends to $\mathbf{0}$ as $t \to \infty$.

Note that in the above definition, we allow the size of the region D to be large; otherwise, the suppressing problem may be adequately solved using linear control.

Asymptotic Tracking Problem: Given a nonlinear dynamic system described by

$$\dot{\mathbf{x}} = \mathbf{f}(\mathbf{x}, \mathbf{u}, t)$$

$$\mathbf{y} = \mathbf{h}(\mathbf{x})$$

and a desired output trajectory $\mathbf{x}_d(t)$, find a control law for the input $\mathbf{u}(t)$ such that, starting from any initial state in a region D, the tracking errors $\mathbf{e}(t) = \mathbf{y}(t) - \mathbf{x}_d(t)$ go to zero while the whole state $\mathbf{x}(t)$ remains bounded.

When the closed-loop system is such that proper initial states imply zero tracking error for all the time,

$$\mathbf{y}(t) \equiv \mathbf{x}_d(t) \quad \forall\, t \geq 0$$

the control system is said to be capable of perfect tracking. Asymptotic tracking implies that perfect tracking is asymptotically achieved; similarly, exponential tracking convergence can be defined.

Finally, we discuss the relation between suppressing and tracking problems. Normally, tracking problems are more difficult to solve than suppressing problems. Because in

tracking problems the controller should not only keep the whole state suppressed but also drive the system output toward the desired output. In fact, suppressing problems can be regarded as a special case of tracking problem, which means a desired trajectory $x_d(t)=0$.

2. Specifying the Desired Behavior

In linear control, the desired behavior of a control system can be systematically specified, either in the time-domain or in the frequency domain. However, systematic specification for nonlinear system is much less obvious because the response of a nonlinear system to one command does not reflect its response to another command, and furthermore a frequency-domain description is not possible.

As a result, for nonlinear systems, we often look instead for some qualitative specifications of the desired behavior in the operating region of interest. Computer simulation is an important complement to analytical tools in determining whether such specifications are met. To achieve the desired performance of wing rock control, we need to consider the following characteristics:

(a) *Stability* must be guaranteed for the nominal model (the model used for design), either in a local sense or in a global sense. The region of stability and convergence are also of interest.

(b) *Robustness* is the sensitivity to effects that are not considered in the design, such as disturbances, measurement noise, unmodeled dynamics, etc. The system should be able to withstand these neglected effects when performing the tasks of interest.

(c) *Accuracy and speed* of response may be considered for some "typical" motion trajectories in the region of operation. Appropriate controller design can actually guarantee fast tracking and very small tracking errors.

(d) *Simplicity and reliability* may be an aim of control system design. Among all feasible designs, we should prioritize to use a simple and reliable controller so that it can be applied for practical control. This also means considering the number and type of actuators and sensors and designed controller complexity for the low cost of a control system.

We need to do some explanations. Stability does not imply the ability to withstand persistent disturbances of even small magnitude. The reason is that stability of a nonlinear system is defined with respect to initial conditions, and only temporary disturbances may be translated as initial conditions. The effects of persistent disturbance on nonlinear system behavior are addressed by the concept of robustness. In addition, the above qualities conflict to some extent, and a good control system can be obtained only based on effective trade-offs in terms of stability/robustness, stability/performance, simplicity/performance, etc.

3. Control schemes of nonlinear systems with disturbances

The tracking control for uncertain nonlinear system with disturbances is a challenging problem. There is no general method for this problem. We will briefly discuss several useful control methods such as sliding-mode control, adaptive control, fuzzy control, neural network control, and neuro-fuzzy control.

On the other hand, in pure model-based control, the control law is designed based on a nominal model of the physical system. In practice, the model is usually imprecise. The model imprecision may come from actual uncertainty about the plant or from the purposeful choice of a simplified representation of the dynamics of systems. From a control point of view, modeling inaccuracies can be classified into two major kinds: parametric uncertainties and unmodeled dynamics. It is well known that modeling inaccuracies can have strong adverse effects on nonlinear control systems. Three major approaches to dealing with model uncertainty are sliding-model control, adaptive control, and fuzzy control.

3.1 Sliding-Mode Control

Sliding-mode control (SMC) is a kind of robust nonlinear controls. Robust control can handle model uncertainties associated with time varying systems. The goal of robust system design is to retain assurance of system performance in spite of model inaccuracies and changes. A system is robust when it has acceptable changes in performance due to model changes or inaccuracies. Hence, a robust control system exhibits the desired performance despite the presence of significant plant uncertainty.

The most significant property of SMC is its robustness. Loosely speaking, when a system is in a sliding mode, it is insensitive to parameter changes or external disturbances. Clearly, SMC is a good candidate for tracking control of uncertain nonlinear systems.

In practical application, a pure SMC suffers from the following main disadvantages. First,

there is the problem of chattering, which is the high-frequency oscillations of the controller output. Second, SMC may employ unnecessarily large control signals to overcome the parametric uncertainties. Last, but not the least, there exists appreciable difficulty in the calculation of what is known as the equivalent control.

For enhancing the performance of SMC, we are interested in intelligent controls such as fuzzy logic, neural networks, evolutionary computing, and other techniques adapted from artificial intelligence. These methodologies provide an extensive freedom for control engineers to exploit their understanding of the problem, to deal with problems of vagueness, uncertainty, or imprecision, and to learn by experience. Therefore, they are useful tools for alleviating the problems associated with SMC. In other words, the new control scheme from SMC combining with some intelligent control techniques usually has a better performance than only SMC does.

3.2 Adaptive Control

Many dynamic systems have constant or slowly varying uncertain parameters. Adaptive control is an approach to the control of such systems. The basic idea of adaptive control is to estimate the uncertain plant parameters on-line based on the measured system signals, and use the estimated parameters in the control input computation. In short, it can be regarded as a control system with on-line parameter estimation.

The basic objective of adaptive control is to maintain consistent performance of a system in the presence of uncertainty or unknown variation in plant parameters. Since such

parameter uncertainty or variation occurs in many practical problems, adaptive control is useful in many industrial fields. These include robotic manipulation, aircraft and rocket control, chemical processes, power systems, ship steering, and bioengineering.

In practice, the adaptive control system is often used to handle time-varying unknown parameters. The time-varying plant parameters must vary considerably slower than the parameter adaptation. This is often satisfied in most practical cases.

Generally, adaptive control is superior to SMC in dealing with uncertainties in constant or slowly varying parameters. The basic reason lies in the learning behavior of adaptive control systems: an adaptive controller improves its performance as adaptation goes on, whereas a robust controller simply attempts to keep consistent performance. Another reason is that an adaptive controller requires little or no a *priori* information about the unknown parameters, whereas a robust controller usually requires reasonable a *priori* estimates of the parameter bounds. Actually, SMC may be combined with adaptive control, leading to robust adaptive controllers in which uncertainties on constant or slowly-varying parameters is reduced by parameter adaptation and other sources of uncertainty are handled by robustness techniques.

However, for the case of the time-varying wing rock with unknown disturbances we will consider in the latter Chapters 7-8, a pure adaptive control is limited. There is reason to seek some new control schemes with effective algorithms to guarantee the robustness and stability of the time-varying control system.

3.3 Fuzzy Logic Control

Fuzzy logic control (FLC) is much closer in spirit to human thinking and natural language than the traditional logical systems. Basically, it provides an effective means of capturing the approximate, inexact nature of the real world. Viewed in this perspective, the essential part of FLC is a set of linguistic control rules related by the dual concepts of fuzzy implication and the compositional rule of inference. In essence, FLC provides an algorithm that can convert the linguistic control strategy based on expert knowledge into an automatic control strategy. It may be viewed as a step toward a rapprochement between conventional precise mathematical control and human-like decision.

Besides, FLC has the ability to perform effectively even in situations where the information about the plant is inexact and the operating conditions are uncertain. This ability of FLC makes it suitable for control applications to plants like aircraft that have nonlinear dynamics and operate in uncertain environments.

We should point out that the control performance of FLC, to some degree, depends on the fuzzy membership functions and rule-base. For a complex nonlinear system, several dozen fuzzy rules based on expert knowledge usually are needed in the control scheme, which makes the fuzzy design to be a tedious and time-consuming process. However, in this thesis we propose to use only four fuzzy rules instead of several dozen fuzzy rules in the control system. Meanwhile, we have developed adaptive algorithms or the NN with on-line learning algorithms to modify the parameters of fuzzy membership functions and to generate rule base from zero. The details are provided in Chapter 6.

3.4 Neural Network Control

Of the many different intelligent approaches, neural networks (NNs) appear to be growing in popularity due to the fact that are potentially capable of coping with some of the difficulties associated with conventional control approaches, such as computational complexity, presence of nonlinearities, and uncertainty. Their massively parallel architecture permits computation to be performed at high speeds. Because they can approximate nonlinear maps to any desired degree of accuracy, they possess at least the capacity to identify nonlinear dynamic systems. The fact that various rules are currently available for the adjustment of the parameters of the network on the basis of observed behavior implies that the networks can deal with uncertainty. In view of the versatility, neural networks have emerged as very powerful tools for designing intelligent control systems.

Generally, NN control strategies can be broadly classified into off-line and on-line scheme based on how the parameters of the network are tuned. When the neural controller operates in an on-line mode, it has no a *priori* knowledge of the system to be controlled, and the parameters of the network are updated while the input-output data is received. However, in the off-line control, the network's parameters are determined from the known training pairs, and then those parameters are fixed for control purposes.

3.5 Neuro-Fuzzy Control

FLC provides an effective means of capturing the approximate, qualitative aspects of human reasoning and decision–making processes. However, without adaptive capability,

the performance of FLC relies exclusively on two factors: the availability of human experts and the knowledge acquisition techniques to convert human expertise into appropriate fuzzy if–then rules and membership functions.

In practice, control engineers consider NNs as a tool for function approximation, self-learning and adaptive algorithms. The self-learning features of NNs are applied in learning the system dynamics, thereby tuning the controller parameters accordingly to provide a satisfactory or desired control response. Of course, it can be used in fuzzy inference systems. As a result, a fuzzy inference system can not only take linguistic information from human experts, but also adapt it using numerical input/output pairs to achieve better performance. This gives fuzzy inference systems an edge over NNs, which cannot take linguistic information directly.

Neuro-fuzzy control is especially suitable for the adaptive flight control where the system dynamics is dominated by the uncertain nonlinearities. In addition, among different choices of network structures, Gaussian function neural network shows its potential for on-line identification and control and thus arouses much interest.

Chapter 6

Fuzzy Control of Wing Rock Phenomenon

In this chapter, we first design the fuzzy proportional-derivative (PD) control for wing rock suppression and then propose the variable universe fuzzy PD control for wing rock tracking control with unknown disturbances. This chapter is organized as follows: A fuzzy logic system (FLS) is introduced in Section 6.1. In Section 6.2, the fuzzy PD control of wing rock phenomenon is designed. In the case of wing rock undergoing unknown disturbances, the variable universe fuzzy PD control scheme is proposed to track a desired trajectory in Section 6.3. Section 6.4 is the summary of this chapter.

6.1 Fuzzy Logic Systems

A FLS is a static nonlinear mapping between its inputs and outputs. Figure 6.1 plotted from Reference [103] shows this system where the system inputs are $x_i \in X_i$ (i=1, 2 ..., n) and the outputs are $y_i \in Y_i$ (i=1, 2 ..., m). x_i and y_i are "crisp", that is, they are real numbers, not fuzzy sets. Then the fuzzification block converts the crisp inputs to fuzzy sets. Next, the inference mechanism uses the fuzzy rules to produce fuzzy conclusions. Finally, the defuzzification block converts these conclusions into the crisp outputs.

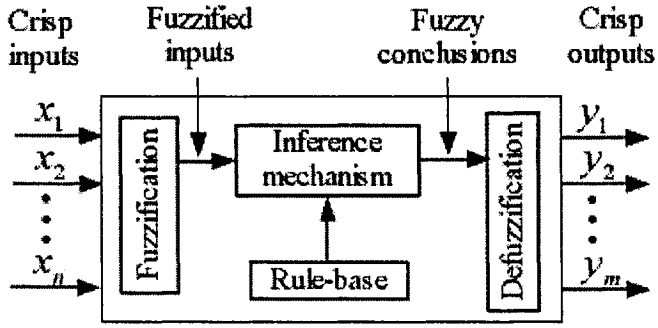

Figure 6.1 Fuzzy logic systems [103]

For discussing convenience, we also give several notions related to a FLS:

Universes of Discourse: The crisp sets X_i and Y_i are called the "universes of discourse" for x_i and y_i, respectively.

Linguistic Variable: For the fuzzy system, linguistic variables denoted by $\bar{x}_i$ are used to describe the inputs x_i. Similarly, linguistic variables denoted by $\bar{y}_i$ are used to describe outputs y_i.

Linguistic Values: Let $\bar{A}_i^j$ or $\bar{B}_i^j$ denote the j^{th} linguistic value of the linguistic variable $\bar{x}_i$ or $\bar{y}_i$ defined over the universe of discourse X_i or Y_i, that is,

$$\bar{A}_i = \{ \bar{A}_i^j : j = 1, 2 \ldots, N_i \}$$

$$\bar{B}_i = \{ \bar{B}_i^j : j = 1, 2 \ldots, M_i \}$$

Linguistic values are generally as "positive large," "zero," "negative big," etc.

Linguistic Rules: The mapping of the inputs to the outputs for a fuzzy system is in part

characterized by a set of condition/action rules, or If-Then form,

$$IF \text{ premise } THEN \text{ consequent} \tag{6.1}$$

Usually, the inputs of fuzzy system are associated with the premise, and the outputs are associated with the consequent.

Membership Functions: The function $\mu(x_i)$ associated with $\overline{A}_i^j$ that maps X_i to [0,1] is called a "membership function."

6.2 Fuzzy PD Control of Wing Rock Phenomenon

As we know, the fuzzy logic control has the ability to perform effectively even in situations where the information about the plant is inexact and the operating conditions are uncertain. This feature of the fuzzy logic control makes it suitable for controlling plants like aircraft that have nonlinear dynamics and operate in uncertain environments.

In the literature, Tarn and Hsu in Reference [55] developed a fuzzy controller with 9 fuzzy rules for wing rock suppression. Sreenatha *et al.* in Reference [56] presented the design and implementation of a FLC for wing rock suppression. The forty-nine fuzzy rules are tried out with the delta wing model in the wind tunnel. Malki *et al.* in Reference [104] derived an analytical structure for this fuzzy PD controller and also studied bounded-input/bounded-output (BIBO) stability analysis of a nonlinear fuzzy PD controller with small gain theorem. Mohan and Patel in Reference [105] presented the discrete version of this research.

In this preliminary study, fuzzy PD control is used for suppressing wing rock and tracking a constant roll angle or trajectory, as examined in Reference [102].

6.2.1 Properties of Conventional Linear PD Control

To begin with, we recall that the PD control law is described by

$$u(t) = K_p e(t) + K_d \dot{e}(t) \tag{6.2}$$

where K_p and K_d are the proportional and derivative gains of the controller, respectively, and $e(t)$ is the error signal defined by $e(t) = r(t) - x(t)$ in which $r(t)$ is the reference signal and $x(t)$ is the system output.

Equation (6.2) can be written as

$$\dot{e} = -\frac{K_p}{K_d} e + \frac{1}{K_d} u \tag{6.3}$$

Let $u = 0$, $u > 0$, and $u < 0$, respectively. We can draw three straight lines on phase plane, as shown in Figure 6.2, where H denotes the distance between a line $u = 0$ and lines $u \neq 0$ and can be expressed as

$$H = \frac{u}{\sqrt{K_p^2 + K_d^2}} \tag{6.4}$$

From the Figure 6.2, we can outline the properties of the PD controller on phase plane:

(a) There is the "zero line" on which the controller output is equal to zero.

(b) The control output is positive (negative) in upper (lower) part of the zero line.

(c) The magnitude of the control output is linearly proportional to the distance H from the zero line in Figure 6.2.

These properties are useful to design a fuzzy PD control system.

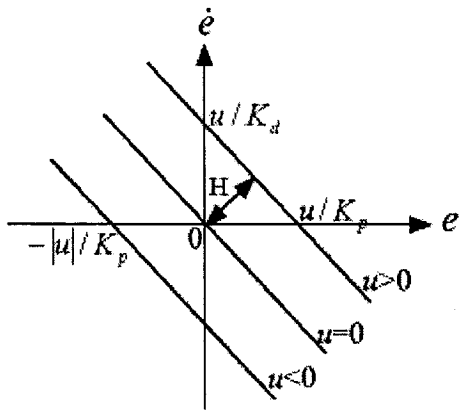

Figure 6.2 Phase-plane expressions of PD control

6.2.2 Fuzzy PD Control

Fuzzy control system design usually includes four parts: 1) fuzzification, 2) fuzzy rule-base, 3) fuzzy inference, and 4) defuzzification. The structure of fuzzy PD control is shown in Figure 6.3.

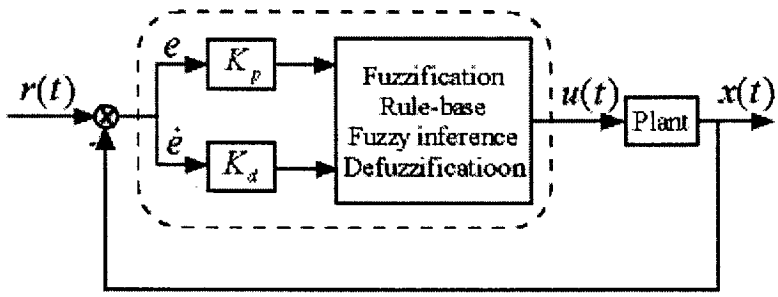

Figure 6.3 Fuzzy PD control diagram

1) Fuzzification

The two input variables are the error $e(t)$ and the rate of its change $\dot{e}(t)$, and the one output variable $u(t)$ is fed to the controlled plant. Membership functions of $e(t)$ and $\dot{e}(t)$

are shown in Figure 6.4(a). Each has two membership values: positive and negative, whereas $u(t)$ with a singleton membership function has three values: positive, negative and zero, as shown in Figure 6.4(b).

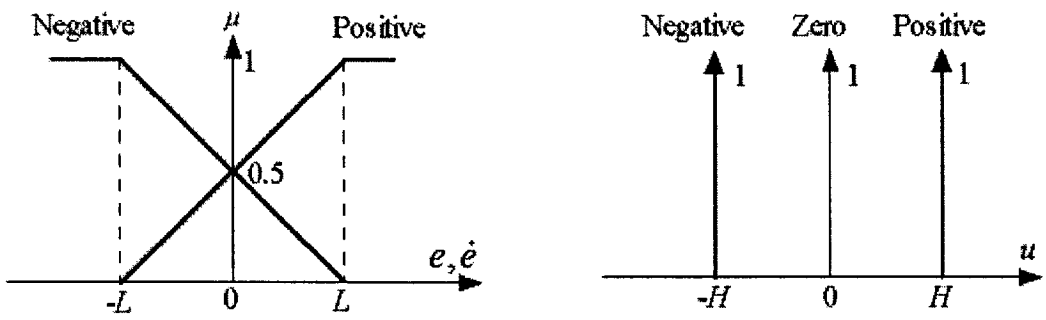

(a) Inputs $e(t)$ and $\dot{e}(t)$ (b) Output $u(t)$

Figure 6.4 Membership functions

Next, we discuss the universes of fuzzy variables. Let $X_i = [-L \quad L]\,(i = 1, 2)$ be the universes of input variables $e(t)$ and $\dot{e}(t)$. To employ the same membership functions on the two inputs, two scaling factors, K_P and K_d, are introduced to magnify input signal values. Similarly, let $Y = [-H \quad H]$ be the universe of output variable $u(t)$. The constants L and H, which are used in the definition of the membership functions in Figure 6.4, are chosen by the designer, according to the value ranges of the error, the rate of its change, and the output signal. After being determined, they are fixed.

2) Fuzzy Rule Base

Based on the defined membership functions, the corresponding fuzzy rule-base is specified as follows:

R1: *IF* $e(t)$ =*ep* *AND* $\dot{e}(t)$=*rp* *THEN* output =**op**

R2: *IF* $e(t)$ =*ep* *AND* $\dot{e}(t)$=*rn* *THEN* output =**oz**

R3: *IF* $e(t)$ =*en* *AND* $\dot{e}(t)$=*rn* *THEN* output =**on**

R4: *IF* $e(t)$ =*en* *AND* $\dot{e}(t)$=*rp* *THEN* output =**oz**

where *ep* is denoted as a positive error, *en* as a negative one, *rp* as the rate of positive error change, *rn* as the rate of negative error change, **op** as a positive output, **oz** as a zero output, and **on** as a negative output.

What is the reason for establishing these fuzzy rules? We give an illustrational explanation in Figure 6.5, assuming the output error signal of wing rock control to be an approximate sinusoidal wave. In addition, for suppressing control the reference signal is $r(t) = 0$; thus, we have $e(t) = r(t) - x(t) = -x(t)$ and $\dot{e}(t) = \dot{r}(t) - \dot{x}(t) = -\dot{x}(t)$. This explanation relates to the sign of input variables $e(t)$ and $\dot{e}(t)$ with time as follows.

(a) *For Rule 1:* In phase I, the condition $ep = e > 0$ implies that $x < 0$, and the condition $rp = \dot{e} > 0$ implies that $\dot{x} < 0$. In this case, the controller should drive the system output upward. We let output be **op**.

(b) *For Rule 2:* In phase II, the condition $ep = e > 0$ implies that $x < 0$, and the condition $rn = \dot{e} < 0$ implies that $\dot{x} > 0$. In this case, the controller will automatically perform the expected task to drive the system output toward zero. Thus the controller needs not to take any action; we can set output to be **oz**.

(c) *For Rule 3:* In phase III, the condition $en = e < 0$ implies that $x > 0$, and the condition $rn = \dot{e} < 0$ implies that $\dot{x} > 0$. In this case, the controller should drive the system output downward. We let output be **on**.

(d) *For Rule 4*: In phase IV, the condition $en = e < 0$ implies that $x > 0$, and the condition $rp = \dot{e} > 0$ implies that $\dot{x} < 0$. In this case, the controller is driving the system output toward zero. It is similar to *Rule 2* that we set output to be **oz**.

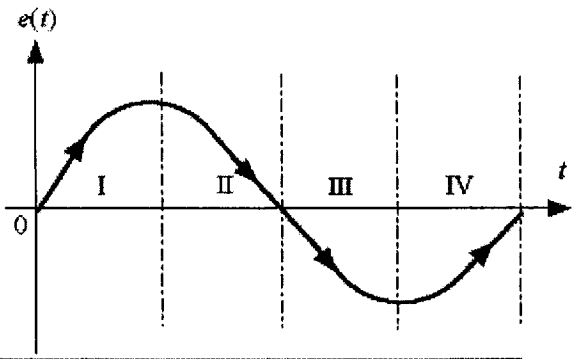

	I	II	III	IV
Input $e(t)$	>0	>0	<0	<0
Input $\dot{e}(t)$	>0	<0	<0	>0
Output $u(t)$	**op**	**oz**	**on**	**oz**

Figure 6.5 The four different phases of the output error signal

3) Fuzzy Inference

Fuzzy inference is the process of formulating the mapping from a given input to an output by using fuzzy logic. This mapping provides a basis from which decisions can be made. Mamdani's fuzzy inference method is the most commonly used fuzzy methodology. Consider *Max-Min* composition with Mamdani implication for the four fuzzy rules with two antecedents.

$$R_i: \quad IF\ e\ is\ A_i\ AND\ \dot{e}\ is\ B_i\ THEN\ u\ is\ C_i \qquad i=1,2,3,4.$$

If the crisp inputs are a_0 and b_0, the firing strength α_i of the rules is computed by

$\alpha_i = A_i(a_0) \cap B_i(b_0)$. Each rule conclusion is obtained by $C_i^* = (\alpha_i \cap C_i)$. The entire system conclusion is obtained by $C^* = (C_1^* \cup C_2^* \cup C_3^* \cup C_4^*)$.

4) Defuzzification

Defuzzification is a process to convert the fuzzy set obtained from an inference mechanism into a single value. Perhaps the most popular defuzzification method is the centroid calculation or COG, which returns the center of the area under the curve.

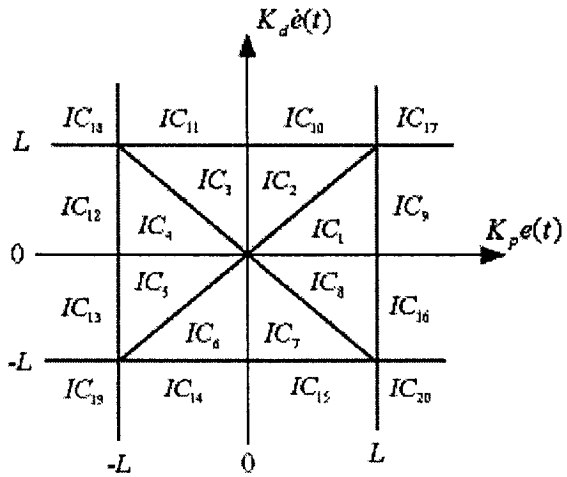

Figure 6.6 Regions of possible input combinations (ICs) [104]

All possible input combinations (ICs) of '$e(t)$' and '$\dot{e}(t)$' are shown graphically in Figure 6.6 from Reference [104]. The control rules, the membership functions, and IC regions are used to evaluate an appropriate fuzzy control law to each region.

By employing the formula of center of gravity, we can obtain the closed-form fuzzy PD control law

$$u(t) = u_{fuzzy}(t) \tag{6.5}$$

where

$$u_{fuzzy}(t) = \frac{L(K_p e(t) + K_d \dot{e}(t))}{2(2L - K_p|e(t)|)} \quad \text{in } IC_1, IC_4, IC_5, \text{ and } IC_8.$$

$$= \frac{L(K_p e(t) + K_d \dot{e}(t))}{2(2L - K_p|\dot{e}(t)|)} \quad \text{in } IC_2, IC_3, IC_6, \text{ and } IC_7.$$

$$= \frac{(L + K_d \dot{e}(t))}{2} \quad \text{in } IC_9 \text{ and } IC_{16}.$$

$$= \frac{(L + K_p e(t))}{2} \quad \text{in } IC_{10} \text{ and } IC_{11}.$$

$$= \frac{(-L + K_d \dot{e}(t))}{2} \quad \text{in } IC_{12} \text{ and } IC_{13}.$$

$$= \frac{(-L + K_p e(t))}{2} \quad \text{in } IC_{14} \text{ and } IC_{15}.$$

$= L$ or $-L$ in IC_{17} or IC_{19}.

$= 0$ in IC_{18} and IC_{19}.

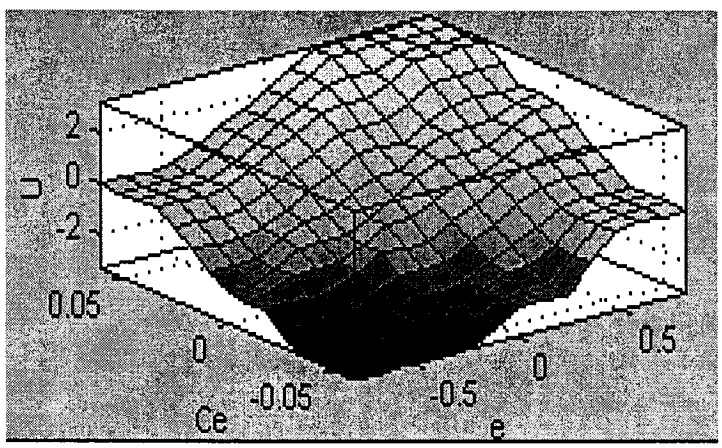

Figure 6.7 Output surface views of fuzzy PD control

In addition, using Fuzzy Logic Toolbox, we can see the entire output surface of the fuzzy PD control in Figure 6.7, which implies that the entire span of the output set is based on the entire span of the input set, $u(t) = f(e, \dot{e})$. With the number of fuzzy rules increasing, the output surface in Figure 6.7 will become smoother surface.

6.2.3 Stability Analysis

There are a considerable amount of efforts devoted to the stability analysis of fuzzy control systems in the literature. As for the fuzzy PD control system, Malki *et al.* in Reference [104] presented the bounded-input/bounded-output (BIBO) stability analysis with small gain theorem. The following is the stability statement.

Theorem: A sufficient condition for the nonlinear fuzzy PD control systems to be stable is that the given nonlinear process has a bounded norm (gain) $\|N\| < \infty$ and the parameters of the fuzzy PD controller, K_P, K_d, and K_u, satisfy

$$\frac{\gamma K_M K_u}{2T(H - K_m)}\|N\| < 1 \tag{6.6}$$

where $\gamma = \min\{1, H\}$, $K_m = \max\{K_P, K_d\}$, $K_M = \max\{K_P M_e, K_d M_r\}$, $M_e = \sup_{n\geq 0}|e(nT)|/T$, $M_r = \sup_{n\geq 1}\frac{1}{T}|e(nT) - e(nT - T)| \leq 2M_e$, and T is the sampling period.

6.2.4 Simulation Results

Wing rock suppression is used as an example to illustrate the performances of the proposed fuzzy PD control. The control model has been given in Equation (5.8).

The following three cases are used to illustrate the effectiveness of the proposed controller. The parameters of the controller in Equation (6.5) are designed as $L = \pm 0.7$ rad, $K_P = 1$, $K_d = 0.07$, and $H = \pm 3.2$.

Case 1: The comparison of three control schemes

In this case, we compare the proposed control scheme with the schemes in References [55-56] to suppress wing-rock at a big initial roll angle, for example, $\phi(0) = 55^0$ and $\dot{\phi}(0) = 0$. The simulation results of three different control schemes are shown in Figure 6.8, including the output responses $\phi(t)$ and the control inputs $u(t)$. The results show that the proposed fuzzy PD controller gives a better regulation as compared with Reference [55] and has similar performance as compared with Reference [56] where 49 fuzzy rules are used.

Case 2: Tracking constant trajectory $r(t) = -10^0$

To verify the tracking performance of the proposed fuzzy PD control, we assume the desired constant trajectory $r(t) = -10^0$ at the initial condition $\phi(0) = 43^0$ and $\dot{\phi}(0) = 0$. The controller can be activated in any time, for example, at t =200 time steps. Figure 6.9(a) shows the output response of the wing rock control, and Figure 6.9(b) shows the same output response on phase plan. The results show that the proposed control scheme can track a constant trajectory.

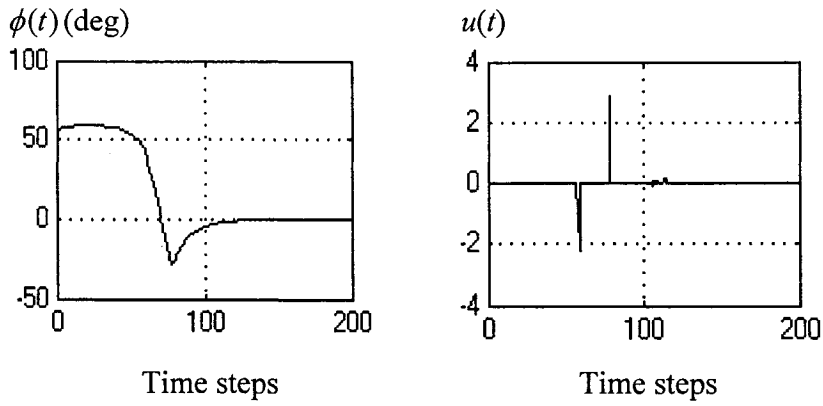

(a) Reference [55] with 9 fuzzy rules

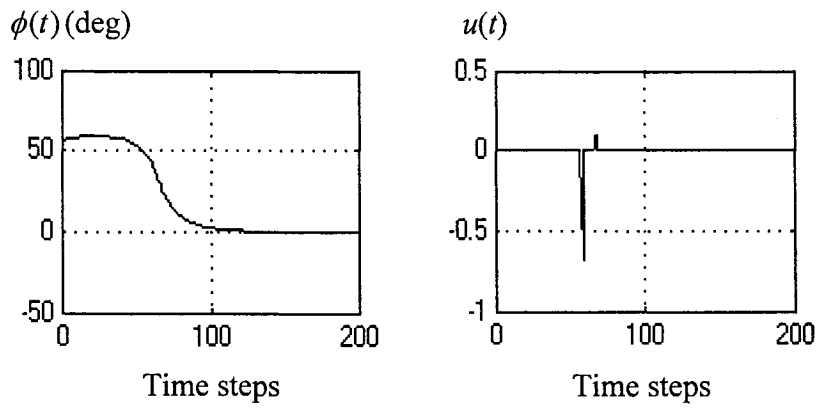

(b) Reference [56] with 49 fuzzy rules

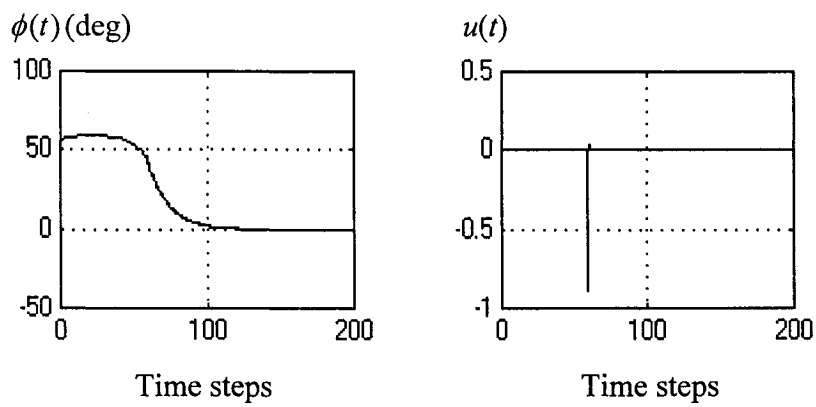

(c) The proposed controller with 4 fuzzy rules

Figure 6.8 Comparisons between three fuzzy controllers

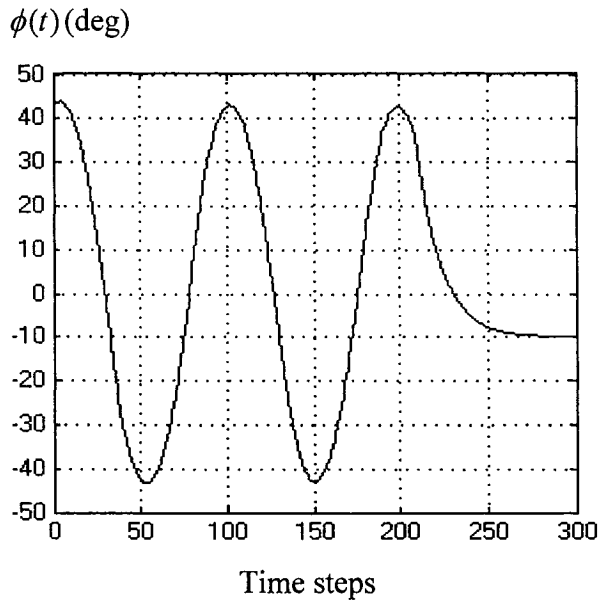

(a) Output response

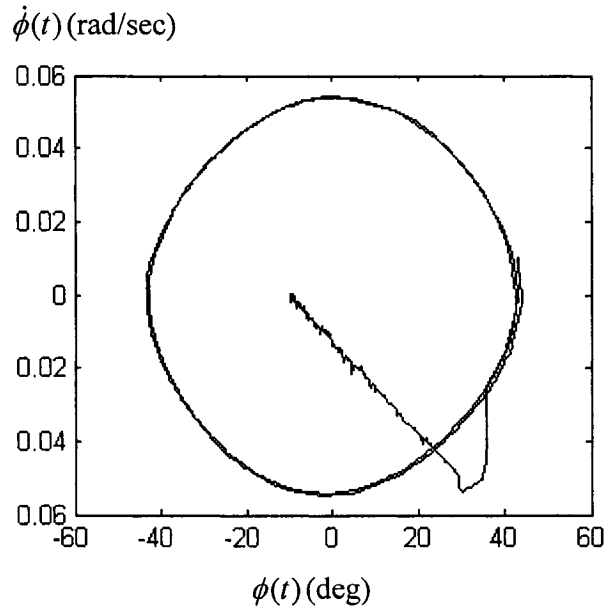

(b) Output response on phase plane

Figure 6.9 Tracking $r(t) = -10^0$ at $\phi(0) = 43^0$ and $\dot{\phi}(0) = 0$

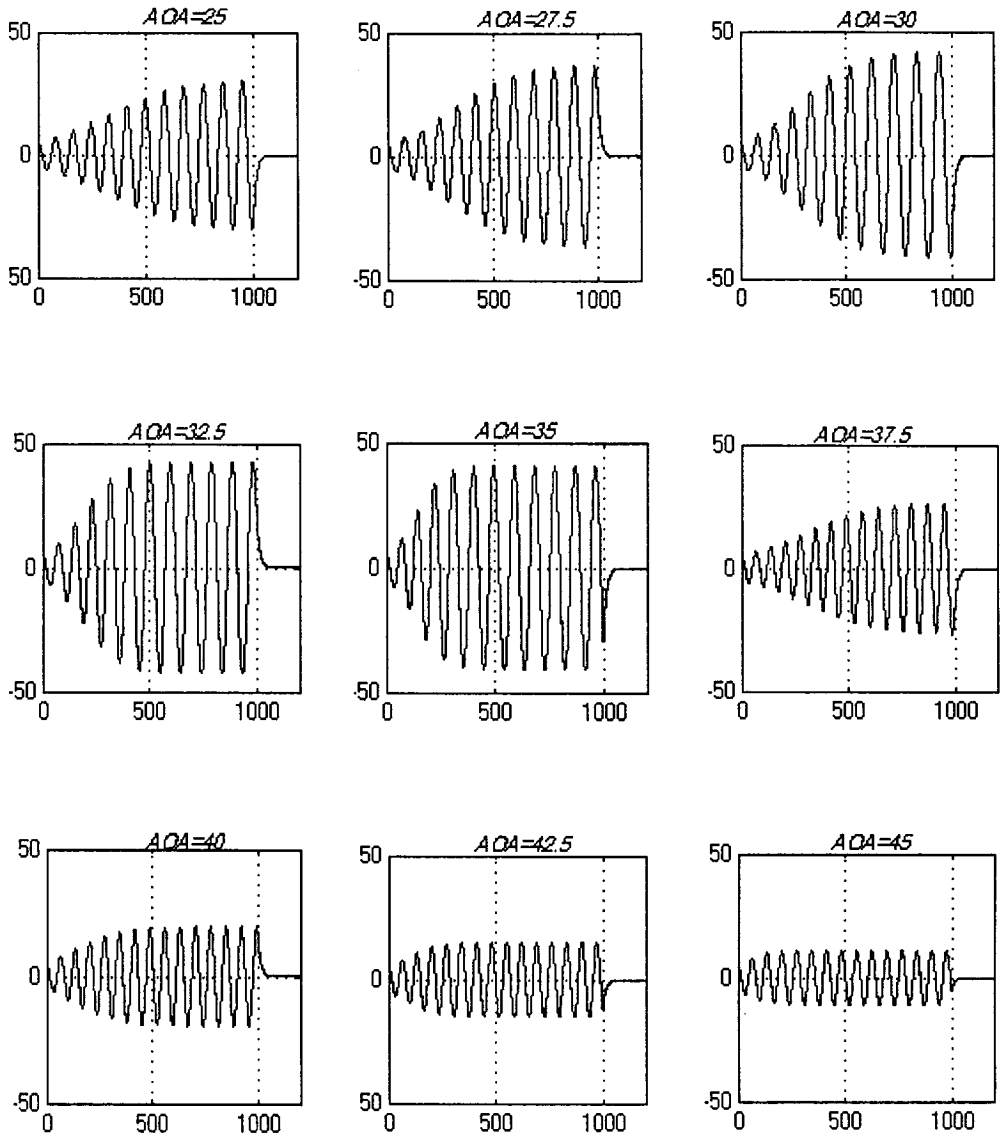

$\phi(t)$ (deg) versus time steps

Figure 6.10 Simulation results at the nine different AOAs

Case 3: Suppress wing rock at different AOAs

To verify the robustness of the proposed controller, we use the proposed controller to suppress wing rock phenomenon at nine different AOAs, assuming the initial condition

as $\phi(0) = 5^0$ and $\dot{\phi}(0) = 0$ and the controller activated at t =1000 time steps; of course, you can choose any initial time. Even though the parameters of the proposed fuzzy PD controller are fixed and the AOA in Equation (5.8) vary in a wide range from 25^0 to 45^0, wing rock phenomenon can be quickly suppressed, as shown in Figure 6.10.

Observations:

(a) The fuzzy PD controller can switch control actions in Equation (6.5), which depends on the change of input signals with time. Moreover, the control action in Figure 6.7 is always continuous and smooth.

(b) The designed fuzzy PD controller, by nature, is a nonlinear controller, that is, $u(t) = f(e, \dot{e})$. In contrast, the conventional PD controller is a simple linear controller.

(c) The fuzzy PD control has better robustness than the conventional PD control.

6.2.5 Conclusions

We have designed a fuzzy PD control scheme for wing rock control. First we have discussed the properties of conventional PD controller, which leads to the design of fuzzy PD controller. Next we have presented the numerical simulation results to verify the effectiveness and robustness of the proposed fuzzy PD control. Even though the proposed fuzzy PD control uses only four fuzzy rules, the numerical simulation results show that the proposed control scheme is simpler and more effective than the schemes of References [55-56] to control wing rock phenomenon.

6.3 Variable Universe Fuzzy PD Control

6.3.1 Introduction

For a large class of second order nonlinear systems, the fuzzy PD control is designed with respect to phase plane determined by error $e(t)$ and the rate of error change $\dot{e}(t)$ according to the states $x(t)$ and $\dot{x}(t)$. As discussed in Section 6.2.4, the fuzzy PD control has a nonlinear regulation law and is better than the conventional PD control. However, if the system suffers from some disturbance, the fuzzy PD control exhibits a big steady-state error, in essence, because of lacking an integral component in the controller.

In the literature, the selection of appropriate membership functions in FLC is an important issue because a change of fuzzy membership function may alter the performance of the fuzzy controller significantly. Several algorithms of tuning of the fuzzy membership function have been proposed in References [106-109]. These algorithms have an important characteristic of global tuning of the fuzzy membership functions, but they need off-line preprocessing or need repeated simulations. Moreover, to improve the precision of fuzzy control, we usually rely on adding the number of fuzzy rules, which makes the fuzzy design a tedious and time-consuming process.

In this study, variable universe fuzzy PD scheme, based on an interpolation mechanism of FLS, is utilized for the on-line tuning of fuzzy membership functions to improve the tracking precision and robustness of the control system with several fuzzy rules when the system undergoes unknown disturbances.

To verify the effectiveness of the proposed method, we demonstrate the suppressing and tracking control of wing rock motion with unknown disturbances, which include un-modeled dynamics and external disturbances.

6.3.2 Fuzzy Control with Switching Mechanism

1) Control Scheme

As discussed in Section 6.2.4, the fuzzy PD control is a nonlinear controller and has better performance than the conversional PD control. But when the system is near steady state, the fuzzy PD control can be interpreted as an approximation of a linear PD controller (see Appendix B in detail). If the control system is with disturbances, the system output may lead to an unaccepted error.

To improve the tracking precision and robustness of the fuzzy PD control in the steady state of the system, we propose a variable universe fuzzy control algorithm, which can be considered as a fine controller.

The developed control strategy, as illustrated in Figure 6.11, is limited to a second-order nonlinear system such as the wing-rock motion. A switching mechanism in this scheme is introduced. In the initial control stage, the tracking error usually has a big value, that is, $|e(t)| > e_0$, where e_0 is a switch threshold value given by designers, the task of the control system is to eliminate the tracking error. During this stage, the fuzzy PD control designed in Section 6.2.2 with fixed membership functions is used. In fact, it is a coarse controller. The aim of the fuzzy PD control is to keep the fast adjustment. When the system tends to

the steady state, and the output signal enters in a small error range, $|e(t)| \le e_0$, the controller is switched to a fine fuzzy controller, that is, the variable universe fuzzy control.

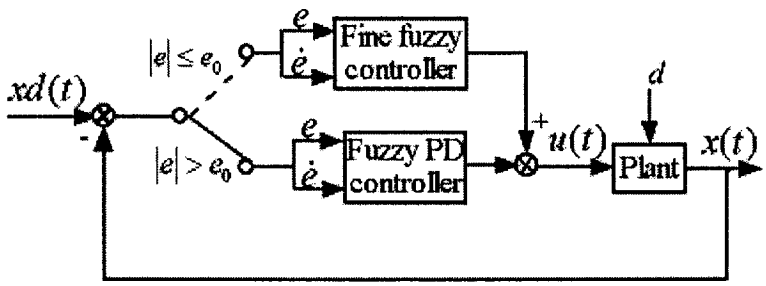

Figure 6.11 Variable universe fuzzy PD control diagram

2) Variable Universe Fuzzy Control

A so-called variable universe means that some universes, such as input universes X_1 and X_2 and output universe Y, can respectively change along with the changing of variables $e(t)$, $\dot{e}(t)$ and $u(t)$. In References [110-111], they are expressed as:

$$X_1(e) = [-\alpha_1(e)L \quad \alpha_1(e)L] \tag{6.7}$$

$$X_2(\dot{e}) = [-\alpha_2(\dot{e})L \quad \alpha_2(\dot{e})L] \tag{6.8}$$

$$Y(u) = [-\beta(u)H \quad \beta(u)H] \tag{6.9}$$

where $\alpha_1(e)$, $\alpha_2(\dot{e})$ and $\beta(u)$ are called contraction-expansion factors of the universes X_1, X_2, and Y, respectively. Being relative to variable universes, the original universes X_1, X_2 and Y are naturally called initial universes. Figure 6.12 shows an example of variable universe of input variables.

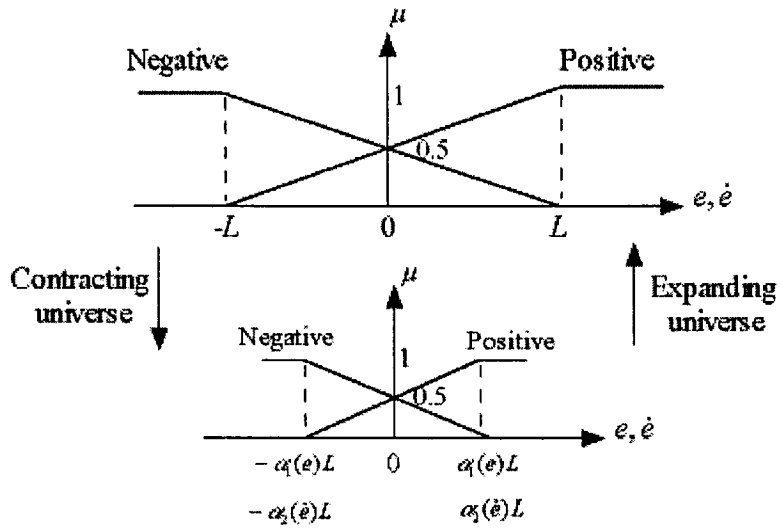

Figure 6.12 Contracting/expanding universe L

Now, the problem is how to select $\alpha_1(e)$, $\alpha_2(\dot{e})$ and $\beta(u)$ to design variable universe fuzzy control. Generally, a function α: $X \to [0, 1]$, $e \to \alpha_1(e)$ and $\dot{e} \to \alpha_2(\dot{e})$ is called a contraction-expansion factor on $X_i = [-L, L]$ if it satisfies the following axioms [111]:

(a) Duality: $\forall e \in X_1$, $\forall \dot{e} \in X_2$, $\alpha_1(e) = \alpha_1(-e)$ and $\alpha_2(\dot{e}) = \alpha_2(-\dot{e})$;

(b) Near zero: $\alpha_1(0) = \varepsilon_1 > 0$ and $\alpha_2(0) = \varepsilon_2 > 0$ (ε_1 and ε_2 are very small constants);

(c) Monotonicity: α_1 and α_2 is strictly monotonically increasing on $[0, L]$;

(d) Normality: $\alpha_1(\pm L) = 1$ and $\alpha_2(\pm L) = 1$.

For the fuzzy control with two input variables and one output variable, the following contraction-expansion factors are suggested:

$$\alpha_1(e) = \varepsilon_1 + \left(\frac{|e|}{L}\right)^{\tau_1} \tag{6.10}$$

$$\alpha_2(\dot{e}) = \varepsilon_2 + \left(\frac{|\dot{e}|}{L}\right)^{\tau_2} \tag{6.11}$$

$$\beta(e,\dot{e}) = \left(\alpha_1(e)\alpha_2(\dot{e})\right)^{\tau_3} \tag{6.12}$$

where $0 < \tau_1, \tau_2, \tau_3 \leq 1$ and $\varepsilon_1, \varepsilon_2 > 0$ is a very small constant, for example, taken as $\varepsilon_1 = \varepsilon_2 = 0.001$.

The structure of variable universe fuzzy control is the same as shown in Figure 6.3 except the different gains K_P and K_d as well as the variable universes L and H, as shown in Figure 6.4. The reason for using different gains K_P and K_d in the different controllers is that when the controller switch to the fine fuzzy controller, the gain K_P should be changed to a small value and the gain K_d should be changed to a big value in order to reduce overshoot and to make the system stable. For example, we choose the new gains $K_{PF} = K_p/m$ and $K_{dF} = m \times K_d$, where $m > 1$ and is a constant.

Based on the new gains, the variable universe algorithm is used to modify fuzzy universe parameters L and H, whereas the fuzzy rules will keep the same at the all time.

3) The Switching Control Law

The proposed variable universe fuzzy PD controller can be expressed as

$$u(t) = \begin{cases} u_{fuzzy}(t) & |e| > e_0 \\ u_{fine}(t) & |e| \leq e_0 \end{cases} \tag{6.13}$$

where $u_{fuzzy}(t)$ is defined in Equation (6.5), and $u_{fine}(t)$ is defined as:

$$u_{fine}(t) = \frac{L(\alpha_1(e)K_{PF}e(t) + \alpha_2(\dot{e})K_{dF}\dot{e}(t))}{2(2\beta(e,\dot{e})H - K_{PF}|e(t)|)} \quad \text{in } IC_1, IC_4, IC_5, \text{ and } IC_8,$$

$$= \frac{L(\alpha_1(e)K_{PF}e(t) + \alpha_2(\dot{e})K_{dF}\dot{e}(t))}{2(2\beta(e,\dot{e})H - K_{PF}|\dot{e}(t)|)} \quad \text{in } IC_2, IC_3, IC_6, \text{ and } IC_7,$$

$$= \frac{\beta(e,\dot{e})H + K_{dF}\dot{e}(t)}{2} \quad \text{in } IC_9 \text{ and } IC_{16},$$

$$= \frac{\beta(e,\dot{e})H + K_{PF}e(t)}{2} \quad \text{in } IC_{10} \text{ and } IC_{11},$$

$$= \frac{-\beta(e,\dot{e})H + K_{dF}\dot{e}(t)}{2} \quad \text{in } IC_{12} \text{ and } IC_{13},$$

$$= \frac{-\beta(e,\dot{e})H + K_{PF}e(t)}{2} \quad \text{in } IC_{14} \text{ and } IC_{15},$$

$$= \beta(e,\dot{e})H \text{ or } -\beta(e,\dot{e})H \quad \text{in } IC_{17} \text{ or } IC_{19},$$

$$= 0 \quad \text{in } IC_{18} \text{ and } IC_{19}.$$

6.3.3 Wing Rock Control Model

To evaluate the proposed control scheme, we modify the control model of wing rock phenomenon in Equation (5.8) as

$$\ddot{\phi} + a_0\phi + a_1\dot{\phi} + a_2|\dot{\phi}|\dot{\phi} + a_3\phi^3 + a_4\phi^2\dot{\phi} = u + d \tag{6.14}$$

where a_i (i=0, 1, 2, 3, 4) are the parameters illustrated in Figure 2.5, $u(t)$ is the control input, and $d(t)$ includes the un-modeled dynamics and external disturbance.

6.3.4 Simulation Results

In this section, we will simulate the control of wing rock phenomenon with unknown disturbances. In particular, we compare the simulation results of variable universe fuzzy

PD control in Figure 6.11 with the previous fuzzy PD control in Figure 6.3.

Before simulation, we design some parameters of the controller:

(a) The switch threshold value in Equation (6.13) is $e_0 = 0.02$ rad or 1.15^0.

(b) For the fuzzy PD controller, $u_{fuzzy}(t)$, we choose $L = \pm 0.7$ rad, K_P =1, K_d =0.3, and $H = \pm 20$.

(c) For the fine controller, $u_{fine}(t)$, we choose $L = \pm$ 0.7rad, m=4, K_{PF} =1/4, K_{dF} =0.3×4, H = ±20, and other parameters $\tau_1 = 0.9$, $\tau_2 = \tau_3 = 0.1$, $\varepsilon_1 = 0.001$, and $\varepsilon_2 = 0.001$.

Assume to track a time-varying trajectory $xd(t) = 10^0 + 5^0 \sin(0.01\pi t)$ or a constant trajectory $xd(t) = 10^0$ under a time-varying disturbance $d(t) = 1.5\sin(2\pi t) + \sin(5\pi t)$ or a constant disturbance $d = 2$ to evaluate the proposed control scheme. The initial condition is $\phi(0) = 2^0$ and $\dot{\phi}(0) = 0$ at AOA=32.5^0. We allow the uncontrolled wing rock to have some LCOs and then activate the controller, for example, at t =1000 time steps.

The following five cases are used to illustrate the effectiveness of the proposed controller. In each case, we compare the tracking errors of two fuzzy PD control schemes.

Case 1: Suppression control with $xd(t) = 0$ *and* $d = 0$

In this case, the output responses of two control schemes are almost the same, as shown in Figure 6.13. This result means that the two control schemes have almost the same performance and both of the tracking errors are $e(t) \approx 0$.

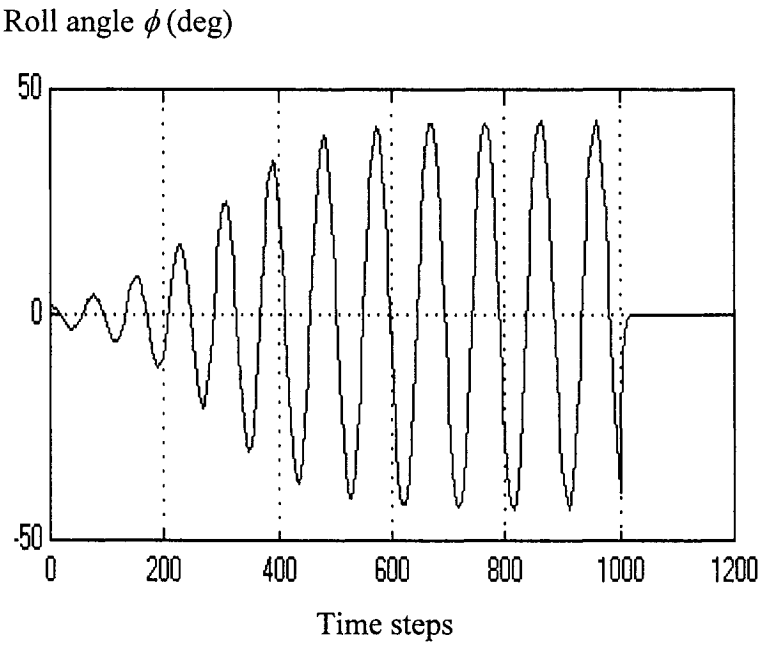

Figure 6.13 Fuzzy control for wing rock suppression

Case2: Tracking control: $xd(t) = 10^0$ *and* $d = 0$

Assume to track the desired constant trajectory $xd(t) = 10^0$ without the disturbances. The simulation results show that the tracking error of the fuzzy PD control is $|e(t)| \le 0.01^0$ while the tracking error of the proposed control scheme is $|e(t)| \le 0.0002^0$.

Case3: Tracking control: $xd(t) = 10^0$ *and* $d = 2$

Assume to track the same constant trajectory $xd(t) = 10^0$ as *Case 2* except the constant disturbance $d = 2$. Figure 6.14(a) shows the tracking error of the fuzzy PD control to be $|e(t)| \le 13.355^0$ while the tracking error of the proposed control scheme is $|e(t)| \le 0.061^0$, as shown in Figure 6.14(b).

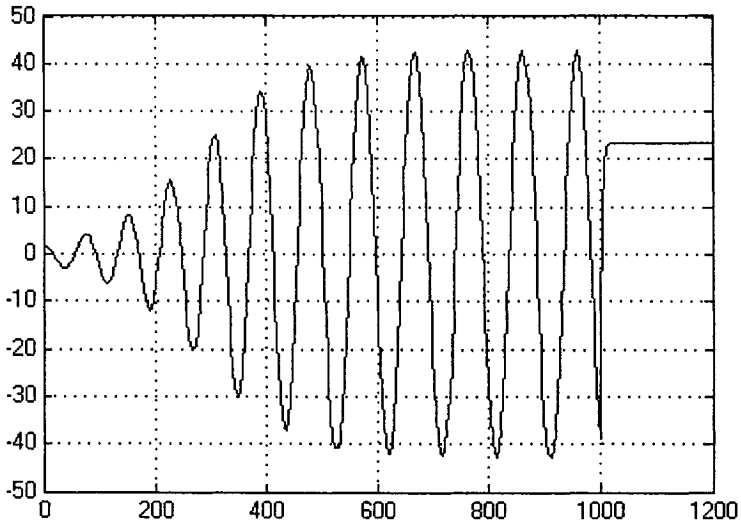

Time steps

(a) Output responses ($|e(t)| \leq 13.355^0$) of the fuzzy PD control

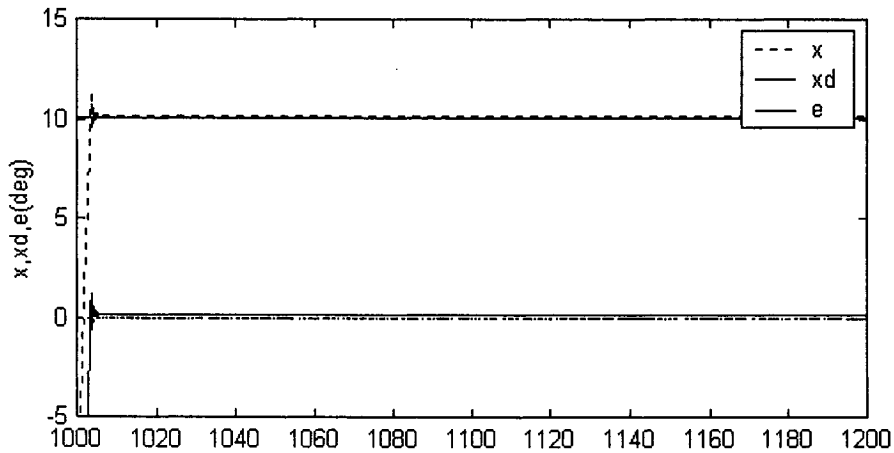

Time steps

(b) Tracking errors $|e(t)| \leq 0.061^0$ of the proposed controller

Figure 6.14 The response comparisons of tracking $xd(t) = 10^0$ with the disturbance d =2

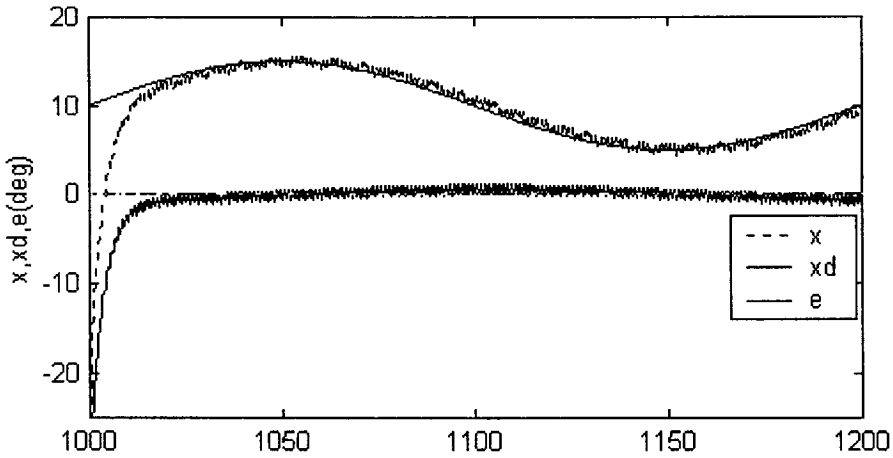

Figure 6.15 The tracking error $|e(t)| \leq 1.1^0$ of the fuzzy PD control for tracking $xd(t) = 10^0 + 5^0 \sin(0.01\pi t)$ under $d(t) = 1.5\sin(2\pi t) + \sin(5\pi t)$

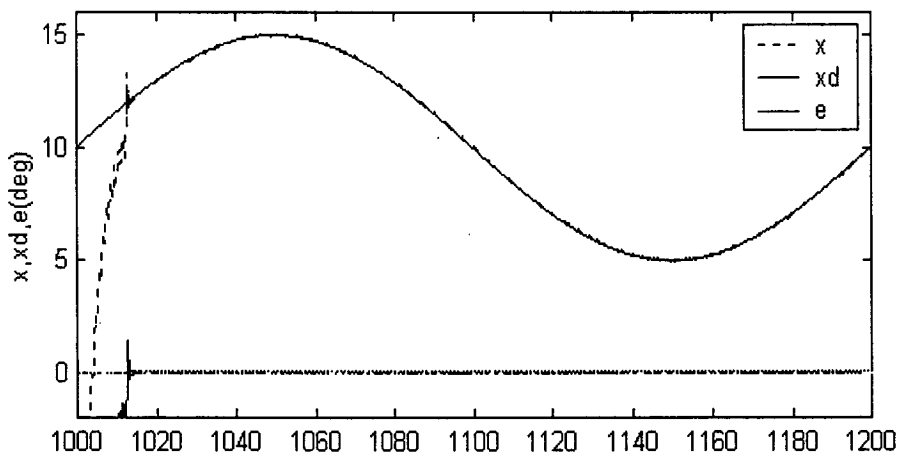

Figure 6.16 The tracking error $|e(t)| \leq 0.0005^0$ of the proposed controller for tracking $xd(t) = 10^0 + 5^0 \sin(0.01\pi t)$ under $d(t) = 1.5\sin(2\pi t) + \sin(5\pi t)$

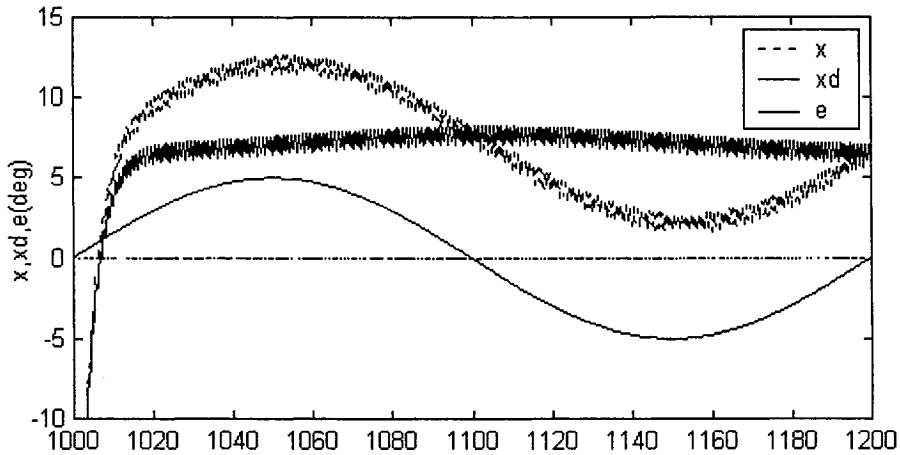

Figure 6.17 The tracking error $|e(t)| \leq 8.1^0$ of the fuzzy PD control for tracking

$xd(t) = 5^0 \sin(0.01\pi t)$ under $d(t) = 1 + 1.5\sin(2\pi t) + \sin(5\pi t)$

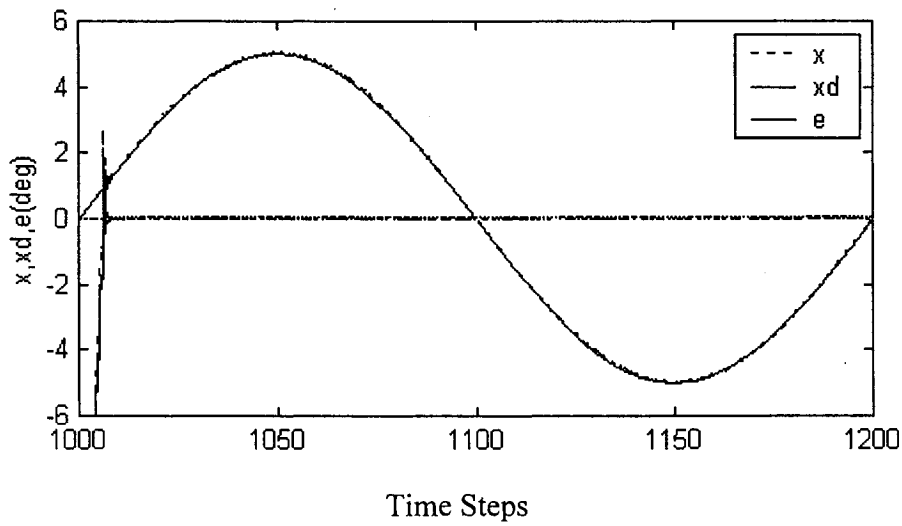

Figure 6.18 The tracking error $-0.05 \leq e(t) \leq 0.1^0$ of the proposed controller for tracking $xd(t) = 5^0 \sin(0.01\pi t)$ under $d(t) = 1 + 1.5\sin(2\pi t) + \sin(5\pi t)$

Case4: Tracking control: $xd(t) = 10^0 + 5^0 \sin(0.01\pi t)$ *and* $d(t) = 1.5\sin(2\pi t) + \sin(5\pi t)$

Assume to track the desired time-varying trajectory $xd(t) = 10^0 + 5^0 \sin(0.01\pi t)$ under the time-varying disturbance $d(t) = 1.5\sin(2\pi t) + \sin(5\pi t)$. Figure 6.15 shows the tracking error of the fuzzy PD control to be $|e(t)| \le 1.1^0$ while the tracking error of the proposed control scheme is $|e(t)| \le 0.0005^0$, as shown in Figure 6.16.

Case 5: Tracking control: $xd(t) = 5^0 \sin(0.01\pi t)$ *and* $d(t) = 1 + 1.5\sin(2\pi t) + \sin(5\pi t)$

Assume to track the desired time-varying trajectory $xd(t) = 5^0 \sin(0.01\pi t)$ under the complex disturbance $d(t) = 1 + 1.5\sin(2\pi t) + \sin(5\pi t)$, which include a constant disturbance and a time-varying disturbance. Figure 6.17 shows the tracking error of the fuzzy PD controller to be $|e(t)| \le 8.1^0$ while the tracking error of the proposed scheme is $-0.05 \le e(t) \le 0.1^0$, as shown in Figure 6.18.

6.3.5 Conclusions

A variable universe fuzzy PD control has been proposed to improve the precision and robustness of wing rock tracking control with unknown disturbances. In this new scheme, when the tracking error is bigger, we take the advantage of the fast and simple adjustment of fuzzy PD control to reduce big tracking errors; when the tracking error enters into the small range, we take the advantage of fine tuning of variable universe fuzzy control. The simulation results show that the proposed control scheme has much better tracking performance and robustness than the fuzzy PD control scheme. The main features of the proposed method are precise tracking and fast responses with only four fuzzy rules.

6.4 Summary

In this chapter, after brief introducing fuzzy logic systems, two fuzzy control schemes have been proposed to control wing rock phenomenon. The numerical results show that the two control schemes almost have the same performance if the disturbance of wing rock phenomenon is ignored, but if the disturbance is considered, the variable universe fuzzy PD control has much better tracking performance and robustness than the fuzzy PD control.

Chapter 7

The NDOFEL Control of Time-Varying Wing Rock Phenomenon

In this chapter, a new learning control scheme, called NDOFEL, based on a feedback-error-learning (FEL) control strategy combining with a nonlinear disturbance observer (NDO), is proposed for a class of time-varying nonlinear systems with unknown disturbances. The nominal model of wing rock phenomenon in this scheme is assumed available. This chapter is organized as follows: Section 7.1 is an introduction. The NDOFEL design is then presented in Section 7.2. Next, we discuss the time-varying wing rock control model in Section 7.3. Finally, Sections 7.4 is the simulation results of time-varying wing rock phenomenon with unknown disturbances, and Section 7.5 is the summary of this chapter.

7.1 Introduction

It is well known that tracking control for uncertain nonlinear systems with disturbances is a challenging issue. To achieve good tracking, the three mechanisms for nonlinear control

systems with uncertainties and disturbances are usually applied as summarized in Reference [112]: adaptation, plant-inversion, and high-gain. In general, direct adaptive algorithms, based on the system performance, adjust the control gains and require little knowledge of system structures and parameter values. However, the control input might become large. In addition, adaptive control methods, as studied in Reference [113], may be limited to a nonlinear system with constant disturbances. Inverse control methods based on input-output linearization presented in Reference [114] focus on canceling known nonlinearities and achieving response characteristics, but the robustness to modeling errors is a serious problem. High-gain approaches such as SMC could guarantee stability but have chattering problems and also require large control inputs.

A disturbance observer (DO) is another approach of dealing with disturbance problems. But, the designs of most disturbance observers are based on linearized models or using linear system techniques, as shown in References [115-117]. There are several pieces of work where the applications of the disturbance observer for the nonlinear friction compensation are reported [118-121]. Recently, Chen *et al.* in Reference [122] have proposed a new nonlinear disturbance observer (NDO) for robotic manipulators. The uncertainties and disturbances can be integrated into a lumped disturbance term $d(t)$ where they assume $\dot{d}(t) = 0$ in Reference [122]. If $\dot{d}(t) \neq 0$, then the performance of the nonlinear disturbance observer will be limited.

On the other hand, if the uncertainties and disturbances in control systems are reduced into a small range, a neural network (NN) control with the feedback-error-learning (FEL)

strategy, first proposed in References [123-124], could be used. This control scheme is adopted because it has the advantage of generating the desired control input, but the neural network does not require initially off-line training. In practice, different neural network algorithms with the FEL strategy were applied in References [125-128].

In this study, inspired by both the NDO algorithm and the neural network control with the FEL strategy, a new learning control scheme, NDOFEL, is proposed to control a class of time-varying nonlinear systems with unknown disturbances.

In the NDOFEL, we take two steps to estimate the time-varying disturbance term $d(t)$ for improving the precision of tracking control. The nonlinear disturbance observer is first used to estimate $d(t)$; as a result, the observer error does not converge to zero but to a small range. To reduce the observer error, a sliding-mode fuzzy neural network (SFNN) with the FEL strategy is then applied to estimate the error so that the output of the plant follows the desired trajectory. This SFNN with on-line learning algorithms derived from Lyapunov methods is developed to modify the parameter of fuzzy membership functions and to generate rule-base from zero. The presented SFNN algorithm is motivated by the following reasons:

(a) The most significant property of sliding-mode control is its robustness, but this approach suffers from inherent chattering problems.

(b) Fuzzy logic control provides human reasoning capabilities to capture uncertainties that cannot be described by precise mathematical models. However, most fuzzy controllers have difficulties in determining suitable fuzzy control

rules and membership functions, and trial-and-error tuning procedure is time-consuming.

(c) The connection structure of neural networks provides powerful abilities such as adaptive learning, parallelism, fault tolerance, and generalization, but neural networks need off-line preprocessing.

The proposed SFNN algorithm combines the advantages of different methods, and at the same time it tries to overcome the drawbacks of each individual method. Furthermore, the new algorithm is required to be simple, stable, and fast for real time control.

The tracking control during wing rock phenomenon with unknown disturbances is used as an example to illustrate the application of the NDOFEL. As mentioned earlier, wing rock phenomena occur at low-speed high AOA and high-speed moderate AOA. Although some control schemes in References [41, 46-47, 49-51, 55-57, 100-102] can suppress wing rock phenomenon, the tracking control performance may be poor if wing rock motions suffer from some uncertainty and disturbance. For this reason, we propose the NDOFEL to achieve the goal of precise tracking control of time-varying wing rock with a lumped disturbance term $d(t)$.

7.2 NDOFEL

7.2.1 Problem Statement

Consider a class of time-varying nonlinear systems with unknown disturbances of the form

$$\ddot{x} = f(\mathbf{x},t) + \Delta + u(t) + d_e \tag{7.1}$$

where the scalar variable $x(t)$ is the output of interest, $\mathbf{x}(t) = [x \quad \dot{x}]^T \in \mathbf{R}^2$ is the state vector, $f(\mathbf{x},t) = f_n(\mathbf{x}) + \Delta f(\mathbf{x},t)$ in which $f_n(\mathbf{x})$ is the known function and $\Delta f(\mathbf{x},t)$ is the unknown function variation, $\Delta(t)$ is the non-modeled dynamics, $u(t)$ is the control input, and $d_e(t)$ is the unknown external disturbance.

Equation (7.1) can be written in the nominal model form

$$\ddot{x} = f_n(\mathbf{x}) + u + d \tag{7.2}$$

where $d(t)$ represents a lumped disturbance, that is

$$d = \Delta f(\mathbf{x},t) + \Delta + d_e$$

To estimate the time varying lumped disturbance term $d(t)$, we first design the nonlinear disturbance observer to estimate $d(t)$.

7.2.2 Nonlinear Disturbance Observer Design

The objective of this section is to design an observer such that the estimation $\hat{d}(t)$ yielded by the observer approaches the disturbance term $d(t)$ under any $x(t)$, $\dot{x}(t)$, and $t \in [t_0, \infty)$.

Rewrite Equation (7.2) as

$$d = \ddot{x} - f_n(\mathbf{x}) - u \tag{7.3}$$

Then, a disturbance observer can be proposed

$$\dot{\hat{d}} = -L\hat{d} + L(\ddot{x} - f_n(\mathbf{x}) - u) \tag{7.4}$$

where $L > 0$ is an observer gain.

However, in most applications, it is difficult to obtain the acceleration signal $\ddot{x}(t)$ due to measurement noise. The disturbance observer cannot be implemented. For this purpose, the disturbance observer can be modified as a nonlinear disturbance observer.

First, we need to define an auxiliary variable

$$z = \hat{d} - L\dot{x} \tag{7.5}$$

Invoking Equation (7.4) with Equation (7.5), we have

$$\dot{z} = -Lz - L(f_n(\mathbf{x}) + u + L\dot{x}) \tag{7.6}$$

Then, the nonlinear disturbance observer is given by

$$\begin{cases} \hat{d} = z + L\dot{x} \\ \dot{z} = -Lz - L(f_n(\mathbf{x}) + u + L\dot{x}) \end{cases} \tag{7.7}$$

Now, define the observer error

$$e_d = d - \hat{d} \tag{7.8}$$

The observer error equation can be derived from Equations (7.3), (7.5), (7.7), and (7.8) as

$$\begin{aligned} \dot{e}_d(t) &= \dot{d} - \dot{\hat{d}} \\ &= \dot{d} - \dot{z} - L\ddot{x} \\ &= \dot{d} - L(-z - f_n(\mathbf{x}) - u - L\dot{x} + \ddot{x}) \\ &= -L(d - \hat{d}) + \dot{d} \\ &= -Le_d(t) + \dot{d} \end{aligned} \tag{7.9}$$

In Equation (7.9), if $\dot{d}(t) = 0$, the observer error is with the desired exponential convergence rate by choosing the observer gain $L > 0$, that is, $e_d(t) \to 0$. However, in this study, we assume $\dot{d}(t) \neq 0$. As a result, $e_d(t)$ does not converge to zero but to a small range. To further estimate $e_d(t)$, we will study the SFNN with a learning algorithm.

7.2.3 SFNN Algorithm

The SFNN with on-line learning algorithms relates to sliding-mode control, fuzzy logic control, and neural networks.

To begin with, define the tracking error vector

$$E = [\mathbf{x}_d - \mathbf{x}]^T = [e \quad \dot{e}]^T \tag{7.10}$$

where $\mathbf{x}_d(t) = [x_d \quad \dot{x}_d]^T \in \mathbf{R}^2$, $x_d(t)$ is a desired trajectory, and $e(t)$ is a tracking error.

The researchers in References [129-134] claimed that sliding-mode control is one of the effective nonlinear robust control approaches since it provides system dynamics with an invariance property to uncertainties once the system dynamics are controlled in the sliding mode.

To estimate the observer error $e_d(t)$, we choose $E(t)$ in Equation (7.10) as the input signals of the SFNN and define a sliding surface as

$$s(E) = \dot{e} + \lambda e \tag{7.11}$$

where $\lambda > 0$ is a strictly positive constant. Since bounds on $s(E)$ can be directly translated

into bounds on the tracking error vector $E(t)$, the scalar $s(E)$ represents a true measure of tracking performance. We can choose $s(E)$ as the input variable of the fuzzy systems as used in Reference [129]. In this way, we can reduce the size of fuzzy rule-base. For example, if each of two fuzzy variables $e(t)$ and $\dot{e}(t)$ has 5 linguistic variables, then there are 25 fuzzy rules. By comparison, if $s(E)$ is chosen as the input variable with 5 linguistic variables, only 5 fuzzy rules are needed.

The discontinuous control is designed by fuzzy control methods such that the system enters in the sliding mode $s(E) = 0$ and remains it forever. The well-known conditions $s \to 0$ and $s\dot{s} < 0$ are used as discussed in Reference [135]. When the error trajectory approaches the switching surface, $s \to 0$, the output signal of fuzzy control should be small; when the error trajectory is not near the switching surface, the large output should increase the reaching rate, as explained in Reference [130].

In this case, a fuzzy rule-base is specified as

$$R_i\text{: IF } s \text{ is } A_i\text{, THEN } u_r \text{ is } r_i, \quad i=1, 2, \ldots, h \tag{7.12}$$

where $s(E)$ is a input linguistic variable with a linguistic value A_i defined on the universe of discourse $s \in S$, $s(E)$ uses Gaussian membership functions, $\mu_i(s) = \exp[-\frac{1}{2}(s-c_i)^2/\sigma_i^2]$, where c_i and σ_i represent the center and width of membership functions, respectively, u_r is the output linguistic variable with singular membership functions, r_i are the singleton actions, and h is the number of total rules.

The fuzzy control rules in Equation (7.12) can be implemented by

$$u_n = \sum_{i=1}^{h} p_i(s, \sigma_i, c_i) \times r_i \tag{7.13}$$

where the fuzzy base function is

$$p_i(s,\sigma_i,c_i)=\frac{\exp[-\frac{1}{2}(s-c_i)^2/\sigma_i^2]}{\sum_{i=1}^{h}\exp[-\frac{1}{2}(s-c_i)^2/\sigma_i^2]} \tag{7.14}$$

To reduce the number of learning premise parameters in Equation (7.13), inspired by the fuzzy variable (contracting/expanding) universe method discussed in detail in Section 6.3, the input variable universe S varies only with the width parameter σ, $s \in S(\sigma)$, and other parameters are obtained by a simple algebra relationship. For example, a proper and initial membership function can be defined as

$$\sigma_i=\sigma=2 \tag{7.15a}$$

$$c_{h-1}=-(h-1)\sigma, \ldots, c_4=-4\sigma, c_2=-2\sigma, c_1=0, c_3=2\sigma, c_5=4\sigma, \ldots, c_h=(h-1)\sigma \tag{7.15b}$$

For example, if we design h =5 in Equation (7.15), Figure 7.1 will illustrate the fuzzy base function in Equation (7.14), where Figure 7.1(b) shows the fuzzy base function of a contracting universe σ =1 against the initial universes σ =2 in Figure 7.1(a). It should be

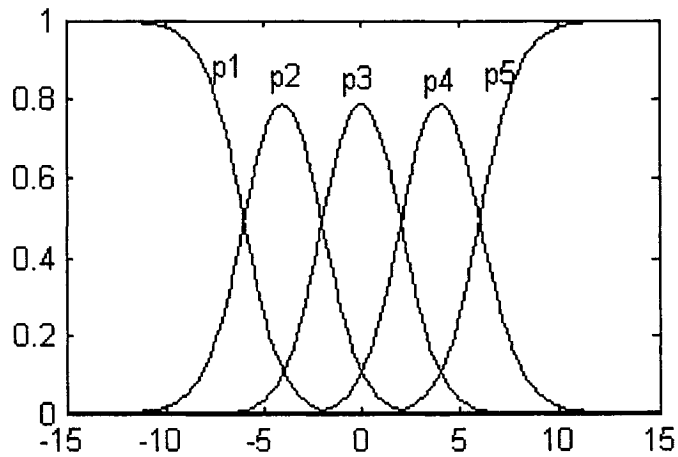

(a) σ=2

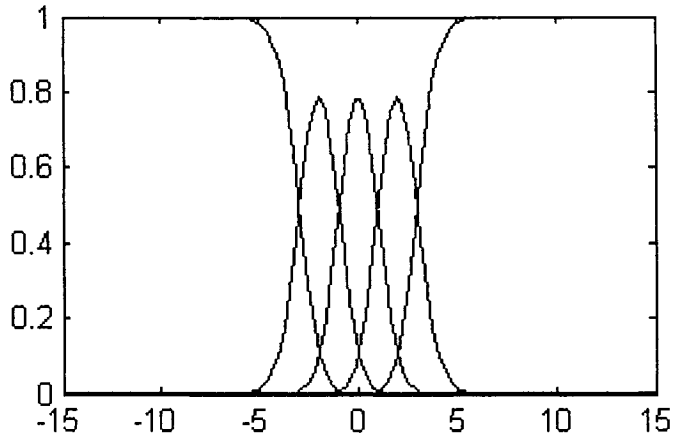

(b) σ=1

Figure 7.1 The fuzzy base function comparison of the different universes

noted that the membership functions are updated iteratively and automatically because a change in the membership functions may alter the performance of the fuzzy controller significantly.

Finally, a feedforward three-layer neural network is constructed to achieve the on-line learning of the SFNN parameters. With Equation (7.15), Equation (7.13) can be written in the matrix form

$$u_n = W^T \Theta \tag{7.16}$$

where $W^T = [r_1 \quad r_2 \quad \cdots \quad r_h]$ and $\Theta = [p_1(s,\sigma,0) \quad p_2(s,\sigma,-2\sigma) \quad \cdots \quad p_h(s,\sigma,(h-1)\sigma)]^T$.

7.2.4 NDOFEL Structure

Using the universal approximation theory [136-137], $e_d(t)$ can be approximated by the SFNN through the on-line learning

$$e_d = W^{*T}\Theta^* + \varepsilon_n \tag{7.17}$$

where W^* is the optimal weight vector of W, Θ^* is the optimal parameter vector of Θ, and ε_n is the inherent approximation error. According to the approximation theory, ε_n can be reduced by increasing the number of fuzzy rules. It is reasonable to assume ε_n is bounded.

If there exists a control law

$$u^* = KE - W^{*T}\Theta^* - \varepsilon_n + \ddot{x}_d - f_n(\mathbf{x}) - \hat{d} \tag{7.18}$$

where $K = [k_1 \quad k_2]$ are the constant gains.

Substituting Equation (7.18) into Equation (7.2), with Equations (7.8), (7.10), and (7.17), we obtain

$$\ddot{e} + k_2\dot{e} + k_1 e = 0 \tag{7.19}$$

where $s^2 + k_2 s + k_1$ is a Hurwitz polynomial. Thus, $u^*(t)$ is called the ideal control law and can guarantee perfect tracking, that is, $x(t) \equiv x_d(t)$, if $\mathbf{x}(0) = \mathbf{x}_d(0)$.

Let $u_c(t) = KE$ in Equation (6.18) and $u_n(t) = W^T\Theta = \hat{e}_d(t)$ denotes the output of the SFNN to estimate $e_d(t)$. The total control input $u(t)$ of the nonlinear system (7.2) is

$$u = u_c - u_n + x_d^{(n)} - f_n(\mathbf{x}) - \hat{d} \tag{7.20}$$

Figure 7.2 shows the proposed NDOFEL control structure.

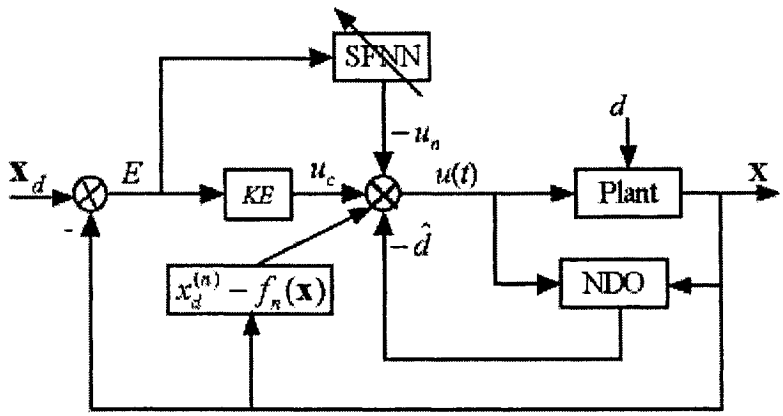

Figure 7.2 The proposed NDOFEL diagram

7.2.5 Error Dynamics

Substituting Equation (7.20) into Equation (7.2), with Equations (7.8), (7.10), (7.16), and (7.17), we obtain the error dynamics

$$e^{(n)} = -KE - (W^{*T}\Theta^{*} - W^{T}\Theta + \varepsilon_n) \tag{7.21}$$

Let $\tilde{W} = W^{*} - W$ and $\tilde{\Theta} = \Theta^{*} - \Theta$. The error dynamics can be written as

$$e^{(n)} = -KE - (\tilde{W}^{T}\tilde{\Theta} + \tilde{W}^{T}\Theta + W^{T}\tilde{\Theta} + \varepsilon_n) \tag{7.22}$$

where $(\tilde{W}^{T}\tilde{\Theta} + \tilde{W}^{T}\Theta + W^{T}\tilde{\Theta})$ is the learning error.

For convenience, Equation (7.22) can be denoted as

$$\dot{E} = AE + B(\tilde{W}^{T}\tilde{\Theta} + \tilde{W}^{T}\Theta + W^{T}\tilde{\Theta} + \varepsilon_n) \tag{7.23}$$

where $A = \begin{bmatrix} 0 & 1 & \cdots & 0 \\ \vdots & \vdots & \ddots & \vdots \\ 0 & 0 & \cdots & 1 \\ -k_1 & -k_2 & \cdots & -k_n \end{bmatrix}$ is stable matrix, and $B = \begin{bmatrix} 0 \\ \vdots \\ 0 \\ -1 \end{bmatrix}$.

7.2.6 Stability Analysis and Adaptive Laws

The following Lyapunov candidate function is chosen

$$V(t) = \tfrac{1}{2} E^T PE + \tfrac{1}{2}\tilde{W}^T R\tilde{W} + \tfrac{1}{2}\tilde{\Theta}^T \Lambda\tilde{\Theta} \tag{7.24}$$

where $P = P^T$ is a symmetric and positive definite matrix and satisfies the following relationship

$$PA + A^T P = -Q \tag{7.25}$$

where Q is a symmetric positive definite matrix, and R and Λ are non-negative definite matrixes.

The derivative of Equation (7.24) is given by

$$\dot{V}(t) = \tfrac{1}{2}(\dot{E}^T PE + E^T P\dot{E}) + \tilde{W}^T R\dot{\tilde{W}} + \tilde{\Theta}^T \Lambda\dot{\tilde{\Theta}} \tag{7.26}$$

Substituting Equations (7.23) and (7.25) into Equation (7.26), we have

$$\begin{aligned} \dot{V}(t) &= -\tfrac{1}{2} E^T QE + \varepsilon_n^T B^T PE + \tilde{\Theta}^T \tilde{W} B^T PE + \tilde{\Theta}^T WB^T PE \\ &\quad + \Theta^T \tilde{W} B^T PE + \tilde{W}^T R\dot{\tilde{W}} + \tilde{\Theta}^T \Lambda\dot{\tilde{\Theta}} \\ &= -\tfrac{1}{2} E^T QE + (\tilde{\Theta}^T \tilde{W} + \varepsilon_n^T) B^T PE \\ &\quad + \tilde{\Theta}^T (WB^T PE + \Lambda\dot{\tilde{\Theta}}) + \tilde{W}^T (\Theta B^T PE + R\dot{\tilde{W}}) \end{aligned} \tag{7.27}$$

If in Equation (7.27) we choose

$$\dot{\tilde{W}} = -R^{-1}\Theta B^T PE \tag{7.28}$$

$$\dot{\tilde{\Theta}} = -\Lambda^{-1} WB^T PE \tag{7.29}$$

then

$$\dot{V}(t) = -\tfrac{1}{2} E^T QE + (\tilde{\Theta}^T \tilde{W} + \varepsilon_n^T) B^T PE \tag{7.30}$$

The higher order item $\tilde{\Theta}^T\tilde{W}$ is neglected and $(\tilde{\Theta}^T\tilde{W}+\varepsilon_n^T)$ is bounded by a constant ε_H.

$\dot{V}$ can be demonstrated negative as follows:

$$\dot{V}(t) \le -\frac{1}{2}\|E\|\lambda_{\min}(Q)\|E\| + \|E\|\lambda_{\min}(P)\|B\|\varepsilon_H$$
$$= -\frac{1}{2}\|E\|\lambda_{\min}(Q)\|E\| + \|E\|\lambda_{\max}(P)\varepsilon_H$$

When

$$\|E\| > \frac{2\lambda_{\max}(P)}{\lambda_{\min}(Q)}\varepsilon_H = E_a \tag{7.31}$$

we can obtain

$$\dot{V} < 0 \tag{7.32}$$

If the control system satisfies the condition in Equation (7.31), we can draw a conclusion that the overall control system is stable, the tracking error is convergent, $E(t) \to 0$ as $t \to \infty$, by application of Barbalat's lemma given in Reference [96], and the uniform ultimate boundedness (UUB) of the tracking error can be achieved.

As we know, $\dot{\tilde{W}} = \dot{W}^* - \dot{W}$ and $\dot{\tilde{\Theta}} = \dot{\Theta}^* - \dot{\Theta}$ with $\dot{W}^* = 0$ and $\dot{\Theta}^* \approx 0$, we can obtain the adaptive laws of the parameters from Equations (7.28) and (7.29) as

$$\dot{W} = R^{-1}\Theta B^T PE \tag{7.33}$$

$$\dot{\Theta} = \Lambda^{-1}WB^T PE \tag{7.34}$$

Finally, if the approximation error is very large at the initial learning phase, the parameters of the network may drift to infinity. To avoid this situation, we modify the

control law in Equation (7.16) as

$$u_n = \begin{cases} W^T\Theta, & if\ |e| < e_0 \\ 0 & if\ |e| \geq e_0 \end{cases} \tag{7.35}$$

where e_0 is an important threshold value. We suggest choosing a little bigger value than maximum $|e_d(t)|$. Equation (7.35) means that during the initial learning period or when $|e(t)| \geq e_0$, the control law (7.20) is simplified as $u = u_c + x_d^{(n)} - f_n(\mathbf{x}) - \hat{d}$ and achieves fast but coarse tracking. When $|e(t)| < e_0$, the overall control law achieves fine tracking.

7.3 Time-Varying Wing-Rock Control Model

In practice, since aircraft at a high AOA operate in an unstable aerodynamic region, it is quite difficult to obtain the model of aircraft's roll dynamics. It is reasonable to assume the practical model of wing rock phenomenon to include time-variable aerodynamics part, non-modeled dynamics, and external disturbances. Therefore, we define a lumped disturbance term $d(t) = \Delta f(\mathbf{x}, t) + \Delta + d_e$ to denote the three parts and add $d(t)$ to the right side of Equation (5.8).

According to above discussion, the time-varying wing-rock control model for 80^0 swept back wing in Equation (5.8) is modified as

$$\ddot{\phi} + a_0\phi + a_1\dot{\phi} + a_2|\dot{\phi}|\dot{\phi} + a_3\phi^3 + a_4\phi^2\dot{\phi} = u + d \tag{7.36}$$

where $a_i(t)$ (i=0, 1, 2, 3, 4) are the time-varying parameters illustrated in Figure 2.8.

7.4 Simulation Results

We first choose the wing rock model at AOA =32.5^0 as a nominal model and assume L =10, $K=[3 \quad 2]$, and h =5. If $Q=\begin{bmatrix}6 & 0\\ 0 & 6\end{bmatrix}$ and $A=\begin{bmatrix}0 & 1\\ -3 & -2\end{bmatrix}$, then $P=\begin{bmatrix}8 & 1\\ 1 & 2\end{bmatrix}$. Then the adaptive laws (7.33) and (7.34) in the SFNN control can be obtained as $\dot{W}=[-\eta_1 p_1(e+2\dot{e}) \quad -\eta_2 p_2(e+2\dot{e}) \quad -\eta_3 p_3(e+2\dot{e}) \quad -\eta_4 p_4(e+2\dot{e}) \quad -\eta_5 p_5(e+2\dot{e})]^T$ and $\dot{\Theta}=-\eta_6 r_3(e+2\dot{e})$ where η_i (i=1,2,3,4,5,6) are learning rates. The reason for choosing $r_3(t)$ is that it is more effective than the other $r_i(t)$ (i=1,2,4,5).

The numerical simulations of wing rock tracking control are implemented in Matlab and Simulink environments. Figure 7.3 shows the corresponding Simulink block diagram.

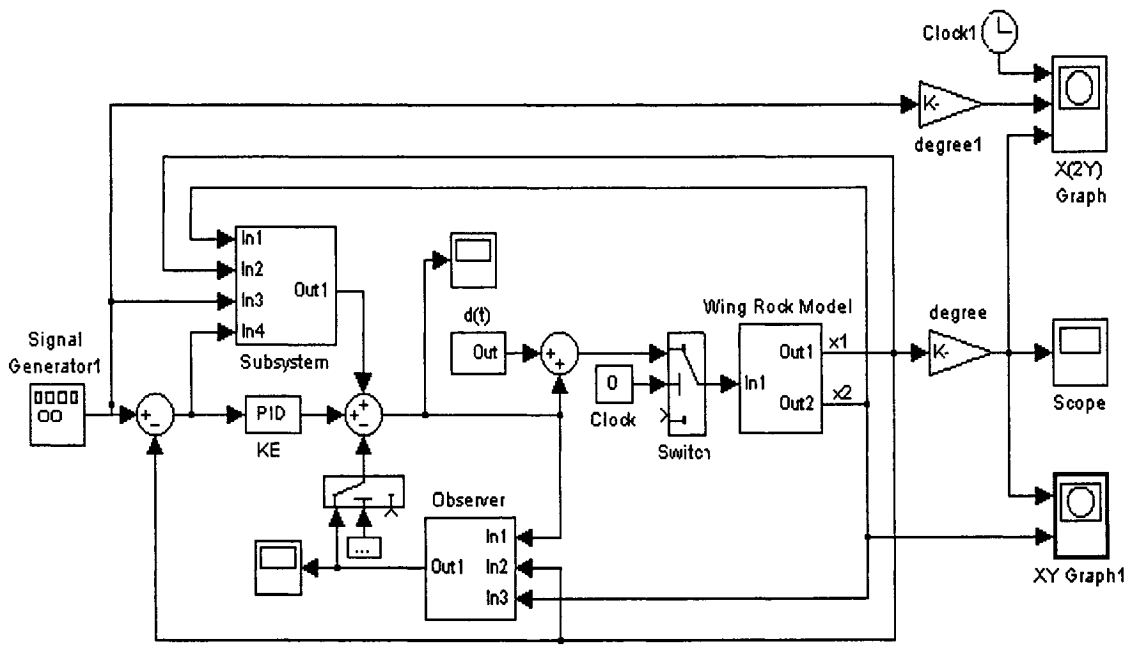

Figure 7.3 Simulink diagram of the NDOFEL for wing rock control

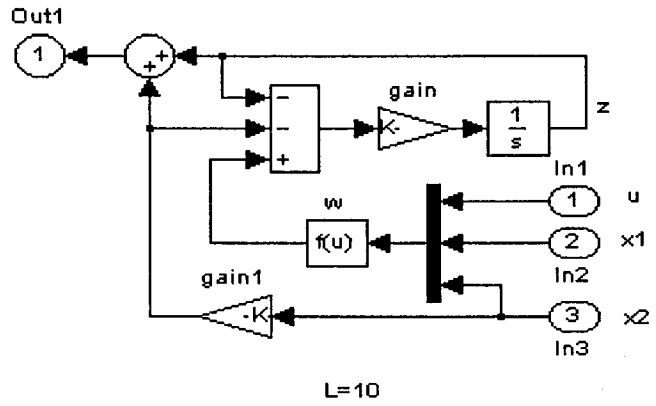

Figure 7.3(a) The NDO diagram

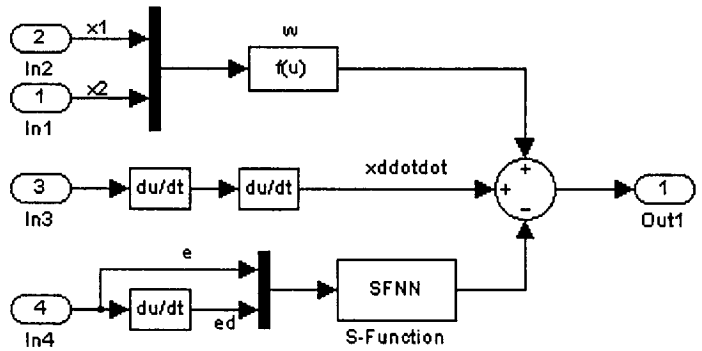

Figure 7.3(b) The control subsystem diagram

The following six cases are used to illustrate the effectiveness and main features of the proposed controller.

Case1: The suppressing control with $u_c = KE$

Figure 7.4 shows the simulation results at $\phi(0) = 2^0$ and $\dot{\phi}(0) = 0$, where the controller is activated at t=800 time steps. Obviously, the control law $u_c(t) = KE = 3e + 2\dot{e}$ can suppress wing rock. However, if the plant undergoes some disturbance, for example, the disturbance is $d(t) = 2\sin 2\pi t + \sin 5\pi t + 1.5$, the output response of control system will have an unreceptive steady-state error up to 50^0, as shown in Figure 7.5.

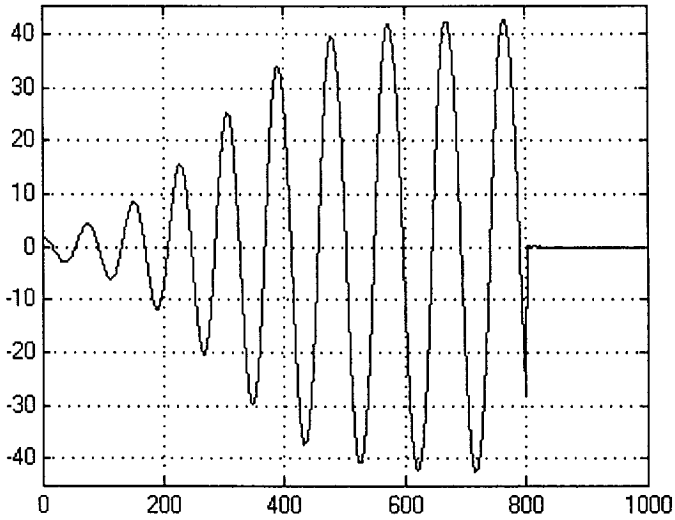

Roll angle (deg) vs. time steps

Figure 7.4 The output response of wing rock suppression with $u_c(t) = KE$

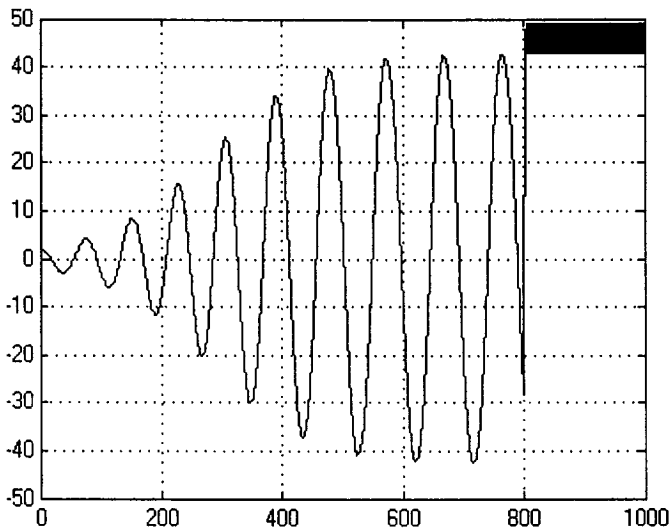

Roll angle (deg) vs. time steps

Figure 7.5 The output response of wing rock suppression with $u_c(t) = KE$

under $d(t) = 2\sin 2\pi t + \sin 5\pi t + 1.5$

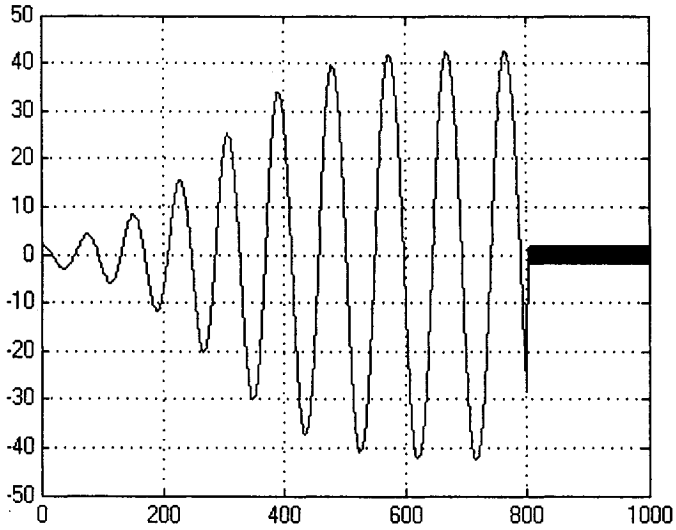

Figure 7.6 The output response $|e(t)| < 2^0$ of wing rock suppression with

$u = u_c + x_d^{(n)} - f_n(\mathbf{x}) - \hat{d}$ under $d(t) = 2\sin 2\pi t + \sin 5\pi t + 1.5$

Case2: The suppressing control with $u_c(t) = KE$ and the NDO

If we use the control law $u = u_c + x_d^{(n)} - f_n(\mathbf{x}) - \hat{d}$ to suppress wing rock phenomenon under the disturbance $d(t) = 2\sin 2\pi t + \sin 5\pi t + 1.5$, the steady-state error 50^0 in Figure 7.5 will be reduced into $|e(t)| < 2^0$, as shown in Figure 7.6.

Case3: The tracking control with $u_c(t) = KE$ and the NDO

Assume to track the desired trajectory $x_d(t) = 40^0 \sin 0.1\pi t$ at the initial condition $\phi(0) = 40^0$ and $\dot{\phi}(0) = 0$. Figure 7.7 shows that the control law $u = u_c + x_d^{(n)} - f_n(\mathbf{x}) - \hat{d}$ under the disturbance $d(t) = 2\sin 2\pi t + \sin 5\pi t + 1.5$ can reduce the tracking error into $|e(t)| < 3.1^0$.

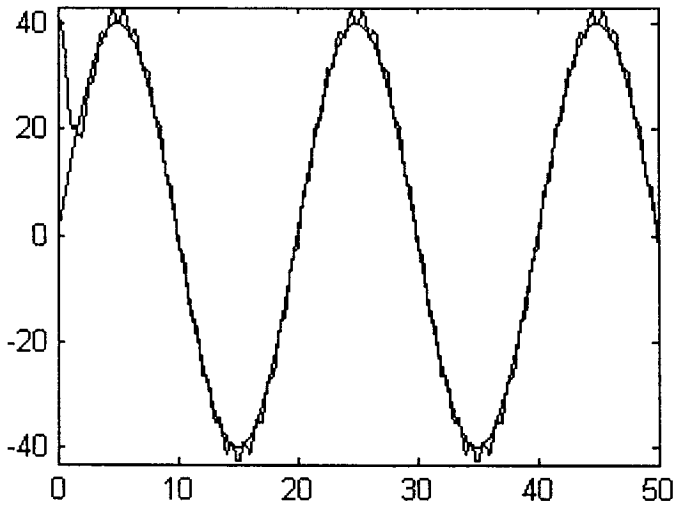

Roll angle (deg) vs. time steps

Figure 7.7 The output response $|e(t)| < 3.1^0$ of tracking control without the SFNN under $d(t) = 2\sin 2\pi t + \sin 5\pi t + 1.5$

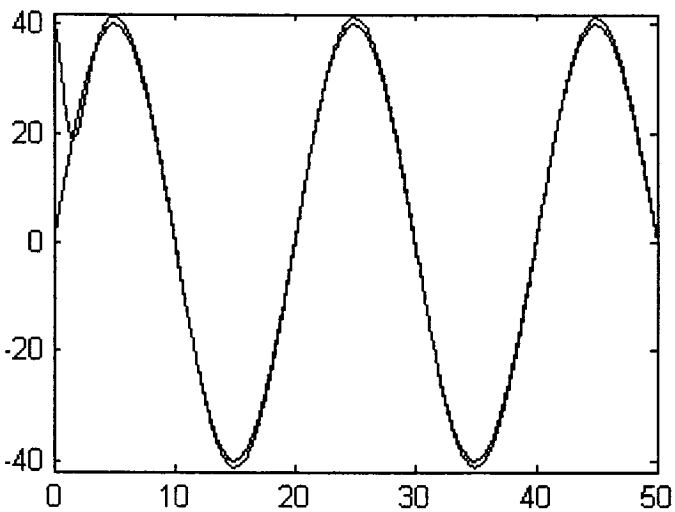

Roll angle (deg) vs. time steps

Figure 7.8 The output response $|e(t)| < 1.5^0$ of tracking control without the SFNN under $d(t) = 1.5$

Case4: The same as Case 3 except the constant disturbance d(t)=1.5

In this case, to verify the performance of the NDO, we repeat the simulation of *Case 3* but with the constant disturbance *d(t)=1.5*, which implied $\dot{d}(t) = 0$. If we use the control law $u = u_c + x_d^{(n)} - f_n(\mathbf{x}) - \hat{d}$ in the control system, the error $|e(t)| < 3.1^0$ in Figure 7.8 can be reduced into the small error range $|e(t)| < 1.5^0$, as shown in Figure 7.8. If we choose a bigger observer gain L, the tracking error will be smaller, and the control system will exhibit a better control performance.

To further reduce the tracking error, the proposed NDOFEL scheme is used in *Cases 5* and *6* for the tracking control during time-varying wing rock phenomenon with unknown disturbances.

Case5: The NDOFEL control

To demonstrate the NDOFEL performance, we simulate the above *Case 3* by using the proposed NDOFEL, instead of the control law $u = u_c + x_d^{(n)} - f_n(\mathbf{x}) - \hat{d}$. Assume λ =40 in Equation (7.11), e_0 =5^0 in Equation (7.35), the initial learning parameters of the SFNN to be $[\sigma \;\; r_1 \;\; r_2 \;\; r_3 \;\; r_4 \;\; r_5] = [2 \;\; 0 \;\; 0 \;\; 0 \;\; 0 \;\; 0]$, and the learning rates to be η_1 =0.5, η_2 =0.5, η_3 =0.8, η_4 =0.5, η_5 =0.5, and η_6 =0.05. When the simulation time is up to 50 time steps, the parameters of the SFNN after the learning are $[\sigma \;\; r_1 \;\; r_2 \;\; r_3 \;\; r_4 \;\; r_5]$ =[0.05 1.29 9.19 −2.20 0.49 0]. Figure 7.9 shows that the tracking error of the time-varying wing rock motion with unknown disturbances is reduced from $|e(t)| < 3.1^0$ into the small range $|e(t)| < 0.05^0$.

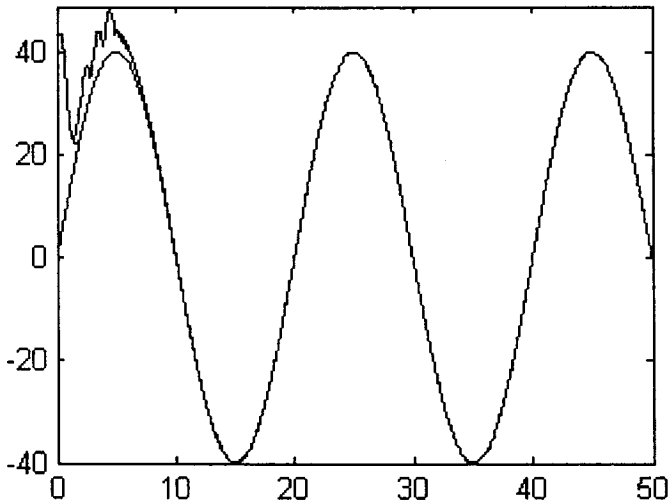

Roll angle (deg) versus time steps

(a) Tracking control output ($|e(t)| < 0.05^0$)

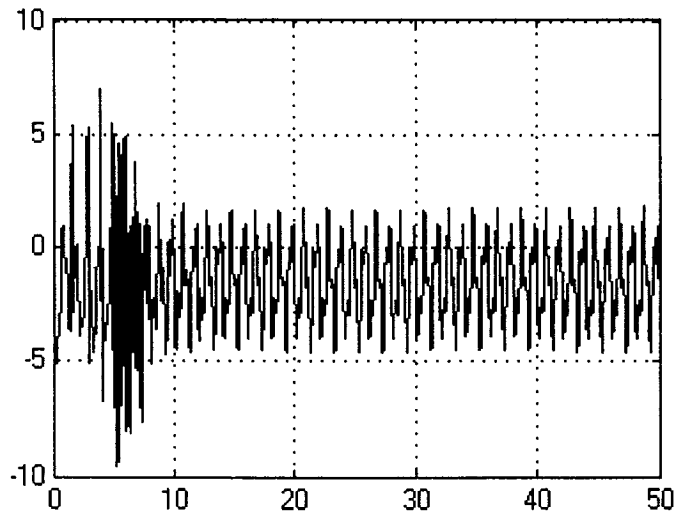

Time steps

(b) Control input $u(t)$

Figure 7.9 The NDOFEL tracking control for $x_d(t) = 40^0 \sin 0.1\pi t$

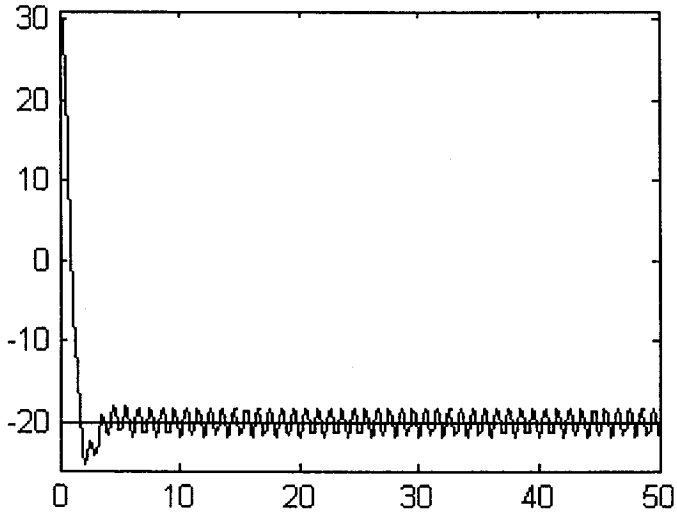

Roll angle (deg) vs. time steps

Figure 7.10 The output response $|e(t)| < 1.8^0$ of tracking control without the SFNN

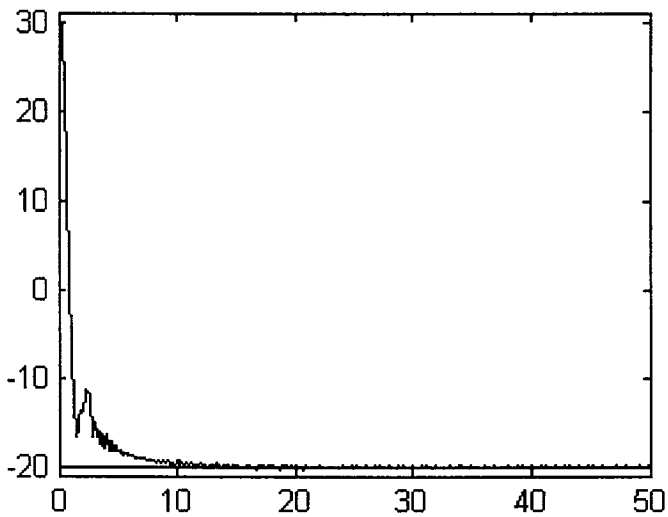

Roll angle (deg) vs. time steps

(a) The tracking control output ($-0.02^0 < e < 0.1^0$)

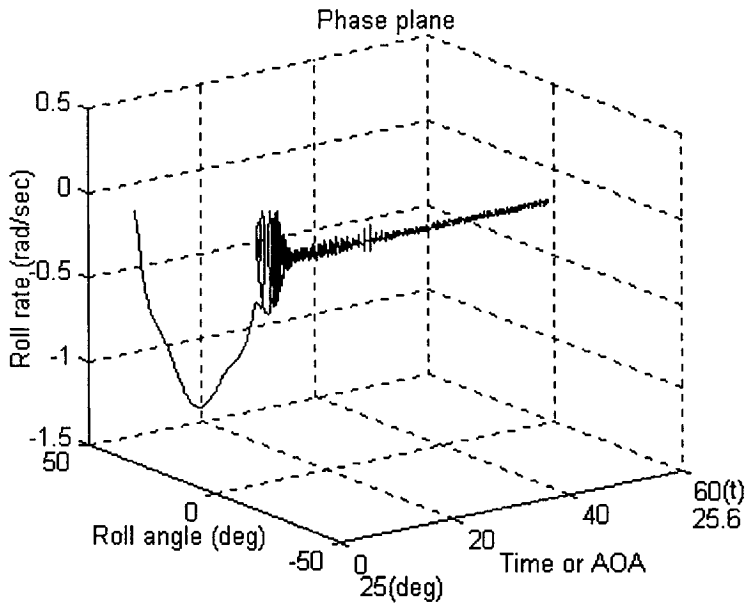

(b) Phase plane

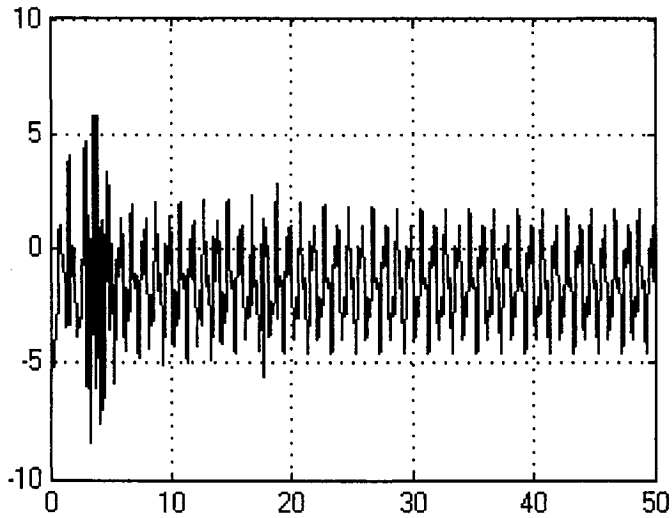

(c) The corresponding control input $u(t)$

Figure 7.11 The NDOFEL tracking control for $x_d(t) = -20^0$

Case 6: The same as Case 5 except the constant trajectory

In the last case, we assume to track the desired constant trajectory or angle, for example, $x_d(t) = -20^0$ at the initial condition $\phi(0) = 30^0$ and $\dot{\phi}(0) = 0$. After the 50 time-step learning, the parameters of the SFNN change from the initial learning parameters $[\sigma \ \ r_1 \ \ r_2 \ \ r_3 \ \ r_4 \ \ r_5]$=[2 0 0 0 0 0] to [0.20 3.34 12.75 −1.29 −1.7 0]. If we use the control law $u = u_c + x_d^{(n)} - f_n(\mathbf{x}) - \hat{d}$, Figure 7.15 shows the tracking error $|e(t)| < 1.8^0$; but, if we use the proposed NDOFEL control, the tracking error $|e(t)| < 1.8^0$ can be further reduced into the small range $-0.02^0 < e(t) < 0.1^0$, as shown in Figure 7.11(a). Figure 7.11(b) is the corresponding output response on phase plan, and Figure 7.11(c) is the corresponding the control input.

7.5 Summary

A novel learning control scheme, NDOFEL, has been proposed to control a class of time-varying nonlinear systems with unknown disturbances. In this scheme, we have taken two steps (the NDO and the SFNN) to estimate the system uncertainties and disturbances. The proposed NDOFEL not only extends the NDO into time-varying nonlinear system, but also improves the precision of tracking control. Lyapunov stability theory is used to derive the updating law of the parameters of the SFNN. The developed SFNN scheme is a simple, stable, and fast learning algorithm such that it can be applied for on-line learning and real-time control. The tracking control during wing rock phenomenon with disturbances is used to demonstrate the NDOFEL performances. Several cases have been used to show its tracking precision, disturbance rejection, and robustness.

To sum up, the proposed NDOFEL has the following features:

(a) Stable online learning ability,

(b) Quickly tracking the desired trajectory,

(c) Maintaining high control performance in the presence of uncertainties and disturbances,

(d) Guaranteeing asymptotical stability of the control system by Lyapunov theorem,

(e) Tuning only *one* fuzzy premise parameter, and

(f) Alleviating the chattering problem of SMC.

Chapter 8

Reinforcement Adaptive Fuzzy Control of Wing Rock Phenomenon

In this chapter, a new reinforcement adaptive fuzzy control scheme is proposed for the tracking control during wing rock phenomenon with uncertainties and disturbances. In this scheme, we assume aircraft's wing rock nominal model unavailable and then derive an adaptive fuzzy control law with a reinforcement-learning (RL) strategy. This chapter is organized as follows: After the introduction in Section 8.1, we provide some preliminary knowledge in Section 8.2. The proposed reinforcement adaptive fuzzy control is designed in Section 8.3. Numerical simulation results of wing rock tracking control are given in Section 8.4. Section 8.5 summarizes this Chapter.

8.1 Introduction

In the previous Chapters 5-7, several nonlinear control schemes have been developed for wing rock suppressing or tracking control, based on the analytical models (2.9) from the free-to-roll test of 80^0 flat-plate delta wing. However, this analytical model may not be

suitable for practical aircraft tracking control. For example, Owens *et al.* in Reference [74] reported that recent free-to-roll test results for four military aircraft (AV-8B, F/A-18C, pre-production F/A-18E, and F-16C) at transonic conditions have shown that *five* types of rolling motions are observed during the tests, and these test results are in agreement with flight test data on all four military aircraft. The test results indicate that aircraft's wing rock phenomenon is a complex, uncertain, and time-varying non-linear system so that its precise analytical modelling is unavailable. Therefore, to guarantee the robustness and stability of the control system, a new reinforcement adaptive fuzzy control scheme is proposed for suppressing or tracking the wing rock phenomena.

Fuzzy logic control (FLC) has recently emerged as one of the most active and fruitful approaches to control complex nonlinear systems. The motivation is often due to the fact that the knowledge and dynamic behavior of systems are qualitative and uncertain, so the fuzzy set theory appears to provide a suitable representation of such knowledge, as described in References [138-140]. In this study, the variable universe technique based on an interpolation mechanism of FLS, as discussed in detail in Section 6.3, is applied to modify the premise parameters of FLS but keep fuzzy rules the same. The remarkable advantage of the variable universe fuzzy control is that it not only needs several fuzzy rules but also keeps a high approximate precision, especially suitable for on-line learning and real time control of control systems.

As to the consequent parameters of FLC, on the other hand, the adaptive law is derived to compensate the uncertain dynamics of wing rock. The learning capability of the adaptive

control in References [54, 141-142] can be achieved by employing an FLS. We design an appropriate adaptation law to tune the parameters of the function approximator. However, the adaptive control systems are usually limited that the time-varying plant parameters must vary considerably slower than the parameter adaptation, and adaptive control methods, as claimed in Reference [113], may be limited to constant disturbances. To obtain fast and precise on-line adaptive ability for the time-varying wing rock phenomenon of aircraft in the uncertain environment, we need to combine the adaptive control law with a reinforcement-learning (RL) strategy in References [143-145] to tune the consequent parameters of the FLC.

The RL stratagem, as discussed in References [143-147], can be used to learn the unknown desired outputs by means of the controller receiving a reinforcement signal (reward or punishment) according to the last action it has performed in the previous state and then the controller adjusting itself with suitable evaluation of its performance.

However, the proposed approach has several important differences from the work of Reference [146] for robots and Reference [147] for friction compensation.

(a) The reinforcement signal is simply equal to the performance measurement, $r(t) = s(t)$, but the $\lambda(t)$ varies with an error signal $e(t)$ in performance measurement function $s(t) = \dot{e}(t) + \lambda(e)e(t)$. By comparison, the adaptive critic element (ACE) in Reference [146] was used to generate a reinforcement signal vector to tune the fuzzy system; the two functions of performance measurement signal in Reference [147] were used to construct a reinforcement signal.

(b) The universe of premise parameters of the fuzzy approximator is modified by a variable universe technique to improve the interpolation precision of the FLS. On the contrary, fixed fuzzy basis functions were used in Reference [146] and fixed sigmoid activation functions were used in Reference [147].

(c) In the FLS, we use only four fuzzy rules. By comparison, 81 fuzzy rules were used in Reference [146], and 40 hidden units in neural network were used in Reference [147].

In addition, the proposed reinforcement adaptive fuzzy control algorithm is derived by Lyapunov theorem to ensure the stability of the closed-loop system and the convergence of the tracking error. In particular, the uniform ultimate boundedness (UUB) of the tracking error with this controller is guaranteed.

The novelty of the proposed control scheme is mainly on the simplicity, robustness, and stability of the control algorithm so that it can be applied for on-line learning and real-time control. Three cases of the time-varying wing rock control under unknown disturbances are used to confirm the effectiveness and robustness of the proposed scheme.

8.2 Preliminaries

1) FLS

As mentioned in Section 6.1, an FLS is mainly concerned with imprecision and approximate reasoning. The fuzzy inference engine uses the fuzzy IF-THEN rules to perform a mapping from an input linguistic vector $\mathbf{x}(t) = (x_1, \cdots, x_n) \in U = U_1 \times \cdots \times U_n$

$\subset R^n$ to an output variable $y(t) \in V \subset R$. The ith fuzzy rule is written as

$$R^i: \ IF \ x_1 \text{ is } A_1^i \text{ and } \ldots \text{ and } x_n \text{ is } A_n^i \ THEN \ y \text{ is } w^i \tag{8.1}$$

where A_j^i is a fuzzy variable and w^i is a singleton number.

If the fuzzifier is a singleton, the inference engine adopts a minimum operator, and the defuzzifier is a center average, then the fuzzy system can be formulated by

$$y(\mathbf{x}) = \frac{\sum_{i=1}^{N} w^i \mu^i}{\sum_{i=1}^{N} \mu^i} = W^T \Phi(\mathbf{x}) \tag{8.2}$$

where $\mu^i = \min(\mu_1^i(x_1), \cdots, \mu_n^i(x_n))$, μ_j^i is the membership function value of fuzzy variable x_j, N is the number of fuzzy rules, $W^T = [w^1 \quad w^2 \quad \cdots \quad w^N]$ is the adjustable consequent parameter vector, and $\Phi = [\Phi^1 \quad \Phi^2 \quad \cdots \quad \Phi^N]^T$ in which $\Phi^i = \mu^i \Big/ \sum_{i=1}^{N} \mu^i$ is the fuzzy basis function.

2) Variable Universe Technique

As described in Section 6.3, a variable universe means that some universe $U_j = [-L_j \quad L_j]$ can change along with changing of variable $x_j(t)$, where L_j is a constant determined by designers according to the change range of $x_j(t)$, which means

$$\overline{U}_j = [-\alpha_j(x_j)L_j \quad \alpha_j(x_j)L_j] \tag{8.3}$$

where $\alpha_j > 0$ is called a contraction-expansion factor of the universe $\overline{U}_j$.

The triangle membership functions are chosen in this work. We denote P and N as fuzzy

subsets of the input variable $x_j(t)$ and define the membership functions $\mu_P(x_j)$ and $\mu_N(x_j)$ as

$$\mu_P(x_j) = \begin{cases} 0 & x_j < -L_j \\ (x_j + L_j)/(2L_j) & -L_j \le x_j \le L_j \\ 1 & x_j > L_j \end{cases} \tag{8.4}$$

$$\mu_N(x_j) = 1 - \mu_P(x_j) \tag{8.5}$$

The following contraction-expansion factor in this chapter is suggested

$$\alpha_i(x_i) = \varepsilon_i + \left(|x_i| / L_i\right)^{\tau_i} \tag{8.6}$$

where ε_i is a very small constant for computing efficiency, for example, taken as ε_1= 0.001, and $0.1 < \tau_i < 1$ is suggested.

3) Reinforcement Learning

To use RL strategy, we first need to understand its basic idea by comparing with supervised learning.

In supervised learning, also called "learning with a master", the learning system knows the error that is committed at all times. For each input vector, the corresponding desired output is known. This difference between the actual and the reference output can be used to modify parameters.

In RL, or "learning with a critic", the received signal is the sanction (positive, negative or neutral) of a behavior; this signal indicates what you have to do without saying how to do

it. The agent uses this signal to determine a policy permitting to reach a long-term objective.

Another difference between these two approaches is that reinforcement learning is fundamentally on-line because the agent's actions modify the environment to determine the policy that will maximize the future rewards.

Figure 8.1 depicts the general process of RL from Reference [148]. At time step t, the agent is in state $x(t)$, and then it chooses one of the possible actions in this state, $a(t)$. Next, it applies the action to produce a new state $x(t+1)$ and to obtain the receipt of the reinforcement $r(t)$. At time step t+1, repeat above actions or stop if the new state is a terminal one.

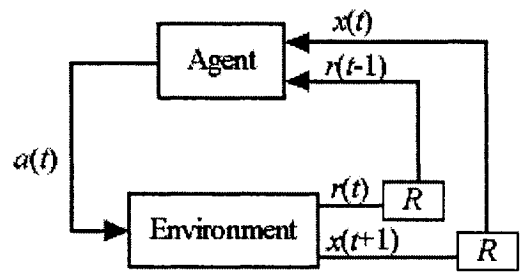

Figure 8.1 Modeling of interaction between the agent and its environment where $\boxed{R}$ represents a delay [148]

The objective of RL is to discover a control policy, a mapping from states to control actions. There is no direct evaluation of the selected control action. Instead, an indirect evaluation is received in terms of satisfaction or dissatisfaction of the control objectives.

RL can discover such control policy that maximizes the reinforcement received.

A general scheme realizing this type of RL consists of two units: the critic (evaluation unit) and the controller (action unit). The task of the critic is to predict the future system performance. The prediction is needed to obtain a more informative signal (internal reinforcement), which can be used to adapt the critic and the controller. In simple RL problems, it is sufficient that the critic predicts one step ahead. When the critic has learned to predict the future system's performance, the controller can be trained to establish an optimal mapping between the system states and the control actions in the sense that the control performance is best.

4) Wing Rock Behavior of Military Aircraft at Transonic Conditions

Authors of Reference [74] have recently analyzed transonic free-to-roll and static wind tunnel tests for four military aircraft: the Av-8B, the F/A-18C, the pre-production F/A-18E, and F-16C. These tests have been conducted in the NASA Langley 16-Foot Transonic Tunnel as a part of the NASA/Navy/Air Force Abrupt Wing Stall Program. During the free-to-roll tests, a wide variety of rolling motions have been observed. The motions can be categorized into five types.

- *Type 1 – Limit-cycle wing rock.* This motion is characterized by wing rock for which the amplitude range is fixed and does not vary with time.
- *Type 2 – Wing rock with nearly constant frequency, but more prominently recognized by varying amplitude.*
- *Type 3 – Occasional damped wing drop and wing rock.* Occasional means there

may be many seconds between wing drop/rock events where there is not any significant lateral activity.

- *Type 4 – Frequent damped wing rock and wing drop. Type 4* tends to occur more often during the heart of the stall.
- *Type 5 – Divergent wing rock and wing drop.* The motion of *Type 5* is determined by the static and dynamic stability.

With the exception of having a perfect limit-cycle wing-rock motion, rolling motions of all five types were observed during the test. Obviously, wing rock phenomena of aircraft at a high AOA are complex, uncertain, and time-varying nonlinear systems. Generally, a satisfactory analytical model cannot be obtained for such systems. Thus, we can assume that wing rock model of aircraft is a second-order unknown nonlinear system with the lumped disturbances term $d(t)$.

5) Nonlinear Systems

Consider second-order nonlinear systems of the form

$$\begin{aligned} \ddot{x}(t) &= f(\mathbf{x}) + u(t) + d(t) \\ y(t) &= x(t) \end{aligned} \tag{8.7}$$

where $f(\mathbf{x})$ is an *unknown* nonlinear continuous function, $\mathbf{x}(t) = [x_1(t) \quad x_2(t)]^T = [x(t) \quad \dot{x}(t)]^T \in R^2$ is the state vector of the system, $d(t)$ is an unknown external disturbance, $u(t) \in R$ and $y(t) \in R$ are the input and output of the system, respectively. Moreover, we assume that $f(\mathbf{x})$ and $d(t)$ to have upper bounds $\bar{f}(\mathbf{x})$ and $\bar{d}$, that is, $|f(\mathbf{x})| \le \bar{f}(\mathbf{x})$ and $|d(t)| \le \bar{d}$, respectively.

8.3 Controller Design

The control objective in this chapter is to use the adaptive fuzzy control method combined with RL strategy such that the system output $x(t)$ can track the desired trajectory $\mathbf{x}_d(t) = [x_d \quad \dot{x}_d]^T$ in the condition of uncertainties and unknown disturbances.

The tracking error $e(t)$ and performance signal $s(t)$ can be expressed as:

$$e(t) = x_d(t) - x(t) \tag{8.8}$$

and

$$s(t) = \dot{e}(t) + \lambda(e)e(t) \tag{8.9}$$

Assume $\lambda(e) = k_\lambda / (|e| + \varepsilon_\lambda)$, k_λ is a given positive constant, and ε_λ is a small constant, for example, let $\varepsilon_\lambda = 0.2$. We should point out that the idea of varying $\lambda(e)$ is similar to tuning the slope of sliding surface, as used in References [149-150]. The larger it is, the faster will the system response be. But a too large value of $\lambda(e)$ can cause overshoot, or even instability. It would, therefore, be advantageous to adaptively vary the slope in such a way that the slope increases with the decreasing errors.

It is typical to define a performance signal $s(t)$ as a performance measurement; when the performance signal $s(t)$ is small, the system performance is better. With Equations (8.7) and (8.8), the derivative of $s(t)$ in Equation (8.9) can be obtained as

$$\dot{s}(t) = g(\bar{\mathbf{x}}) - u(t) - d(t) \tag{8.10}$$

where the unknown function $g(\bar{\mathbf{x}})$ is given by

$$g(\bar{\mathbf{x}}) = \ddot{x}_d(t) + \dot{\lambda}(e)e(t) + \lambda(e)\dot{e}(t) + f(\mathbf{x}) \tag{8.11}$$

where $\bar{\mathbf{x}}(t) = [\ddot{x}_d(t) \quad e(t) \quad \mathbf{x}(t)]^T$.

We assume that the terms $\lambda(e)\dot{e}(t) + \dot{\lambda}(e)e(t) - f(\mathbf{x})$ in Equation (8.11) can be represented by an ideal fuzzy approximator term $W^T\Phi(\mathbf{x})$ as follows

$$g(\bar{\mathbf{x}}) = \ddot{x}_d(t) + W^T\Phi(\mathbf{x}) + \varepsilon(\mathbf{x}) \tag{8.12}$$

where $\varepsilon(\mathbf{x})$ is the neural network approximation error, $W^T = [w_1 \quad w_2 \quad \cdots \quad w_n]$ is an ideal weight matrix, and $\Phi(\mathbf{x})$ is a fuzzy base function. The function $g(\bar{\mathbf{x}})$ can be identified by a following terms (see Appendix C in detail):

$$\hat{g}(\bar{\mathbf{x}}) = \ddot{x}_d(t) + \hat{W}^T\Phi(\mathbf{x}) \tag{8.13}$$

Define the control law

$$u(t) = Ks(t) + \hat{g}(\bar{\mathbf{x}}) - \hat{d}(t) \tag{8.14}$$

where K represents the fixed gain in the overall control scheme, $\hat{g}(\bar{\mathbf{x}})$ is the output vector of the fuzzy approximator, and $\hat{d}(t)$, see Equation (8.17), is the robustifying term to attenuate disturbances. It should be noted that $Ks(t)$ in Equation (8.14) is similar to a PD controller, which can maintain the system stability; thus, the weight values can be initialized to be zero. This means that there is no need off-line learning or trial and error phase. Figure 8.2 shows the architecture of the proposed wing rock control scheme.

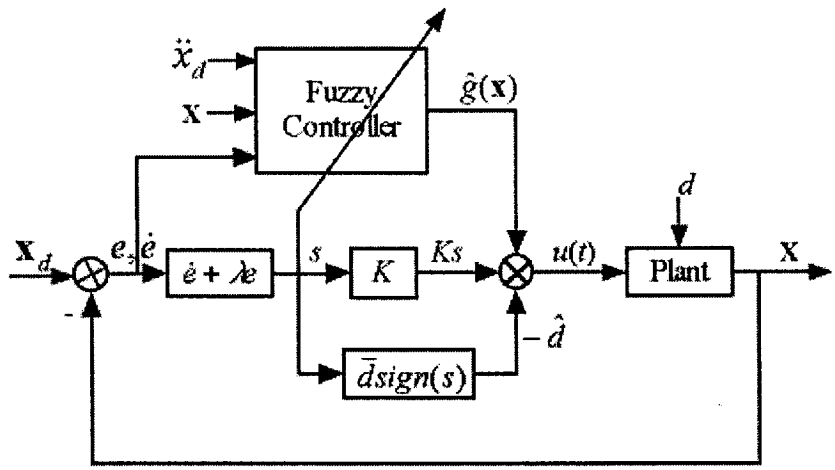

Figure 8.2 The reinforcement adaptive fuzzy control diagram of wing rock

Substituting Equation (8.14) into Equation (8.10), we obtain the closed-loop dynamics as

$$\dot{s}(t) = -Ks(t) + \tilde{g}(\bar{\mathbf{x}}) + \hat{d}(t) - d(t) \tag{8.15}$$

where the approximation error $\tilde{g}(\bar{\mathbf{x}})$ is denoted as

$$\tilde{g}(\bar{\mathbf{x}}) = g(\bar{\mathbf{x}}) - \hat{g}(\bar{\mathbf{x}}) = \tilde{W}^T \Phi(\mathbf{x}) + \varepsilon(\mathbf{x}) \tag{8.16}$$

with $\tilde{W} = W - \hat{W}$ and the robustifying term is given by

$$\hat{d}(t) = \bar{d}sign(s(t)) \tag{8.17}$$

As we see, Equation (8.15) implies that the overall system is driven by the functional estimation error $\tilde{g}(\bar{\mathbf{x}})$ and disturbance error $\tilde{e}_d(t) = \hat{d}(t) - d(t)$.

To achieve fast and precise tracking of an uncertain nonlinear system, the incomplete experts knowledge may not be enough. RL strategy is used in the adaptive fuzzy control scheme. In RL, an internal evaluator called the critic, which can predict the future system performance, is used. This prediction is needed to obtain a more informative signal

(internal reinforcement), which can be used to adapt the critic and the controller, as explained in Reference [151].

.

We assume a special case of reinforcement signal to be

$$r(t) = s(t) \tag{8.18}$$

where $r(t)$ is used to update the weight vector $\hat{W}$. Before the stability analysis, we have two assumptions:

(a) $\|W\|_F \leq W_m$ with a known W_m (the Frobenius norm is defined by $\|W\|_F = [tr(W^T W)]^{1/2} = \sqrt{\sum_{i,j} w_{ij}^2}$);

(b) The approximate error and disturbance error is bounded, that is, $\left|\varepsilon - d + \hat{d}\right| \leq \varepsilon_b$.

Theorem: If the weight tuning law provided for the fuzzy approximator is

$$\dot{\hat{W}} = r(t) K_w \Phi(\mathbf{x}) - \eta K_w |s(t)| \hat{W} \tag{8.19}$$

where K_w is a positive and diagonal constant matrix, η is a positive constant, and the $r(t)$ given by Equation (8.18) is the reinforcement signal, then the control input $u(t)$ given by Equation (8.14) guarantees that the $s(t)$ and $\hat{W}$ are uniformly ultimately bounded (UUB).

Proof: Define the Lyapunov function candidate

$$V(t) = \tfrac{1}{2} s^2 + \tfrac{1}{2} tr\{\tilde{W}^T K_w^{-1} \tilde{W}\} \tag{8.20}$$

with $\tilde{W} = W - \hat{W}$. Evaluating the time derivative of $V(t)$ along the trajectories of the weight tuning laws in Equation (8.19) yields

$$\dot{V}(t) = s\dot{s} + tr\{\tilde{W}^T K_w^{-1} \dot{\tilde{W}}\} \tag{8.21}$$

Substituting Equations (8.15) and (8.17)-(8.19), noting that $\dot{\tilde{W}} = \dot{W} - \dot{\hat{W}}$ with $\dot{W} = 0$, into Equation (8.21), we can rewrite it as

$$\begin{aligned} \dot{V}(t) &= s(-Ks + \tilde{W}^T \Phi - d + \hat{d}) - tr\{\tilde{W}^T K_w^{-1}(rK_w \Phi - \eta K_w |s| \hat{W})\} \\ &= -Ks^2 + s\tilde{W}^T \Phi + s\varepsilon_b - tr\{r\tilde{W}^T \Phi - \eta |s| \tilde{W}^T \hat{W}\} \\ &= -Ks^2 + s\varepsilon_b + \eta |s| tr\{\tilde{W}^T \hat{W}\} \end{aligned} \tag{8.22}$$

Applying the matrix inequality $\tilde{W}^T \hat{W} \le \left\|\tilde{W}\right\|_F W_m - \left\|\tilde{W}\right\|_F^2$, Equation (8.22) becomes

$$\begin{aligned} \dot{V}(t) &\le -Ks^2 + s\varepsilon_b + \eta |s| (\left\|\tilde{W}\right\|_F W_m - \left\|\tilde{W}\right\|_F^2) \\ &\le -Ks^2 - \eta |s| \{(\left\|\tilde{W}\right\|_F - W_m/2)^2 - \varepsilon_b/\eta - W_m^2/4\} \end{aligned} \tag{8.23}$$

Therefore, $\dot{V}(t)$ is guaranteed to be negative as long as either Equation (8.24) or (8.25) holds.

$$|s| \ge (\varepsilon_b + \eta W_m^2/4)/K = B_s \tag{8.24}$$

$$\left\|\tilde{W}\right\|_F \ge W_m/2 + \sqrt{\varepsilon_b/\eta + W_m^2/4} = B_w \tag{8.25}$$

Clearly, from inequalities in Equations (8.24) and (8.25), we can define compact set Ω: $\Omega = \{(|s|, \left\|\tilde{W}\right\|_F) \mid 0 \le |s| \le B_s \text{ and } \left\|\tilde{W}\right\|_F \le B_w\}$. By Lyapunov theory, for $s(t_0)$ and $\tilde{W}(t_0) \in \Omega$, there exists numbers $T(B_s, B_w, s(t_0), \tilde{W}(t_0))$ such that $0 \le |s(t)| \le B$ and $\left\|\tilde{W}\right\|_F \le B_w$ for all $t \ge t_0 + T$. In other words, $\dot{V}(s, \tilde{W})$ is negative outside the compact set Ω, and then s and $\tilde{W}$ are UUB. □

8.4 Simulation Results of Wing Rock Control

8.4.1 Wing Rock Model

In Section 8.2, we assume the mathematical model (8.7) of wing rock phenomenon contains the *unknown* continuous nonlinear function $f(\mathbf{x})$. To confirm the effectiveness of the proposed scheme, we regard the differential equation (7.36), a time-varying wing rock motion with the lumped disturbance $d(t)$, as the wing rock model. Equation (7.36) is then rewritten as:

$$\ddot{\phi} = -(a_0\phi + a_1\dot{\phi} + a_2|\dot{\phi}|\dot{\phi} + a_3\phi^3 + a_4\phi^2\dot{\phi}) + u(t) + d(t) \tag{8.26}$$

Comparing Equation (8.26) with Equation (8.7), we can see that the *unknown* term $f(\mathbf{x}) = -(a_0\phi + a_1\dot{\phi} + a_2|\dot{\phi}|\dot{\phi} + a_3\phi^3 + a_4\phi^2\dot{\phi})$.

8.4.2 Simulation Results

To evaluate the robustness of the proposed control scheme, we assume the lumped disturbance $d(t) = 2\sin 2\pi t + \sin 5\pi t + 1.5$, which is added in the close-loop system at $t = 20$ time steps for all cases. The initial condition we choose is $\phi(0) = 40^0$ and $\dot{\phi}(0) = 0$. The parameters used in this simulations are $L_1 = 0.7$ rad, $L_2 = 1$ rad/sec, $\varepsilon_1 = \varepsilon_2 = 0.001$, and $\tau_1 = \tau_2 = 0.9$ in Equation (8.6), $k_\lambda = 10$ and $\varepsilon_\lambda = 0.2$ for solving $\lambda(e)$, and $\tau = 0.01$, $K_w = K = 50$, and $\eta = 0.08$ in Equation (8.26).

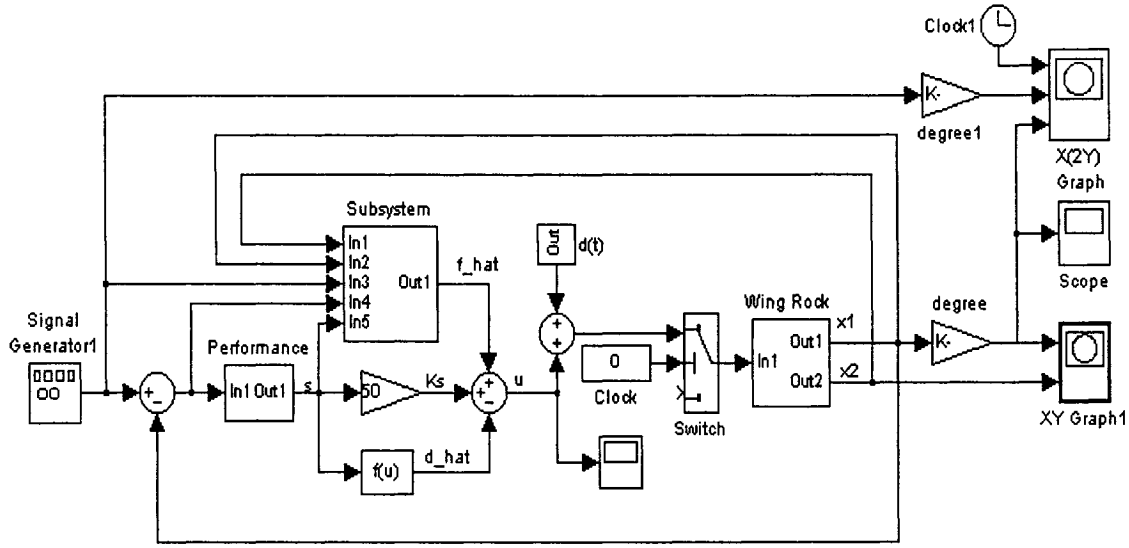

Figure 8.3 Simulink diagram of the reinforcement adaptive fuzzy control

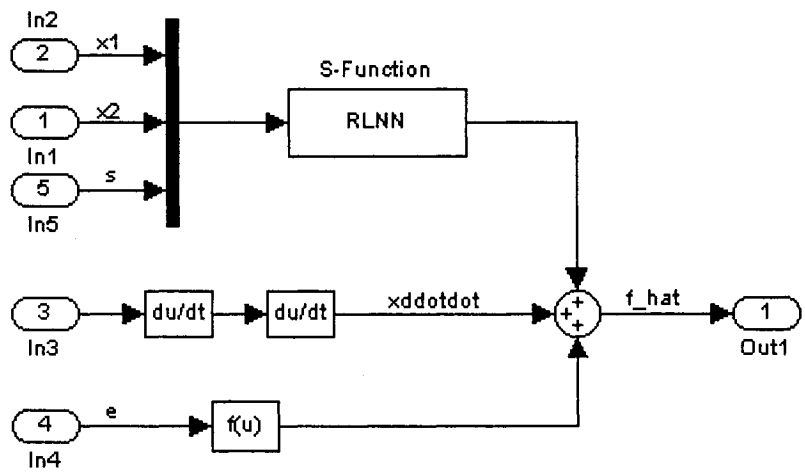

Figure 8.3(a) The control subsystem diagram

The numerical simulations of wing rock tracking control are implemented in Matlab and Simulink environments. Figure 8.3 shows the corresponding Simulink block diagram.

We are interested in the following three cases for the suppressing and tracking control of wing rock phenomenon with unknown disturbances.

Case1: Wing rock suppression

We first verify the suppressing control of the proposed control scheme. Figure 8.4(a) shows the output response of wing rock control on phase plane. The results show that the proposed control scheme can suppress wing rock quickly and then maintains the states at the equilibrium point with the error $0 < e(t) < 0.14^0$, even though the system is time varying and with disturbances. Figure 8.4(b) shows the corresponding control input, and Figure 8.4(c) shows the stable four updating weights over time.

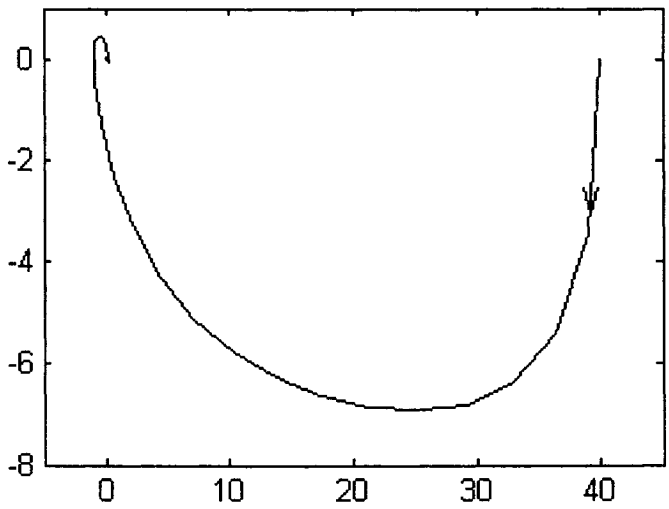

Roll rate $\dot{\phi}(t)$ (rad/sec) versus $\phi(t)$ (deg)

(a) Wing rock suppression on phase plan

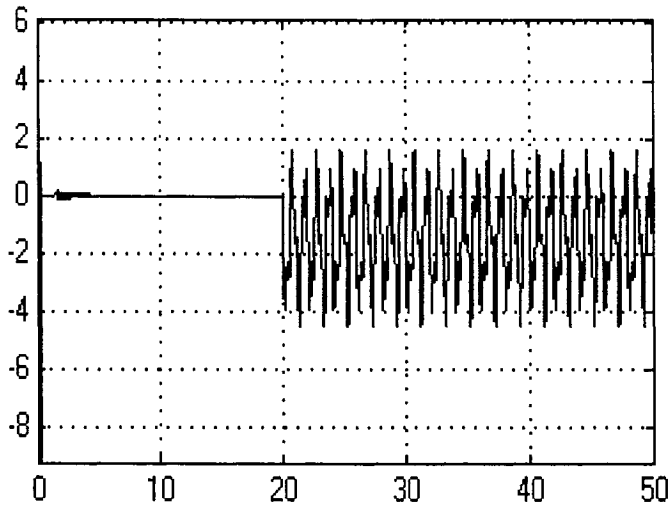

(b) Suppressing control input $u(t)$

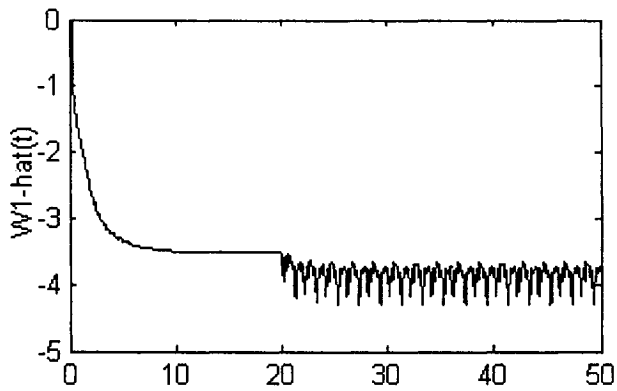

Time steps

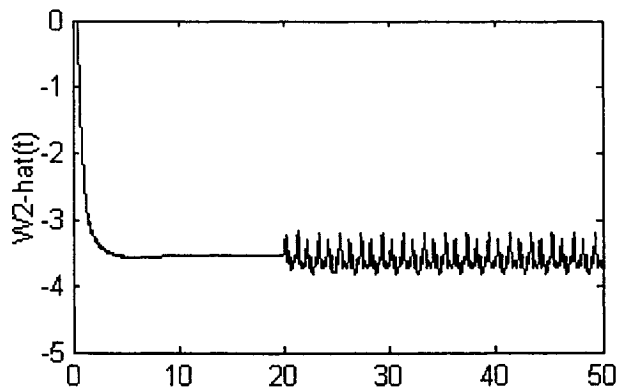

Time steps

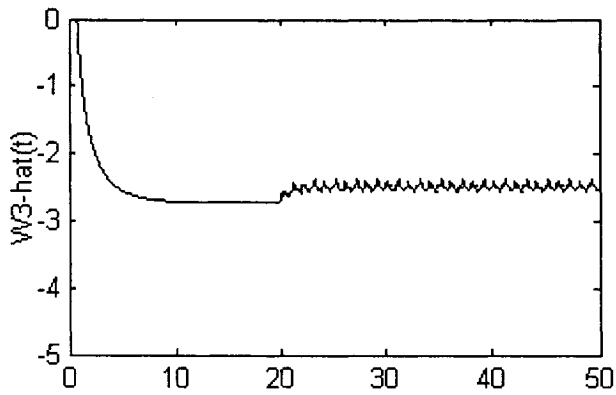

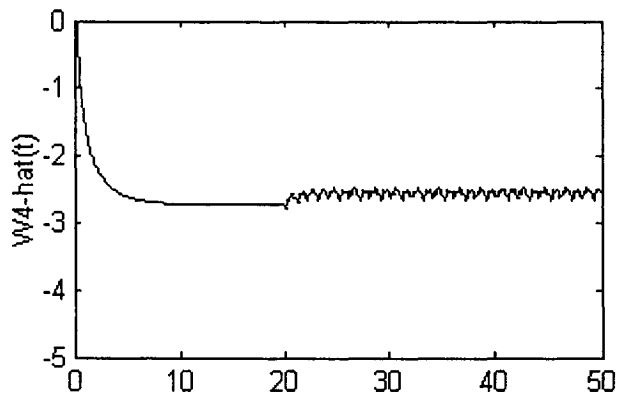

(c) Weight updating $\hat{W}^T(t) = [\hat{W}_1 \quad \hat{W}_2 \quad \hat{W}_3 \quad \hat{W}_4]$

Figure 8.4 Wing rock suppression for *Case 1*

Case2: Tracking control for $x_d(t) = 40^0 \sin 0.05\pi t$

In *Case 2* and *Case 3*, we will verify the tracking performance of the proposed control scheme. Assume to track the time-varying trajectory $x_d(t) = 40^0 \sin 0.05\pi t$. Figure 8.5(a) shows that the proposed control scheme can achieve satisfactory performances, where the output roll angle follows the desired trajectory almost simultaneously. If the disturbance is added in the time-varying system at t =20 time steps, the control output keeps almost same performances with the error $|e(t)| < 0.15^0$. Figure 8.5(b) shows the corresponding control input. The weight updating is shown in Figure 8.5(c), where we observe that the four weights with respect to the four fuzzy rules alternately make a big tuning when the system states enter the different phases.

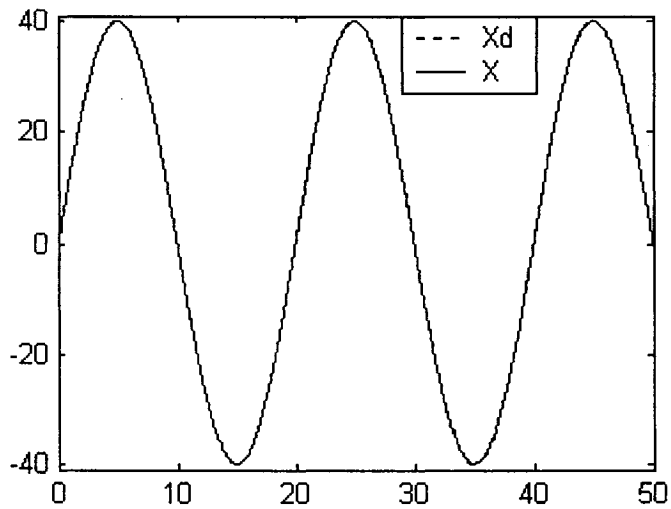

Roll angle $\phi(t)$ (deg) versus time steps

(a) Wing rock tracking control for $x_d(t) = 40^0 \sin 0.05\pi t$

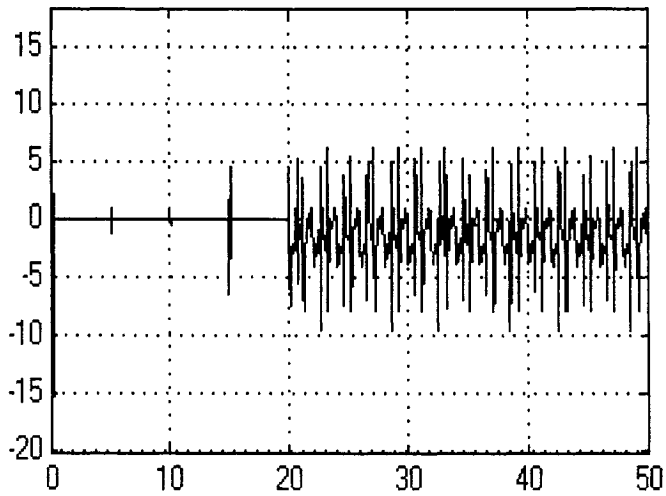

(b) Tracking control input $u(t)$

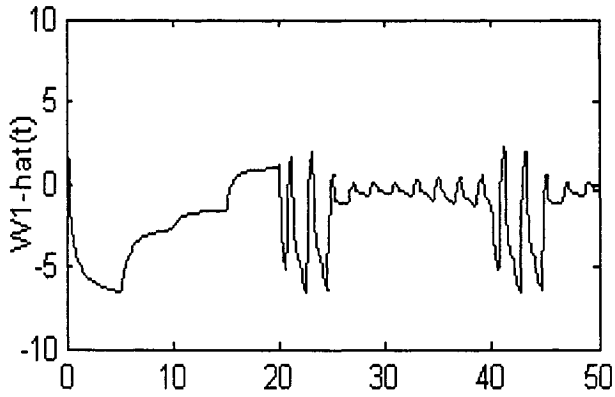

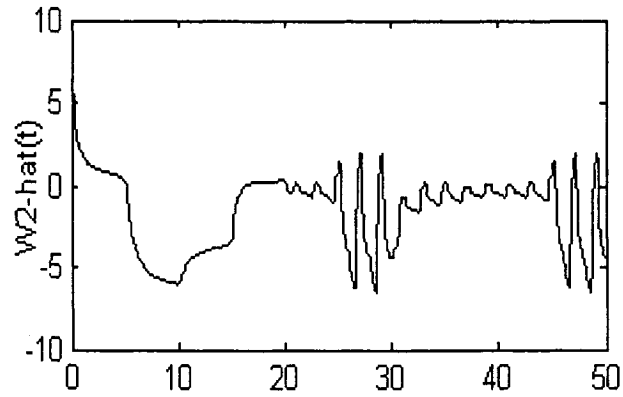

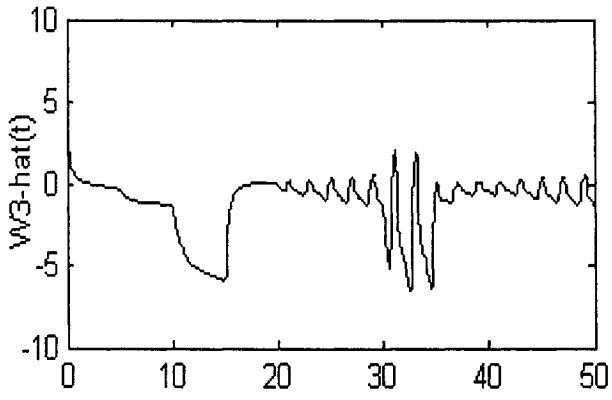

Time steps

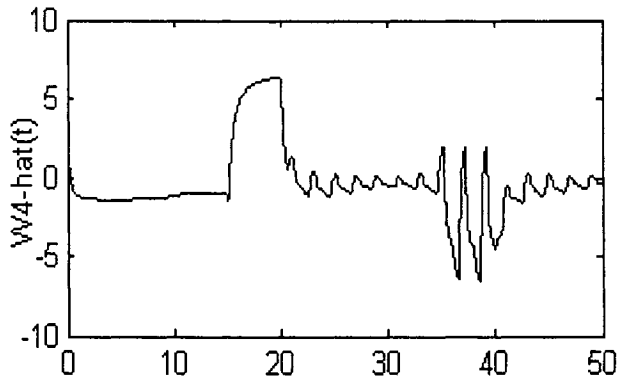

Time steps

(c) Weight updating $\hat{W}^T(t) = [\hat{W}_1 \quad \hat{W}_2 \quad \hat{W}_3 \quad \hat{W}_4]$

Figure 8.5 Tracking a time-varying trajectory $x_d(t) = 40^0 \sin 0.05\pi t$

Case3: Tracking a constant trajectory $x_d(t) = -20^0$

In fact, tracking a constant trajectory in wing rock phenomenon usually results in a big tracking error. Figure 8.6(a) shows the output response of tracking $x_d(t) = -20^0$ on phase plane. Figure 8.6(b) shows that if the disturbance is added in the system, the proposed control scheme can reject disturbances and can maintain the tracking error in the small range $|e(t)| < 0.23^0$. Figure 8.6(c) shows the corresponding weight updating.

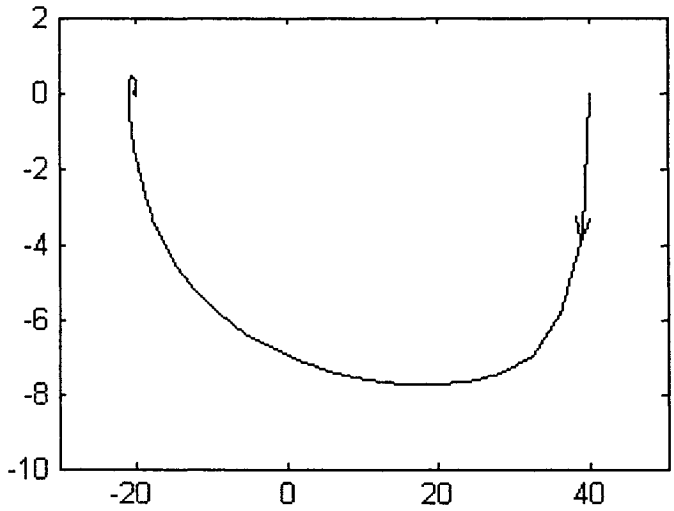

Roll rate $\dot{\phi}(t)$ (rad/sec) versus $\phi(t)$ (deg)

(a) Tracking $x_d(t) = -20^0$ on phase plane

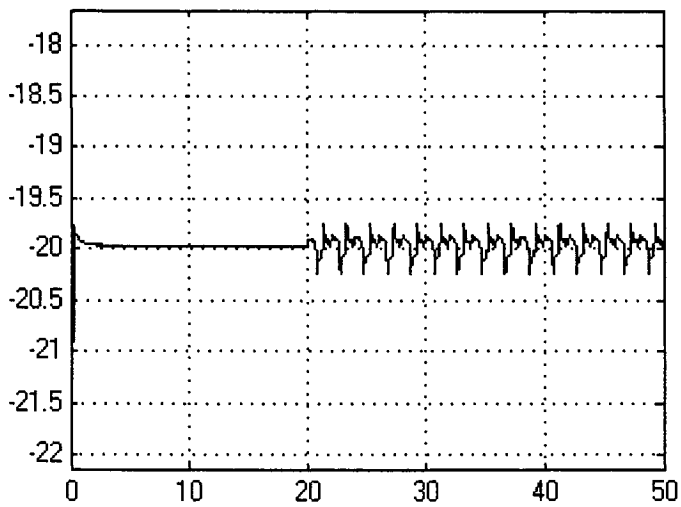

(b) Output response $\phi(t)$

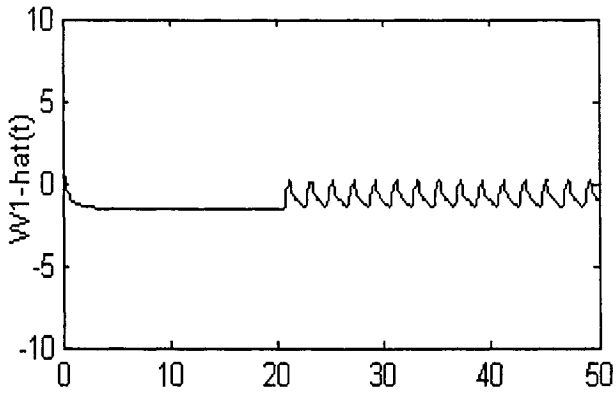

Time steps

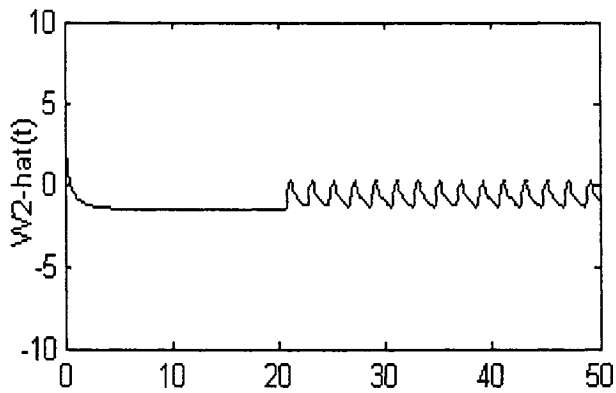

Time steps

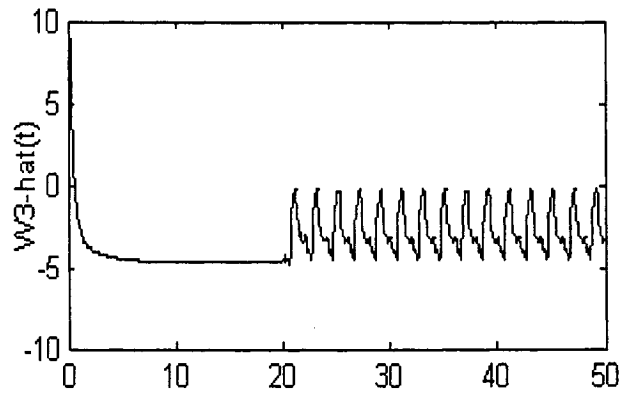

Time steps

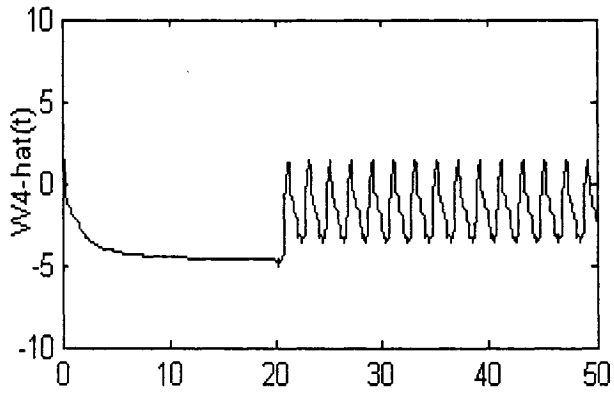

(c) Weight updating $\hat{W}^T(t) = [\hat{W}_1 \quad \hat{W}_2 \quad \hat{W}_3 \quad \hat{W}_4]$

Figure 8.6 Tracking a constant trajectory $x_d(t) = -20^0$

8.5 Summary

A new reinforcement adaptive fuzzy control scheme has been proposed for wing-rock tracking control in which we assume aircraft's wing rock nominal model unavailable. The fuzzy approximator is used to identify the unknown nonlinear function. The variable universe technique is applied to modify the premise parameters of the approximator. Its consequent parameters can be tuned by the reinforcement adaptive law, which is the on-line adaptive algorithm derived from Lyapunov stability theory. Therefore, all the signals in the closed-loop system are bounded even in the presence of the uncertainties and disturbances. Simulation results confirm the effectiveness and robustness of the proposed scheme. Even though the fuzzy approximator uses only four fuzzy rules, it can achieve precise tracking. Moreover, if the system is with the disturbances, it can still maintains high tracking performances.

Chapter 9

Discussions and Future Work

9.1 Discussions

The increased interest in improving the safety and handling qualities of highly maneuverable fighter airplanes and very slender space-plane configurations results in a focused effort to study the phenomenon of wing rock. In this thesis, we have studied the phase plane of wing rock phenomenon, the mechanism of wing rock hysteresis, and the suppressing and tracking control problems during nonlinear wing rock phenomena without and with the unknown disturbances. More important, we have emphasized the control and simulation investigation of the time-varying wing rock with unknown disturbances for the practical environment consideration of aircraft at a high AOA.

Based on the different control objectives, the control issues of wing rock phenomenon in this investigation are divided into two parts:

(a) In Part I (Chapter 2-5), we have introduced one-DOF wing rock models, investigated wing rock phenomena on phase plane, analyzed the hysteresis mechanism of wing rock phenomenon, and then proposed the variable phase

control (VPC) scheme to suppress wing rock with hysteresis.

(b) In Part II (Chapter 6-8), the nonlinear control problems of wing rock phenomenon with uncertainties have been studied, especially for the tracking control of the time-varying wing rock phenomenon with unknown disturbances. These control schemes include fuzzy PD control, variable universe fuzzy PD control, the NDOFEL control, and the reinforcement adaptive fuzzy control.

Some important discussions from this study can be summarized as follows:

(a) At present, the description of wing rock phenomena is based on numerous tests observations. In these free-to-roll tests, an 80^0 flat-plate delta wing is used to develop some one-degree-of-freedom (one-DOF) wing rock models. Most control schemes of wing rock phenomenon in the literature focus on the suppressing problem of the typical limit-cycle wing rock. They usually assume that the wing rock model is known and has no disturbance. Their work helps us understand wing rock control design.

(b) As for the mechanism of wing rock motion, through the free-to-roll tests of 80^0 slender delta wing at a high AOA, most researches think that hysteresis (as discussed in Chapter 4) with three loops provides clues about where wing rock phenomenon is being driven and where it is being damped. They have observed that one central loop of hysteresis indicates that oscillations are unstable and the energy from the free steam flows into the system to drive the wing rolling motion. On the contrary, another two outer loops of hysteresis make the system to be dissipated and stable, resulting in limit-cycle wing rock phenomenon.

(c) However, above test observations lack of mathematical analysis. Based on Lyapunov's direct method, the method of energy analysis of limit-cycle wing rock phenomenon is proposed in order to derive the rate of energy change of the phenomenon, *dE/dt*, and then to analyze the hysteresis mechanism of wing rock phenomenon. A defined critical angle divides the wing-rock hysteresis into two parts: absorbing energy where the motion is being driven and dissipative energy where the motion is being damped. Numerical simulations reveal much more information of *dE/dt*, as shown in Figures 4.3 and 4.4.

(d) Based on the above analytical method, it is easy to bethink of hysteresis compensation approaches from which we find a solution to compensate wing rock hysteresis to suppress wing rock phenomenon. Inspired by the work of Cruz-Hernandez in References [97-98], which deals with open-loop linear system compensation for piezoceramic actuators, the variable phase control scheme is developed for the closed-loop nonlinear control of wing rock with constant AOAs, as discussed in Chapter 5. The simulation results have shown that the proposed control scheme may be an effective control approach for wing rock suppression. The main features of proposed scheme are simple design and calculation, small control power need, and good robustness.

(e) It should be noted that the current requirements for fighter aircraft demand a high degree of agility and unlimited capability at high AOAs, and the capability to get a first shot has become extremely important in air combat. In view of this, the suppressing control of wing rock phenomenon is not enough, so we need to study its tracking control problems. Even though some nonlinear control schemes in

the literature have been presented, they may not be suitable for tracking problems, especially for real aircraft at a high AOA with uncertainties (such as time-varying aerodynamics parameters and un-modeled dynamics) and unknown disturbances. In fact, the tracking control for uncertain nonlinear system with unknown disturbances is a challenging issue.

(f) FLC has recently emerged as one of the most active and fruitful approaches to control complex nonlinear systems. The motivation is often due to the fact that the knowledge and dynamic behavior of systems are qualitative and uncertain. The fuzzy set theory appears to provide a suitable representation of such knowledge. This feature of FLC makes it suitable for controlling plants like aircraft that have nonlinear dynamics and operate in uncertain environments. Thus, the fuzzy PD control is designed to suppress wing rock, as presented in Chapter 6. Unfortunately, the output response of control system exhibits a bigger steady-state error if the system suffers from unknown disturbances. The variable universe fuzzy PD control is then proposed to overcome this disadvantage. The main advantages of the variable universe fuzzy PD control are precise tracking and fast responses with only four fuzzy rules.

(g) For the time-varying wing rock phenomenon with unknown disturbances, it can be described in the nominal model adding a lumped disturbance term $d(t)$, which includes the system uncertainties and unknown disturbances. If $\dot{d}(t) \approx 0$, then some nonlinear control methods such as adaptive control, fuzzy control, and nonlinear disturbance observer can be used to achieve wing rock tracking control. If $\dot{d}(t) \neq 0$, but it has bounds, there are no any control methods reported in the

literature by the author knowledge. In this thesis, inspired by the nonlinear disturbance observer algorithm and neural networks with the feedback-error-learning strategy, a novel learning control scheme, NDOFEL, have been proposed to control a class of time-varying nonlinear systems with unknown disturbances. In the NDOFEL, the big tracking error can be reduced by two steps: the nonlinear disturbance observer algorithm and the sliding-mode fuzzy neural network (SFNN) algorithm, as designed in Chapter 7. Six cases are used to show the many advantages of the NDOFEL.

(h) In practice, the aircraft's wing rock phenomena reported in Reference [74] are very complex, uncertain, and time-varying nonlinear systems. This means that aircraft's wing rock nominal model is unavailable. Under these circumstances, new design tools and approaches have to be explored. For this reason, the reinforcement adaptive fuzzy control has been proposed in Chapter 8. In this scheme, the unknown nonlinear function can be represented by the fuzzy approximator. The variable universe technique is applied to modify the premise parameters of FLS for improving its interpolation precision, and the derived adaptive law combining with a RL strategy is applied to tune its consequent parameters. Several numerical simulation cases have been presented to show its tracking precision and disturbance rejection.

9.2 Recommendations for Future Work

Possible areas of future work that emerge from this thesis include:

1) Research the mechanism of wing rock phenomenon.

Even though the hysteresis is used to explain wing rock phenomenon, analysis results are not enough. For example, how to obtain a real-time critical angle? What are important factors to affect the uncertainty of rolling motions?

2) The variable phase control scheme needs some further research. The related questions may include:
   (a) In the phase control design, some parameters such as the phase angle φ, input signal frequency range $\omega = [\omega_1 \ \omega_2]$, and phaser gain are important to control design. The questions are how to use adaptive approaches to obtain these parameters and to obtain a valid variable phase control scheme for the time-varying wing rock control of aircraft.
   (b) The stability of the phase control also needs to be proved mathematically.
3) The stability of variable universe fuzzy PD control needs to be proved mathematically.
4) The NODFEL algorithm is a valid scheme for tracking control, but we need to know the nominal model of wing rock phenomenon. The related questions may include:
   (a) How to identify this nominal model?
   (b) How to obtain multi-DOF NDOFEL scheme?
5) The reinforcement adaptive fuzzy control scheme seems to be good for the system with uncertainty and disturbance, but the results we derived is only for a second-order nonlinear system. The general solution for nth-order nonlinear systems needs to be derived and proved.
6) In above control schemes, actuator (or aileron) dynamics is not included in the close-loop control systems.

7) From the point of view of entire aircraft flight dynamics, wing rock modeling should be integrated with the multi-DOF model of aircraft. Of course, nonlinear control schemes should also be extended to the multi-DOF LCO control such as Dutch roll limit cycle control.

8) Last, but not the least, all control algorithms may be tested on aircraft to evaluate their stability, robustness, accuracy, simplicity, and reliability.

In conclusion, this thesis has addressed the control and simulation issues of wing rock phenomenon, especially for the tracking control problems of the system with uncertainties and disturbances. The five new schemes of wing rock control in this thesis have been proposed. The novelties of the proposed control schemes emphasize the stability, robustness, and simplicity of the algorithms so that they can be applied for on-line learning and real-time control. Many numerical simulation cases presented strongly support the proposed algorithms. Finally, we should point out that LCO phenomena are very common in the nonlinear dynamics of aircraft. The proposed algorithms may be used to solve these LCO problems. Thus, we still have a lot of work need to do in the future.

Appendix A

A Six-Order Approximate *Phaser*

The form of the six-order linear filter is given by

$$L_{pa}(s) = \frac{s^6 + p_5 s^5 + ... + p_1 s + p_0}{s^6 + q_5 s^5 + ... + q_1 s + q_0} \tag{A1}$$

For a given frequency $\omega = [\omega_1 \quad \omega_2]$ and a phase angle φ, the location for the pole and the zero can be found. The location of the first zero z_1 is located somewhere behind the location of ω_1; for example, $z_1 = \omega_1 - \omega_1 / 4$. The remainder of the zeros will be located between ω_1 and ω_2. They are logarithmically equally spaced between ω_1 and ω_2, as shown in Figure A1.

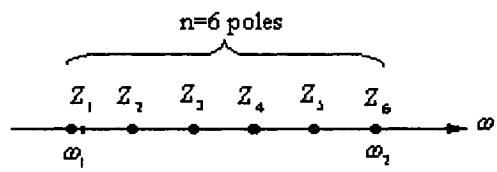

Figure A1 Six-zero logarithmical equal space

The values of the $p_i's$ are obtained using the values of the zeros:

$$\begin{aligned} num(s) &= (s+z_1)(s+z_2)(s+z_3)(s+z_4)(s+z_5)(s+z_6) \\ &= s^6 + p_5 s^5 + p_4 s^4 + p_3 s^3 + p_2 s^2 + p_1 s + p_0 \end{aligned} \tag{A2}$$

Substituting $s = j\omega$ into Equation (A1), we have

$$\begin{aligned} L_{ph}(j\omega) &= \frac{(j\omega)^6 + p_5(j\omega)^5 + p_4(j\omega)^4 + p_3(j\omega)^3 + p_2(j\omega)^2 + p_1 j\omega + p_0}{(j\omega)^6 + q_5(j\omega)^5 + q_4(j\omega)^4 + q_3(j\omega)^3 + q_2(j\omega)^2 + q_1 j\omega + q_0} \\ &= \frac{\left(-\omega^6 + p_4\omega^4 - p_2\omega^2 + p_0\right) + j\left(p_5\omega^5 - p_3\omega^3 + p_1\omega\right)}{\left(-\omega^6 + q_4\omega^4 - q_2\omega^2 + q_0\right) + j\left(q_5\omega^5 - q_3\omega^3 + q_1\omega\right)} \\ &= \frac{(K_1K_3 + K_2K_4) + j(K_2K_3 - K_1K_4)}{K_3^2 + K_4^2} \end{aligned} \tag{A3}$$

where $K_1 = -\omega^6 + p_4\omega^4 - p_2\omega^2 + p_0$, $K_2 = p_5\omega^5 - p_3\omega^3 + p_1\omega$,

$K_3 = -\omega^6 + q_4\omega^4 - q_2\omega^2 + q_0$, and $K_4 = q_5\omega^5 - q_3\omega^3 + q_1\omega$.

The phase angle of the transfer function is

$$\angle L_{ph}(j\omega) = \Phi(\omega) = \tan^{-1}\left(\frac{K_2K_3 - K_1K_4}{K_1K_3 + K_2K_4}\right) \tag{A4}$$

Substituting the values of K_3 and K_4 into Equation (A4), we obtain

$$(-\omega^6 + q_4\omega^4 - q_2\omega^2 + q_0)[\tan(\Phi(\omega))K_1 - K_2)] + (q_5\omega^5 - q_3\omega^3 + q_1\omega)[\tan(\Phi(\omega))K_2 + K_1] = 0$$

Let $K_5 = \tan(\Phi(\omega))K_1 - K_2$ and $K_6 = \tan(\Phi(\omega))K_2 + K_1$; we have

$$-K_5\omega^6 + K_5q_4\omega^4 - K_5q_2\omega^2 + K_5q_0 + K_6q_5\omega^5 - K_6q_3\omega^3 + K_6q_1\omega = 0 \tag{A5}$$

The unknown variables in Equation (A5) are the q_i's and ω.

We can make the value of the phase angle equal to φ at the values where the zeros are

located. If $\omega = [\omega_1 \quad \omega_2]$, then we have $\angle L_{pa}(j\omega) = \Phi(\omega) = \varphi$ and $\tan(\Phi(\omega)) = \tan(\varphi)$.

The following set of equations are then obtained

$$\begin{cases} -K_7 z_1^6 + K_7 z_1^4 q_4 - K_7 z_1^2 q_2 + K_7 q_0 + K_8 z_1^5 q_5 - K_8 z_1^3 q_3 + K_8 z_1 q_1 = 0 \\ -K_7 z_2^6 + K_7 z_2^4 q_4 - K_7 z_2^2 q_2 + K_7 q_0 + K_8 z_2^5 q_5 - K_8 z_2^3 q_3 + K_8 z_2 q_1 = 0 \\ -K_7 z_3^6 + K_7 z_3^4 q_4 - K_7 z_3^2 q_2 + K_7 q_0 + K_8 z_3^5 q_5 - K_8 z_3^3 q_3 + K_8 z_3 q_1 = 0 \\ -K_7 z_4^6 + K_7 z_4^4 q_4 - K_7 z_4^2 q_2 + K_7 q_0 + K_8 z_4^5 q_5 - K_8 z_4^3 q_3 + K_8 z_4 q_1 = 0 \\ -K_7 z_5^6 + K_7 z_5^4 q_4 - K_7 z_5^2 q_2 + K_7 q_0 + K_8 z_5^5 q_5 - K_8 z_5^3 q_3 + K_8 z_5 q_1 = 0 \\ -K_7 z_6^6 + K_7 z_6^4 q_4 - K_7 z_6^2 q_2 + K_7 q_0 + K_8 z_6^5 q_5 - K_8 z_6^3 q_3 + K_8 z_6 q_1 = 0 \end{cases} \tag{A6}$$

where $K_7 = \tan(\varphi)K_1 - K_2$ and $K_8 = \tan(\varphi)K_2 + K_1$.

Equation (A6) can be re-ordered in the form $A\boldsymbol{x} = C$

$$\begin{bmatrix} K_7 & K_8 z_1 & -K_7 z_1^2 & -K_8 z_1^3 & K_7 z_1^4 & K_8 z_1^5 \\ K_7 & K_8 z_2 & -K_7 z_2^2 & -K_8 z_2^3 & K_7 z_2^4 & K_8 z_2^5 \\ K_7 & K_8 z_3 & -K_7 z_3^2 & -K_8 z_3^3 & K_7 z_3^4 & K_8 z_3^5 \\ K_7 & K_8 z_4 & -K_7 z_4^2 & -K_8 z_4^3 & K_7 z_4^4 & K_8 z_4^5 \\ K_7 & K_8 z_5 & -K_7 z_5^2 & -K_8 z_5^3 & K_7 z_5^4 & K_8 z_5^5 \\ K_7 & K_8 z_6 & -K_7 z_6^2 & -K_8 z_6^3 & K_7 z_6^4 & K_8 z_6^5 \end{bmatrix} \begin{Bmatrix} q_0 \\ q_1 \\ q_2 \\ q_3 \\ q_4 \\ q_5 \end{Bmatrix} = \begin{Bmatrix} K_7 z_1^6 \\ K_7 z_2^6 \\ K_7 z_3^6 \\ K_7 z_4^6 \\ K_7 z_5^6 \\ K_7 z_6^6 \end{Bmatrix} \tag{A7}$$

Now, the values of the q_i's can be obtained.

Appendix B

The Relationship of Fuzzy PD Control and PD Control

The following material is adopted from the Chapter 10 of Reference [110].

Let $X=[-E,E]$ and $Y=[-EC,EC]$ be the universe of input variables and $V=[-U,U]$ be the universe of output variables. Denote $A=\{A_i\}_{(1\le i\le p)}$, $B=\{B_j\}_{(1\le j\le q)}$ and $D=\{D_{ij}\}_{(1\le i\le p,1\le j\le q)}$, respectively, the peak point of A_i, B_j and D_{ij} satisfying that $-E\le x_1<x_2<\cdots<x_p\le E$, $-EC\le y_1<y_2<\cdots<y_q\le EC$, $-U\le u_{11}<u_{12}<\cdots<x_{pq}\le U$. Here A_i and B_j are defined by triangular membership functions. A, B, and D form a reference rule base R:

$$\text{If } x \text{ is } A_i \text{ and } y \text{ is } B_j, \text{ then } u \text{ is } D_{ij} \tag{B.1}$$

where $i=1,2,\cdots,p$, $j=1,2,\cdots,q$. The fuzzy PD control based on Expression (B.1) can be shown as the following interpolation function:

$$u(t)\overset{\Delta}{=}F(x(t),y(t))=\sum_{i=1}^{p}\sum_{j=1}^{q}\mu_{Ai}(x(t))\mu_{Bj}(y(t))\mu_{ij} \tag{B.2}$$

Theorem: Let $x(t) = e(t)$ and $y(t) = de(t)/dt$, then a fuzzy PD control is a piecewise PD control with mutual affection between $x(t)$ and $y(t)$ and with translation coefficients as the following:

$$u(t) \triangleq F(x(t), y(t)) = \sum_{i=1}^{p-1} \sum_{j=1}^{q-1} u^{(i,j)}(t) \tag{B.3}$$

where

$$u^{(i,j)}(t) = \begin{cases} K_P^{(i,j)}(x(t) + T_D^{(i,j)} y(t) + T_{PD}^{(i,j)} x(t) y(t) + T_C^{(i,j)}), & x_i \le x(t) \le x_{i+1} \\ & y_i \le y(t) \le y_{i+1} \\ 0, & \textit{otherwise} \end{cases} \tag{B.4}$$

and $i = 1,2,\cdots,p-1$, $j = 1,2,\cdots,q-1$; $K_P^{(i,j)}$, $T_D^{(i,j)}$, $T_{PD}^{(i,j)}$, and $T_C^{(i,j)}$ are, respectively, the proportional gain, the differential time constant, the time constant of mutual affection between $x(t)$ and $y(t)$, and the translation coefficient, in $[x_i, x_{i+1}] \times [y_i, y_{i+1}]$. Especially let (x_{i0}, y_{j0}) be the origin of x - y plane, that is, $x_{i0} = 0 = y_{j0}$, then $T_C^{(i0,j0)} = T_C^{(i0,j0-1)} = T_C^{(i0-1,j0-1)} = T_C^{(i0-1,j0)} = 0$; thus, when $i = i_0 - 1,\ i_0$, and $j = j_0 - 1,\ j_0$, Expression (B.4) can be simplified as follows:

$$u^{(i,j)}(t) = \begin{cases} K_P^{(i,j)}(x(t) + T_D^{(i,j)} y(t) + T_{PD}^{(i,j)} x(t) y(t)), & x_i \le x(t) \le x_{i+1} \\ & y_i \le y(t) \le y_{i+1} \\ 0, & \textit{otherwise} \end{cases} \tag{B.5}$$

Remark 1: It is not difficult to learn that PD control

$$u(t) = K_P(x(t) + T_D y(t))$$

is a plane passing through the origin in *xyu* space, which means that it is of linear regulation law. However, fuzzy PD control is a piecewise quadratic surface passing

through the origin in the space, in which the whole surface can approximate a nonlinear regulation law. So whole merit of fuzzy PD control is much better than the PD control. But in the neighborhood of the origin, as the translation coefficients are zero, there exists (i, j) such that

$$u(t) = u^{(i,j)}(t) = K_P^{(i,j)}(x(t) + T_D^{(i,j)} y(t) + T_{PD}^{(i,j)} x(t) y(t)) \tag{B.6}$$

At this region, $|x(t)|$ and $|y(t)|$ are so small that the higher order terms $T_{PD}^{(i,j)} x(t) y(t)$ can be omitted, so we have

$$u(t) = u^{(i,j)}(t) \approx K_P^{(i,j)}(x(t) + T_D^{(i,j)} y(t) \tag{B.7}$$

This means that the fuzzy PD control is approximately a PD control in the neighborhood of the origin. Hence, the weakness of PD control is inherited by the fuzzy PD control in the neighborhood.

Remark 2: This gives us a conclusion about the effectiveness of fuzzy PD control. In the earlier stage of control processing, the effect of fuzzy PD control is better than the effect of PID control, especially on inhibiting over-regulation. But when $(x(t), y(t))$ is in the neighborhood of the origin, from Expression (B.7), we know that fuzzy PD control is approximately PD control. Of course, the PD control cannot be better than PID control.

Appendix C

Fuzzy Approximator for Triangular Input Membership Functions

In Chapter 5 of Reference [152], Spooner *et al.* stated that a continuous function may be uniformly approximated by a *continuous* piecewise linear function. Since the set of continuous piecewise linear functions is a subset of the set of all piecewise liner functions. This fact, however, leads us to the following important theorem.

Theorem 1: Fuzzy systems with triangular input membership functions and center average defuzzification are universal approximators for $f \in g(1, D)$ with $D = [a, b]$.

Besides, Zeng and Singh in Reference [153] discussed the approximation problem of SISO fuzzy systems. They used pseudo trapezoid-shaped (PTS) membership function. Obviously, triangular-shaped membership function is a special case of PTS membership function.

For a SISO fuzzy system, the fuzzy basic functions (FBFs) are given by

$$B_i(x) = A_i(x) \Big/ \sum_{i=1}^{N} A_i(x), \quad x \in U \subset R, \quad i = 1,2,\cdots,N \tag{C.1}$$

and the fuzzy system can be written as

$$f(x) = \sum_{i=1}^{N} B_i(x) y_i, \quad x \in U \subset R \tag{C.2}$$

Now, we introduce the approximation property and convergent property of fuzzy systems in Equation (C.2). We assume that $g(x)$ is the desired experiential or heuristic control or decision in $U = [a,b]$.

Theorem 2. Basic approximation property: Suppose that fuzzy sets A_i $(i = 1,2,\cdots,N)$ in $U = [a,b]$ are normal, consistent and complete with PTS membership functions $A_i(x) = A_i(x; a_i, b_i, c_i, d_i)$ $(i = 1,2,\cdots,N)$ and $A_1 < A_2 < \cdots < A_N$; and fuzzy system

$$f(x) = \sum_{i=1}^{N} B_i(x) y_i$$

and $B_i(x)$ $(i = 1,2,\cdots,N)$ are FBFs. Then for a given real function $g(x)$ in $U = [a,b]$,

$$|g(x) - f(x)| = |g(x) - y_i|, \quad x \in M(B_i) = [d_{i-1}, a_{i+1}] \tag{C.3}$$

$$\begin{aligned} |g(x) - f(x)| &= |g(x) - B_i(x) y_i - B_{i+1}(x) y_{i+1}| \\ &\le \max\{|g(x) - y_i|, |g(x) - y_{i+1}|\}, \; x \in F(B_i, B_{i+1}) = [a_{i+1}, d_i] \end{aligned} \tag{C.4}$$

Remark 1: Theorem 2 gives a very clear view of the approximation mechanism of fuzzy systems. Such an approximation mechanism is quite similar to the approximation mechanism in mathematical approximation theory. This approximation idea is especially suitable for the practical cases where we know what a good control or decision is in some part of the input space but we are not clear what in some other part of the input space.

Theorem 3. Uniform approximation property: Suppose that fuzzy sets A_i $(i=1,2,\cdots,N)$ in $U=[a,b]$ are normal, consistent and complete with PTS membership functions $A_i(x)=A_i(x;a_i,b_i,c_i,d_i)$ $(i=1,2,\cdots,N)$ and $A_1<A_2<\cdots<A_N$; and fuzzy system

$$f(x)=\sum_{i=1}^{N}B_i(x)y_i$$

and $B_i(x)$ $(i=1,2,\cdots,N)$ are FBFs. For a given function $g(x)$ in $U=[a,b]$, if

$$\varepsilon_i=\sup_{x\in M(B_i)}|g(x)-y_i|,\ \varepsilon=\max\{\varepsilon_i\,|\,1\le i\le N\}, \tag{C.5}$$

then

$$\sup_{x\in U}|g(x)-f(x)|=\varepsilon \tag{C.6}$$

Remark 2: Theorem 3 can be used in the following two ways: 1) to check whether the designed system has the required accuracy; 2) as a guide, to redesign the fuzzy sets C_i (i=1, 2, …, N) in the fuzzy rule base.

Theorem 4. Uniform convergent property: Suppose that fuzzy sets A_i $(i=1,2,\cdots,N)$ in $U=[a,b]$ are normal, consistent and complete with PTS membership functions $A_i(x)=A_i(x;a_i,b_i,c_i,d_i)$ $(i=1,2,\cdots,N)$ and $A_1<A_2<\cdots<A_N$; $\delta=\max\{d_i-a_i\,|\,1\le i\le N\}$; and fuzzy system

$$f(x)=\sum_{i=1}^{N}B_i(x)y_i$$

and $B_i(x)$ $(i=1,2,\cdots,N)$ are FBFs. For any continuous functions $g(x)$ in $U=[a,b]$, if

$$m_i = \min_{x \in [a_i, d_i]} g(x) \le y_i \le M_i = \max_{x \in [a_i, d_i]} g(x), \quad i = 1,2,\cdots,N \tag{C.7}$$

then

$$\lim_{\delta \to 0} \sup_{x \in U} |g(x) - f_\delta(x)| = 0 \tag{C.8}$$

Remark 3: Theorem 4 means that the fuzzy system $f_\delta(x)$ converges to the desired (control or decision) function $g(x)$ when the modulus of the partition $A_1, A_2, \cdots, A_N$ tends to zero under some appropriate conditions.

References

[1] Bunton, R. W. and Denegri, C. M. Jr., "Limit Cycle Oscillation Characteristics of Fighter Aircraft," *Journal of Aircraft,* Vol. 37, No. 5, 2000, pp. 916-918.

[2] Dimitriadis G. and Cooper J. E., "Limit Cycle Oscillation Control and Suppression," *The Aeronautical Journal*, May 1999, pp. 257-263.

[3] Patil, M. J., Hodges, D. H., and Cesnik C. E. S., "Limit-Cycle Oscillation in High-Aspect-Ratio Wings, " *Journal of Fluids and Structures*, No. 15, 2001, pp. 107-132.

[4] Katz, J., "Wing/Vortex Interactions and Wing Rock," *Progress in Aerospace Sciences*, Vol. 35, 1999, pp 727-750.

[5] Olsson, H. and Astrom, K. J., "Friction Generated Limit Cycles," *IEEE International Conference on Control Applications,* Dearborn, MI, USA, September 15-18, 1996.

[6] Wallenborg A. and Astrom, K. J., "Limit Cycle Oscillations in High Performance Robot Drives," In *Preprints Control '88,* University of Oxford, UK, 1988.

[7] Kremer, G. G. and Thompson, D. F., "Robust Stability of Nonlinear Hydraulic Servo Systems Using Closest Hopf Bifurcation Techniques," *American Control Conference,* Philadelphia, PA, June 1998.

[8] Mougenet, F. and Hayward V., "Limit Cycle Characterization, Existence and Quenching in the Control of a High Performance Hydraulic Actuator," *IEEE International Conference on Robotics and Automation,* 1995.

[9] Cox, C. S. and French, I. G., "Limit Cycle Prediction Conditions for a Class of Hydraulic Control Systems," *Journal of Dynamics, Measurement and Control,* Vol. 108, pp. 17-23, March 1986.

[10] Huang Y. J. and Wang Y.-J., "Limit Cycle Analysis of Electro-Hydraulic Control Systems with Friction and Transport Delay," *The 3th Congress on Intelligent Control and Automation,* Hefei, China, June 28-July 2, 2000.

[11] Impram, S. T. and Munro, N., "Limit Cycle Analysis of Uncertain Control Systems with Multiple Nonlinearities," *The 40th IEEE Conference on Decision and Control,* Orlando, Florida, USA, December 2001.

[12] Ko, J., Kurdila A. J., Strganac, T. W., "Nonlinear Control of a Prototypical Wing Section with Torsional Nonlinearity," *Journal of Guidance, Control, And Dynamics,* Vol. 20, No. 6, 1997, pp. 1181-1189.

[13] Denegri, C. M. Jr., "Limit Cycle Oscillation Flight Test Results of a Fighter with External Stores," *Journal of Aircraft*, Vol. 37, No. 5, 2000, pp. 761-769.

[14] Liebst, B. S., "The Dynamics, Prediction, and Control Of Wing Rock in High-Performance Aircraft," *Phil. Trans. R. Soc. Lond.* No. 356, 1998, pp. 2257-2276.

[15] Ross, A. J., "Investigation of Nonlinear Motion Experienced on a Slender-Wing Research Aircraft," *Journal of Aircraft*, Vol. 9, No. 9, 1972, pp. 625-631.

[16] Ross, A. J., 'Lateral Stability at High Angles of Attack, Particularly Wing Rock," Paper 10, *AGARD CP-260*, Sept. 1978.

[17] Pamadi, B. N., Rao, D. M., and Niranjana, T., "Roll Attractor of Delta Wings at High Angles of Attack," *International Council of the Aeronautical Sciences*, 94-7.1.2, Sept. 1994.

[18] Cochran, J. E., and Ho, C. -S., "Stability of Aircraft Motion in Critical Cases," *Journal of Guidance, Control, and Dynamics*, Vol. 6, No. 4, 1983, pp. 272-279.

[19] Araujo, A. D. and Singh, S. N., "Variable Structure Adaptive Control of Wing Rock Motion of Slender Delta Wings," *Journal of Guidance, Control, and Dynamics*, Vol. 21, No. 2, 1998, pp. 251-256.

[20] Shue, S.-P. and Agarwal, R. K., "Nonlinear $H\infty$ Method for Control of Wing Rock motions," *Journal of Guidance, Control, and Dynamics*, Vol. 23, No.1, 2000, pp. 251-256,.

[21] Ananthkrishnan, N., and Sudhakar, K., "Characterization of Periodic Motions in Aircraft lateral Dynamics," *Journal of Guidance, Control, and Dynamics*, Vol. 19, No. 3, 1996, pp. 680-685.

[22] Planeaux, J. B., Beck, J. A., and Baumann, D. D., "Bifurcation Analysis of a Model Fighter Aircraft with Control Augmentation," *AIAA* Paper 90-2836, 1990.

[23] Evans, C., "An Investigation of Large Amplitude Wing-Rock," *Aeronautical Journal*, March 1984, pp. 55-57.

[24] Chaderjian, Neal M., "Navier-Stokes Prediction of Large-Amplitude Delta-Wing Roll Oscillations, " *Journal of Aircraft*, Vol. 31, No. 6, 1994, pp. 1333-1340.

[25] Khrabrov, A. and Zhuk, A., "Using Large Amplitude Free Oscillations in Pitch and Roll to Investigate Unsteady Aerodynamic Characteristics at Separated Flow Regimes," *The 16th ICIASF*, Dayton, OH, July 18-21,1995.

[26] Nelson, R. C., Arena, A. S., and Thompson, S. A., " Aerodynamic and Flow filed Hysteresis of Slender Wing Aircraft Undergoing Large-Amplitude Motions," *AGARD*, Manoeuvring Aerodynamics 11p, 1992.

[27] Kurdila A. J., "Nonlinear Control Methods for High-Energy Limit-Cycle Oscillations," *Journal of Guidance, Control, and Dynamics*, Vol. 24, No. 1, 2001, pp. 185-192.

[28] Nelson, H. C. and Andrew, S. A. Jr., "Experimental Investigation of Wing Rock of Slender Wings and Aircraft Configurations," in Kawamura, R. and Aihara, Y. (Eds.), *Fluid Dynamics of High Angle of Attack,* Springer-Verlag, 1992, pp.413-422.

[29] Levin, D. and Katz, J. "Self Induced Roll Oscillations of Low Aspect Ratio Rectangular Wings," *AIAA Paper* 90-2811,1990.

[30] Pamadi, B. N. and Bandu, N., *Performance, Stability, Dynamic, and Control of Airplanes*, AIAA Education Series, 1998.

[31] Nguyen, L. T., Yip, L. P., and Chambers, J. R., "Self Induced Wing Rock of Slender Delta Wings," *AIAA Paper* 81-1883, 1981.

[32] Johari, H., and Moreira, J., "Delta Wing Vortex Manipulation Using Pulsed and Steady Blowing During Ramp-Pitch," *Journal of Aircraft*, Vol. 33, No. 2, 1994, pp. 304-310.

[33] Wong, G. S., Rock, S. M., and Roberts. L., "Active Control of Wing Rock Using Tangential Leading-Edge Blowing," *Journal of Aircraft*, Vol. 31, No. 3, 1994, pp. 659-665.

[34] Traub, L. W., "Effect of Spanwise Blowing on a Delta Wing with Vortex Flaps,"

Journal of Aircraft, Vol. 32, No. 4, 1994, pp. 884-886.

[35] Johari, H., Olinger, D. J., and Fitzpatrick, K. C., "Delta Wing Vortex Control via Recessed Angled Spanwise Blowing," *Journal of Aircraft*, Vol. 32, No. 4, 1995, pp. 804-810.

[36] Gangulee, D., and Terry, N. T., "Vortex Control over Sharp-Edged Slender Bodies," *Journal of Aircraft*, Vol. 32, No. 4, 1994, pp. 739-745.

[37] Lowson, M. V., Riley, A. J., "Vortex Breakdown Control by Delta Wing Geometry," *Journal of Aircraft*, Vol. 32, No. 4, 1995, pp. 832-83.

[38] Stengel, R. F., "Toward Intelligent Flight Control," *IEEE Transactions on Systems, Man and Cybernetics*, Vol. 23, No. 6, 1993, pp. 1699-1717.

[39] Wahi, P., Raina, R., and Chowdhury, F. N, "A Survey Of Recent Work in Adaptive Flight Control," *Southeastern Symposium on System Theory, 2001. Proceedings of the 33rd*, March 2001, pp. 7-11.

[40] Calise A. J. and Rysdyk, R. T., "Nonlinear Adaptive Flight Control Using Neural Networks," *IEEE Control Systems*, 1998, pp. 14-25.

[41] Monahemi, M. M., and Krstic, M., "Control of Wing Rock Motion Using Adaptive Feedback Linearization," *Journal of Guidance, Control, and Dynamics*, Vol. 19, No. 4, 1996, pp. 905-912.

[42] Gazi, V. and Passino, K. M., "Direct Adaptive Control Using Dynamic Structure Fuzzy System," *American Control Conference*, Chicago, IL, June 28-30, 2000.

[43] Ordonez, R. and Passino, K. M., "Indirect Adaptive Control for a Class of Non-Linear Systems With a Time-Varying Structure," *International Journal of Control*, Vol. 74, No. 7, 2001, pp. 701-717.

[44] Omidvar, O. M. and Elliott, D. L. (Eds.), *Neural Systems for Control*, San Diego: Academic Press, 1997.

[45] Ge, S. S., *Stable Adaptive Neural Network Control*, Boston: Kluwer Academic, 2002.

[46] Singh, S. N., Yim, W., and Wells W. R., "Direct Adaptive and Neural Control of Wing Rock Motion of Slender Delta Wings," *Journal of Guidance, Control, and Dynamics*, Vol. 18, No. 1, 1995, pp. 25-30.

[47] Joshi, S. V., Sreenatha, A. G., and Chandrasekhar, J., "Suppression of Wing Rock of Slender Delta Wings Using a Single Neuron Controller," *IEEE Transaction on Control System Technology*, Vol. 6, No. 5, 1998, pp. 671-677.

[48] Lyshevski, S. E., *Control Systems Theory with Engineering Applications,* Boston: Birkhauser, 2001.

[49] Luo, J., and Lan, C. E., "Control of Wing Rock Motion of Slender Delta Wings," *Journal of Guidance, Control, and Dynamics*, Vol. 16, No. 2, 1993, pp. 225-231.

[50] Rogers, R. M., "Parameter Optimal Control of Wing Rock," *Journal of Guidance, Control, and Dynamics*, Vol. 17, No. 5, 1994, pp. 1131-1133.

[51] Shue, S. P., Sawan, M. E., and Rokhsaz, K., "Optimal Feedback Control of a Nonlinear System: Wing Rock Example," *Journal of Guidance, Control, and Dynamics*, Vol. 19, No. 1, 1996, pp. 166-171.

[52] Tewari, A., "Nonlinear Optimal Control of Wing Rock Including Yawing Motion," *AIAA Guidance, Navigation, and Control Conference and Exhibit*, Denver, CO, Aug. 14-17, 2000.

[53] Lee, H. J., Park J. B., and Chen G., "Robust Fuzzy Control of Nonlinear Systems

With Parametric Uncertainties," *IEEE Transactions on Fuzzy Systems*, Vol. 9, No. 2, 2001, pp. 369-379.

[54] Wang, L.-X., "Stable Adaptive Fuzzy Control of Nonlinear Systems," *IEEE Transactions on Fuzzy Systems*, Vol. 1, No. 2, 1993, pp. 146-155.

[55] Tarn, J. H., and Hsu, F. Y., "Fuzzy Control of Wing Rock for Slender Delta Wings," *American Automatic Control Council*, Vol. 3, 1993, pp. 1159-1161.

[56] Sreenatha, A.G., Patki, M. V., and Joshi, S. V., " Fuzzy Logic Control for Wing-Rock Phenomenon," *Mechanics Research Communications*, Vol. 27, No. 3, 2000, pp. 359-364.

[57] Lim, Y. X. and Sreenatha, A. G., "Stability and Robustness Analysis of Fuzzy Logic Controller for Wing Rock Suppression," *AIAA Atmospheric Flight Mechanics Conference*, Denver, CO, Aug. 14-17, 2000.

[58] Nho, K. and Agarwal, R. K., "Fuzzy Logic Model-Based Predictive Control of Aircraft Dynamics Using ANFIS," *AIAA Paper* 2001-0316.

[59] Zhou, K., Doyle, J., and Glover, K., *Robust and Optimal Control*, Prentice Hall, 1996.

[60] Richard, J. A., Buffington, J. M., Sparks, A. G., and Banda, S. S., *Robust Multivariable Flight Control,* London: Springer-Verlag, 1994.

[61] Crassidis, J. L., "Robust Control of Nonlinear Systems Using Model-Error Control Synthesis," *Journal of Guidance, Control, and Dynamics*, Vol. 22, No. 4, 1999, pp. 595-601.

[62] Stalford, H., "On Robust Control of Wing Rock Using Nonlinear Control," 1987 *American Control Conference*, June 10-12, 1997, pp. 1890-1899.

[63] Littleboy, D.M. and Smith, P.R., "Using Bifurcation Methods to Aid Nonlinear Dynamic Inversion Control Law Design," *Journal of Guidance, Control, and Dynamics*, Vol. 21, No. 4, 1998, pp. 632-638.

[64] Liebst, B. S., DeWitt, B. R., "Wing Rock Suppression in the F-15 Aircraft," *AIAA Atmospheric Flight Mechanics*, New Orleans, LA, Aug. 11-13, 1997.

[65] Goman, M. G. and Khramtsovsky, A. V., "Application of Continuation and Bifurcation Methods to the Design of Control Systems," *Phil. Trans. R. Soc. Lond.* No. 356, 1998, pp. 2277-2295.

[66] Young, K. D., Utkin, V. I., and Ozguner, U. "A Control Engineer's Guide to Sliding Mode Control," *IEEE Transaction on Control Systems Technology,* Vol. 7, No. 3, 1999, pp.328-342.

[67] Hung, J. Y., Gao, W., and Hung, J. C., "Variable Structure Control: A Survey," *IEEE Transaction on Industrial Electronics,* Vol. 40, No. 1, 1993, pp. 2-22.

[68] Hedrich, J. K. and Gopalsawami, S., "Nonlinear Flight Control Design via Sliding Mode Methods," *IEEE Transaction on Aerospace and Electronic Systems,* Vol. 13, No. 5, 1990, pp.850-858.

[69] Jafarov, E. M. and Tasaltin, R., "Robust Sliding-Mode Control for the Uncertain MIMO Aircraft Model F-18," *IEEE Transaction on Aerospace and Electronic Systems,* Vol. 36, No. 4, 2000, pp.1127-1141.

[70] Singh, S. N., Steinberg, M., and Digirolamo, R. D., "Variable Structure Robust Flight Control Systems for the F-14," *IEEE transaction on Aerospace and Electronic Systems,* Vol. 33, No. 1, 1997, pp.77-84.

[71] Fernand, J. M. and Downing, D. R., "Discrete Sliding Mode Control of Wing

Rock," *AIAA Guidance, Navigation and Control Conference*, Scottsdale, AZ, Aug. 1-3, 1994.

[72] Ericsson, L. E., "Some Challenges in High-Alpha Vehicle Dynamics," *Fluid Dynamics of High Angle of Attack*, Springer-Verlag, 1992.

[73] ----------, "Surprising Developments in the Search of Analytical Means for Prediction of Slender Wing Rock". *AIAA Paper* 2002-0712, 2002.

[74] Owens, D. B., Capone, F. J., Hall, R. M., Brandon, J. M. and Cunningham, K., "Free-to-Roll Analysis of Abrupt Wing Stall on Military Aircraft at Transonic Speeds," *AIAA*-2003-0750, January 2003.

[75] Schmidt, L. V., "Wing Rock due to Aerodynamic Hysteresis," *Journal of Guidance, Control, and Dynamics*, Vol. 16, No. 3, 1979, pp. 129-133.

[76] Ericsson, L.E., "The Fluid Mechanics of Slender Wing Rock," *Journal of Aircraft,* Vol. 21, No. 5, 1984, pp 322-328.

[77] Levin, D. and Katz, J. "Dynamic Load Measurement with Delta Wings Undergoing Self Induced Roll Oscillation," *Journal of Aircraft*, Vol. 21, No.1, 1984, pp. 30-36.

[78] Hsu, C., and Lan, C. E., "Theory of Wing Rock," *Journal of Aircraft*, Vol. 22, No. 10, 1985, pp. 920-924.

[79] Konstadinopoulos, P., Mook, D. T., and Nayfeh, A. H., "Subsonic Wing Rock of Slender Delta Wings," *Journal of Aircraft*, Vol. 22, No. 3, 1985, pp. 223-228.

[80] Nayfeh, A. H., Elzebda, J. M., and Mook, D. T., "Analytic Study of the Subsonic Wing Rock Phenomenon for Slender Delta Wings," *Journal of Aircraft*, Vol. 26, No. 9, 1989, pp. 805-809.

[81] Elzebda, J. M., Mook, D. T., and Nayfeh, A. H., "Influence of Pitching Motion on Subsonic Wing Rock of Slender Delta Wings," *Journal of Aircraft*, Vol. 26, No. 6, 1989, pp. 503-508.

[82] Katz J. and Levin D., "Self-induced Roll Oscillations Measured on a Delta Wing/Canard Configuration," *Journal of Aircraft*, Vol. 23, No.11, 1986, pp. 814-819.

[83] Ericsson, L.E., "Various Sources of Wing Rock," *Journal of Aircraft,* Vol. 27, No. 6, June 1990, pp 488-494.

[84] Arena, A. S. Jr., and Nelson, R. C., " An Experimental Study of the Nonlinear Dynamic Phenomenon Known as Wing Rock," *AIAA* - 90-2812, 1990.

[85] ----------, "Experimental Investigation on Limit Cycle Wing Rock of Slender Wings," *Journal of Aircraft*, Vol. 31, 1994, pp. 1148-1155.

[86] Arena, A. S. Jr., *An Experimental and Computational Investigation of Slender Wings Undergoing Wing Rock*, Ph.D Dissertation, University of Notre Dame, Indiana, USA, 1992.

[87] Yoshinaga, T., Tate, A., and Noda, J., "Wing Rock of Delta Wings with an Analysis by the Phase Plane method, " *in Proceedings of the AIAA Atmospheric Flight Mechanics Conference*, Washington, DC, 1993.

[88] Guglieri, G., and Quagliotti, F., "Experimental Observation and Discussion of the Wing Rock Phenomenon," *Aerospace Science and Technology*, 2 (1997) 111-123.

[89] ----------, "Analytical and Experimental Analysis of Wing Rock," *Nonlinear Dynamics*, 24 (2001) 129-146.

[90] Nelson, R. C., *Flight Stability and Automatic Control,* McGraw-Hill, Inc. 1989.

[91] Wanda, S.-S., *The Behavior of Nonlinear Vibrating Systems*, Kluwer Academic Publishers, 1990.

[92] Nayfeh, A. H., *Introduction to Perturbation Techniques,* Wiley & Sons Inc, 1981.

[93] Rudra, P., *Getting Start with MATLAB 5,* Oxford University Press, 1999.

[94] Shinners, S. M., *Advanced Modern Control System Theory and Design,* Wiley & Sons Inc, 1998.

[95] La Salle, L. P. and Lefschetz, S., "Stability by Lyapunov Direct Method," New York, *Academic Press,* 1981.

[96] Slotine, J.-J. E. and Li, W. *Applied Nonlinear Control,* Englewood Cliffs, New Jersey: Prentice Hall, 1991.

[97] Cruz-Hernandez, J. M. and Hayward, V., "Phase Control Approach to Hysteresis Reduction", *IEEE Transaction on Control Systems Technology*, Vol. 9, No. 1, 2001, pp. 17-26.

[98] Cruz-Hernandez, J. M., *Reduction of Hysteresis: A Phase Control Approach*, Ph.D. Dissertation, McGill University, Canada, 1998.

[99] Nguyen, L. T., Whipple, R. D., and Brandon, J. M., "Recent Experiences of Unsteady Aerodynamic Effects on Aircraft Flight Dynamics at High-Angles-of-Attack," Paper 28, *AGARD CP-386*, Sept. 1985.

[100] Liu, Z. L., Su, C.-Y., and Svoboda, J., "A Novel Wing-Rock Control Approach Using Hysteresis Compensation," *America Control Conference*, Denver, USA, June 2003.

[101] Liu, Z. L., Su, C.-Y., and Svoboda, J., "Variable Phase Control of Wing Rock," to appear in *Aerospace Science and Technology*.

[102] Liu, Z. L., Su, C.-Y., and Svoboda, J., "Control of Wing Rock Phenomenon Using Fuzzy PD Controller," *IEEE International Conference on Fuzzy Systems*, St. Louis, USA, May 2003.

[103] Kevin, M. P. and Stephen, Y., *Fuzzy Control,* Addison Wesley Longman, Inc., 1998.

[104] Malki, H. A., Li, H., and Chen, G., "New Design and Stability Analysis of Fuzzy Proportional-Derivative Control Systems," *IEEE Transaction on Fuzzy Systems*, Vol. 2, 1994, pp. 245-254.

[105] Mohan, B. M., and Patel, A. V., "Analytical Structures and Analysis of the Simplest Fuzzy PD Controllers," *IEEE Transaction on Systems, Man, and Cybernetics-Part B: Cybernetics*, Vol. 32, No. 2, 2002, pp. 239-248.

[106] Leu, Y.-G., Lee, T.-T., and Wang, W.-Y., "On-line tuning of fuzzy-neural network for adaptive control of nonlinear dynamical systems," *IEEE Trans. Syst., Man, and Cybern.*, Vol. 27, No. 6, 1997, pp.1034-1043.

[107] Park, D., Kandel, A., and Langholz, G., "Genetic-based new fuzzy reasoning models with application to fuzzy control," *IEEE Trans. Syst., Man, and Cybern.*, Vol. 24, 1994, pp. 39-47.

[108] Nomura, H., Hayashi, I., and Wakami, N., "A learning method fusing fuzzy reasoning and genetic algorithm," in *Proc. IMACS/SICE Int. Symp. Robotics, Mechatronics Systems* '92 Kobe, Japan, pp. 16-20.

[109] Isaka, S., and Sebald, A. V., "An optimization approach for fuzzy controller design," *IEEE Trans. Syst., Man, and Cybern.*, Vol. 22, 1992, pp.1469-1473.

[110] Li, H.-X., Chen, C. L. and Huang, H.-P., "Fuzzy Neural Intelligent Systems:

Mathematical Foundation and the Applications in Engineering" *CRC Press*, c2001.

[111] Li, H.-X., Miao, Z.-H. and Lee, E. S., "Variable Universe Stable Adaptive Fuzz Control of a Nonlinear System," *Computers & Mathematics with Application*, Vol. 2, 2002, pp. 799-815.

[112] Liu, C.-S. and Peng, H., "Disturbance Observer Based Tracking Control," *Journal of Dynamic Systems, Measurement, and Control*, Vol. 122, pp. 332-335, June, 2000.

[113] Roup, A. V. and Bernstein, D. S., "Adaptive Stabilization of a Class of Nonlinear Systems with Nonparametric Uncertainty," *IEEE Transaction on Automatic Control*, Vol. 46, No.11, pp. 1821-1825, 2001.

[114] Bugajski, D. J., Enns, D. F., and Eigersma, M. R., "A Dynamic Inversion Based Control Law with Application to the High Angle of Attack Research Vehicle," *AIAA Paper* 90-3407, 1990.

[115] Ohnishi, K., "A New Servo Method in Mechatronics," *Transaction of Japanese Society of Electrical Engineers*, 107-Do, pp. 83-86, 1987.

[116] Nakao, M., Ohnishi, K., and Miyachi, K., "A Robust Decentralized Joint Control Based on Interference Estimation," *Proc. IEEE Int. Conf. Robotics and Automation*, No. 1, pp. 326-331, 1987.

[117] Umeno T., and Hori, Y., "Robust Speed Control of DC Servomotors Using Modern Two-Degree-of-Freedom Controller Design," *IEEE Transactions on Industrial Electronic*, No. 38, pp. 363-368, 1991.

[118] Bickfl, R. J., "Disturbance Observer Based Robot Control with Applications to Force Control," *Ph. D Dissertation*, University of California, Berkeley, 1996.

[119] Chan, S. P., "A Disturbance Observer for Robot Manipulators with Application to Electronic Components Assembly," *IEEE Transactions on Industrial Electronic*, No. 42, pp. 487-493, 1995.

[120] Ishikawa, J. and Tomizuka, M., "Pivot Friction Compensation Using an Accelerometer and a Disturbance Observer for Hard Disk Drives," *IEEE/ASME Transactions on Mechatronics,* No. 3, pp. 194-201, 1998.

[121] Iwasaki, M., Shibata, T., and Matsui, N., "Disturbance-Observer-Based Nonlinear Friction Compensation in Table Drive System," *IEEE/ASME Transactions on Mechatronics*, No. 3, pp. 194-201, 1998.

[122] Chen, W.-H., Ballance, D. J., Gawthrop, P. J. and O'Reilly, J., "A Nonlinear Disturbance Observer for Robotic Manipulators," *IEEE Transaction on Industrial Electronics,* Vol. 47, No.4, pp. 932-938, 2000.

[123] Gomi, H. and Kawato M., "Neural Network Control for a Closed-Loop System Using Feedback-Error-Learning," *Neural Networks*, Vol. 6, No.7, 1993, pp. 933-946.

[124] ----------, "Learning Control for a Closed Loop System Using Feedback-Error-Learning," *Proceedings of the 29th Conference on Decision and Control*, Hawaii, 1990, pp. 3289-3294.

[125] Rao, D. H. and Gupta, M. M., "Feedback-Error-Learning Scheme Using Recurrent Neural Networks for Nonlinear Dynamic Systems," *Neural Networks, IEEE World Congress, Computer Intelligence*. Vol. 1, 1994, pp. 175-180.

[126] Li, Y., Sundararajan, N., and Saratchandran, P., "Nonlinear Neuro-Flight-Controller Design Using Feedback-Error-Learning Strategy," *Automatica*, Vol. 37,

No. 8, pp. 1293-1301, 2001.

[127] Velthuis, W.J.R., Vries, T.J.A.D., and Amerongen, J.V., "Design Procedure for a Learning Feed-Forward Controller," *The 1st IFAC Conf. on Mechatronics Systems, Darmstadt,* Germany, September 18-20, 2000.

[128] Er, M. J. and Gao, Y., "Robust Adaptive Control of Robot Manipulators Using Generalized Fuzzy Neural Networks," *IEEE Transaction on Industrial Electronics*, Vol. 50, No. 3, pp. 620-628, 2003.

[129] Wai, R.J., Lin, C.-M., and Hsu, C.-F., "Self-Organizing Fuzzy Control for Motor-Toggle Servomechanism via Sliding-Mode Technique," *Fuzzy Sets and Systems* (131), 2002, pp. 235-249.

[130] Liu, Z. L. and Svoboda, J., "Dutch Roll Limit-Cycle Oscillation Suppression Using Fuzzy Sliding-Mode Control," *ICCA '03*, Montreal, Canada, June 9-12, 2003.

[131] Choi, S.-B. and Kim, J.-S., "A Fuzzy-Sliding Mode Controller for Robust Tracking of Robotic Manipulators," *Mechatronics,* Vol. 7, No. 2, 1997, pp. 199-216.

[132] Chen, C.-S. and Chen, W.-L., "Robust Adaptive Sliding-Mode Control Using Fuzzy Modeling for an Inverted-Pendulum System, " *IEEE Transaction on Industrial Electronics*, Vol. 45, No. 2, 1998.

[133] Chen, J.-Y., "Rule Regulation of Fuzzy Sliding Mode Controller Design: Direct Adaptive Approach," *Fuzzy Sets and Systems,* 120, 2001, pp.159-168.

[134] Jafarov, E. M. and Tasaltin, R., "Robust Sliding-Mode Control for the Uncertain MIMO Aircraft Mode F-18," *IEEE Transactions on Aerospace and Electronic Systems,* Vol. 36, No. 4, 2000, pp. 1127-1141.

[135] Hung, J. Y., Gao, W., and Hung, J. C., "Variable Structure Control: A Survey,"

IEEE Trans. on Industrial Electronics, Vol. 40, No. 1, 1993, pp. 2-21.

[136] Wang, L.-X., "Fuzzy Systems are Universal Approximators, " *in Proc. IEEE Int. Conf. Fuzzy Systems*, San Diego, 1992, pp. 1163-1170.

[137] Park, J. and Sandberg, I W., "Approximation and Radial-Basis-Function Network," Neural Computation, Vol. 5 1993, pp.305-316.

[138] Jang, J.-S. R., "ANFIS: Adaptive-Network-Based Fuzzy Inference Systems," *IEEE Trans. on Systems, Man, and Cybernetics,* 23(03), 1993, pp. 665-685.

[139] Jang, J.-S. R., Sun, C.-T., and Mizutani, E., *Neuro-Fuzzy and Soft Computing,* New Jersey: Prentice Hall, 1997.

[140] Sun, Q., Li, R., and Zhang, P. A., "Stable and Optimal Adaptive Fuzzy Control of Complex Systems Using Fuzzy Dynamic Model," *Fuzzy Sets and Systems*, Vol. 133, 2003, pp. 1-17.

[141] Su, C.-Y., and Stepanenko, Y., "Adaptive Control of a Class of Nonlinear Systems with Fuzzy Logic," *IEEE Trans. Fuzzy Systems*, Vol. 2, 1994, pp. 285-294.

[142] Lee, Y., and Zak, S. H., "Uniformly Ultimately Bounded Adaptive Tracking Control of Uncertain Systems," in *proc. 2002 American Control Conf.*, Anchorage, AK, May 8-10, pp. 3419-3424.

[143] Hwang, K.-S., Tan, S.-W., and Tsai, M.-C., "Reinforcement Leaning to Adaptive Control of Nonlinear Systems," *IEEE Trans. Syst., Man, and Cybern.*, Vol. 33, No. 3, 2003, pp.514-521.

[144] Jouffe, L., "Fuzzy Inference System Learning by Reinforcement Methods," *IEEE Trans. Syst., Man, and Cybern.*, Vol. 28, No. 3, 1998, pp.338-355.

[145] Kaelbling, L. P., Littman, M. L., and Moore, A. W., "Reinforcement Learning: A

Survey", *J. Artif. Intell. Res.*, Vol. 4, 1996, pp. 237-285.

[146] Lin, C.-K., " A Reinforcement Learning Adaptive Fuzzy Controller for Robots," *Fuzzy Sets and Systems*, Vol. 137, 2003, pp. 339-352.

[147] Kim, Y. H. and Lewis, F. L., "Reinforcement Adaptive Learning Neural Network Based Friction Compensation for High Speed and Precision," *The 37th IEEE Conf. on Decision & Control*, Florida, USA, Dec. 1998.

[148] Glorennec, P. Y., "Reinforcement Learning: An Overview," *ESIT 2000,* Aachen, Germany, Sept. 14-15, 2000.

[149] Kaynak, O., Erbatur, K., and Ertugrul, M., "The Fusion of Computationally Intelligent Methodologies and Sliding-Mode Control – A Survey," *IEEE Trans. Ind. Electron.*, Vol. 48, No. 1, 2001, pp. 4-17.

[150] Ha, Q. P., Rye, D. C., and Durrant-Whyte, H. F., "Fuzzy Moving Sliding Mode Control with Application to Robotic Manipulators," *Automatica*, Vol. 35, 1999, pp. 607-616.

[151] Buijtenen, W. M., Schram, G., Babuska, R., and Verbruggen, H. B., "Adaptive fuzzy control of satellite attitude by reinforcement learning," *IEEE Trans. Fuzzy Systems*, Vol. 6, pp. 185-194, 1998.

[152] Spooner, J. T., Maggiore, M., Ordonez, R., and PASSINO, K. M., "Stable adaptive control and estimation for nonlinear systems - neural and fuzzy approximator techniques," John Wiley & Sons, Inc., c2002.

[153] Zeng, X.-J. and Singh, M. G., "Approximation theory of fuzzy systems – SISO case," *IEEE Trans. Fuzzy Systems*, Vol. 2, pp. 162-176, 1994.